AD-A119 726 SOUTHWEST RESEARCH INST SAN ANTONIO TX F/G 12/1
THE INFLUENCE OF TUBE SUPPORT CONDITIONS ON MUZZLE MOTIONS.(U)
JUN 82 P A COX, J C HOKANSON DAAG29-79-C-0037
UNCLASSIFIED ARO-15722.2-EG NL

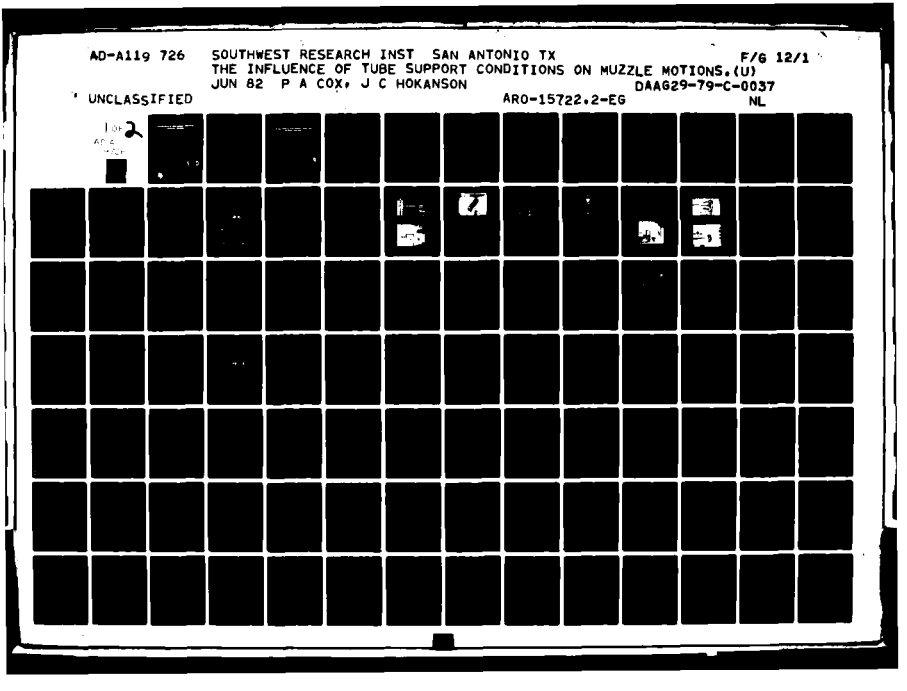

12

THE INFLUENCE OF TUBE SUPPORT CONDITIONS ON MUZZLE MOTIONS

by
P. A. Cox
J. C. Hokanson

FINAL REPORT
Contract No. DAAG29-79-C-0037
SwRI Project No. 02-5622

for
U. S. Army Research Office
Research Triangle Park, North Carolina

August 1982

SOUTHWEST RESEARCH INSTITUTE
SAN ANTONIO HOUSTON

The findings in this report are not to be construed as an official Department of the Army position, unless so designated by other authorized documents.

ARO 15722.2-EG

SOUTHWEST RESEARCH INSTITUTE
Post Office Drawer 28510, 6220 Culebra Road
San Antonio, Texas 78284

THE INFLUENCE OF TUBE SUPPORT CONDITIONS ON MUZZLE MOTIONS

by
P. A. Cox
J. C. Hokanson

FINAL REPORT
Contract No. DAAG29-79-C-0037
SwRI Project No. 02-5622

for
U. S. Army Research Office
Research Triangle Park, North Carolina

August 1982

Approved:

H. Norman Abramson, Vice President
Engineering Sciences Division

UNCLASSIFIED

SECURITY CLASSIFICATION OF THIS PAGE (When Data Entered)

REPORT DOCUMENTATION PAGE	READ INSTRUCTIONS BEFORE COMPLETING FORM
1. REPORT NUMBER	2. GOVT ACCESSION NO. AD-A119 726	3. RECIPIENT'S CATALOG NUMBER
4. TITLE (and Subtitle) THE INFLUENCE OF TUBE SUPPORT CONDITIONS ON MUZZLE MOTIONS	5. TYPE OF REPORT & PERIOD COVERED Final Technical Report March 1979 - June 1982
	6. PERFORMING ORG. REPORT NUMBER 02-5622
7. AUTHOR(s) P. A. Cox, J. C. Hokanson	8. CONTRACT OR GRANT NUMBER(s) DAAG29-79-C-0037
9. PERFORMING ORGANIZATION NAME AND ADDRESS Southwest Research Institute, P. O. Drawer 28510, San Antonio, Texas 78284	10. PROGRAM ELEMENT, PROJECT, TASK AREA & WORK UNIT NUMBERS P-15722-E
11. CONTROLLING OFFICE NAME AND ADDRESS U. S. Army Research Office, P. O. Box 12211, Research Triangle Park, North Carolina 27709	12. REPORT DATE June 1982
	13. NUMBER OF PAGES
14. MONITORING AGENCY NAME & ADDRESS(if different from Controlling Office)	15. SECURITY CLASS. (of this report) Unclassified
	15a. DECLASSIFICATION/DOWNGRADING SCHEDULE N/A

16. DISTRIBUTION STATEMENT (of this Report)

Approved for public release; distribution unlimited.

17. DISTRIBUTION STATEMENT (of the abstract entered in Block 20, if different from Report)

N/A

18. SUPPLEMENTARY NOTES

The findings in this report are not to be construed as an official Department of the Army position, unless so designated by other authorized documents.

19. KEY WORDS (Continue on reverse side if necessary and identify by block number)

Experiments	Support Clearances
Finite Elements	Support Stiffness
Gun Dynamics	Tube Motions
Muzzle Motions	Tube Support

20. ABSTRACT (Continue on reverse side if necessary and identify by block number)

This study addressed the effect of clearances between the tube and its support and the effect of support stiffness on the muzzle motions produced when a weapon is fired. A small-scale test weapon was designed, fabricated, and tested during the study. The test weapon included provisions for changing the clearance between the tube and the tube support sleeve and for changing support stiffness. Breech eccentricity and lubrication between sliding surfaces were also varied. (CONTINUED)

DD FORM 1 JAN 73 1473 EDITION OF 1 NOV 65 IS OBSOLETE

UNCLASSIFIED

SECURITY CLASSIFICATION OF THIS PAGE (When Data Entered)

20. ABSTRACT (Continued)

A series of experiments was conducted in which tube support conditions were systematically varied and transverse motions of the tube were measured at eight locations. Additional measurements included tube recoil, timing of the firing pulse, chamber pressure, muzzle exit time, and muzzle velocity. Tube lateral motions were measured with noncontacting inductance transducers, and instrumentation systems for these and other transducers are described.

Tube motions of the test weapon were calculated by the finite element method for comparison with the experimental results. The initial positions of the tube within the tube support sleeve, tube radial expansion, and tube support stiffness were found to be significant parameters affecting the predicted tube motion.

FOREWORD

This report covers work sponsored by the U. S. Army Research Office (ARO) in the time period March 1979 through June 1982. The work was performed under the cognizance of Dr. Fred Schmeideshoff of ARO. Drs. Tom Simkins and Julian Wu of the Benet Weapons Lab served as Scientific Liaison representatives for ARO. Their suggestions and comments as the work progressed were welcome and helpful.

The authors are pleased to acknowledge Kirt Thistlewaite and Frank Hudson for conducting the experiments, Rosemary Rivas for typing the report, and Victor Hernandez for drawing the illustrations. The authors and the above mentioned technicians were the principal personnel employed under this contract. No technical degrees were earned or awarded as a result of this work.

SUMMARY

This was a combined experimental-analytical program to investigate the effects of tube support conditions on gun tube motions. A 1/5.25-th scale model of the M68 105mm tank gun was designed and fabricated for the experiments. It was used to conduct a 27-test experimental study in which support stiffness and support clearances were systematically varied. Four additional tests were conducted to show the influence of breech mass eccentricity and the viscosity of the lubrication between sliding surfaces. Tube motions were measured with noncontacting inductance transducers. Instrumentation problems encountered with these transducers and with the measurement of chamber pressure are covered in the report.

An analytical model of the test weapon was developed and solved using the two-dimensional finite element program, GUN2D. The model was unique in its treatment of the tube support conditions. Interaction forces between the tube and its support were calculated and applied separately to the tube and to the support as external forces. The support model treated local deformations produced by contact forces, viscous damping based upon the relative lateral velocities between the tube and its support, tube initial position, tube-to-sleeve clearances, tube radial expansion, and, finally, the recoil motion of the tube relative to the support.

Using the analytical model, a parameter study was conducted to show the influence of the Bourdon forces, axial accelerations, initial tube curvature, tube radial expansion, and tube initial position relative to its support. In addition, selected tests were simulated analytically as an aid to understanding the effects produced by changing tube support stiffness and clearances.

The most significant parameters affecting tube motions were found to be the initial tube position relative to its supports and the tube radial expansion. The range of clearances in the experiments produced only small effects on the tube displacements. It was discovered analytically that these clearances were too large to have much influence on the tube motions. The minimum clearance in the tests was about three times the maximum tube radial expansion for the model test weapon. Clearances which were about twice the maximum tube radial expansion sharply altered calculated values. Support stiffness significantly altered tube displacements, but primarily in the support region. Analytically, very different displacement profiles along the tube length were produced by changing tube support stiffness.

TABLE OF CONTENTS

TABLE OF CONTENTS (continued)

LIST OF FIGURES

LIST OF FIGURES (continued)

LIST OF TABLES

I. INTRODUCTION

The U. S. Army is concerned about the first round accuracy of its large caliber weapons. Traditionally, the first round fired has an error in the accuracy of fire which is random and greater than that for subsequent rounds. The cause of this error is often attributed to jump, a variation in the projectile muzzle exit conditions produced by the gun tube motions.

Motions of the tube at the time of shot ejection are influenced by many factors, one of which is the tube support conditions. The importance of the tube support conditions on the tube motions produced during firing was pointed out by Cox and Hokanson [1, 2] in their study of the M68 105mm tank gun.

The research documented in this report focused on the influence of tube support conditions on tube motions produced when a weapon is fired. It was a combined experimental-analytical program in which tube motions, measured under various support conditions, were compared with analytical predictions. The goal of this research was to improve the analytical methods for predicting gun tube motions.

Two basic parameters, which characterize the tube support conditions, were studied in this program. These were the stiffness (both lateral and rotational) of the tube support system and the clearances between the tube and its support. Both of these parameters were varied systematically in the experiments. In addition, a limited series of tests was conducted to observe the effect produced by a heavy viscous lubricant between the tube and its support and also the effect produced by a large breech mass eccentricity. Analytical studies addressed several parameters which influenced the muzzle motions. The most influential of these were the tube radial expansion and the initial position of the tube in the support sleeve.

Analytical predictions of gun tube motions were made using the finite element computer program GUN2D developed by Cox and Hokanson [1, 2]. In applying GUN2D to this study, the interaction forces which occur between the tube and its support were derived as a function of the relative motions between the two parts and applied as external forces.

Following sections of this report describe the small-scale model of the M68 gun which was designed, fabricated and tested in this program (Section II); the test set-up (Section III); the measurement systems

---

1. Cox, P. A., and Hokanson, J. C., "Muzzle Motions of the M68 105mm Tank Gun," Contract Report ARBRL-CR-00418, Prepared by Southwest Research Institute, San Antonio, Texas, March 1980.

2. Cox, P. A., and Hokanson, J. C., "Muzzle Motions of the M68 105mm Gun," Proceedings of the 2nd U. S. Army Symposium on Gun Dynamics, held at The Institute on Man and Science, Rensselaerville, NY, 19-22 September 1978.

(Section IV); the experiments (Section V); the analytical model (Section VI); and the parameter studies (Section VII). Analytical-experimental comparisons are made in Section VIII, support conditions are evaluated in Section IX, and finally conclusions and recommendations are given in Section X. The material contained in Sections II through V has been published as Reference 3. All other material is presented here for the first time.

3. Cox, P. A., and Hokanson, J. C., "The Influence of Tube Support Conditions on Muzzle Motions," Report No. ARLCB-SP-82005, Proceedings of the 3rd U. S. Army Symposium on Gun Dynamics, Vol. II of II, held at The Institute on Man and Science, Rensselaerville, NY, 11-14 May 1982.

II. DESCRIPTION OF THE GUN MODEL

A. Scaling Relationships

The small-scale gun model used in these experiments was patterned after the M68 105mm tank gun. The M68 was chosen because of the authors' earlier work [1, 2] with it and because of the large body of experimental data which has been accumulated for this weapon at the Ballistic Research Laboratories. A small-scale model was needed which would replicate the essential features of the M68 and also could be fired repeatedly in a small range. It was also desirable to minimize unwanted excitations to the gun during firing and to have a simple means of changing stiffness and clearances in the tube support mechanism.

A 20mm bore was chosen for the model weapon, which gave a geometric scaling factor, relative to the M68, of

$$\lambda = \frac{20\text{mm}}{105\text{mm}} = \frac{1}{5.25}$$

Based upon replica scaling, an analysis was performed to derive scaling factors for other model parameters. The resulting scale factors are:

Force:	λ^2
Stress:	1.0
Pressure:	1.0
Displacements:	λ
Velocity:	1.0
Acceleration:	$1/\lambda$
Time:	λ

These scaling factors show that, with replica scaling, stresses, pressures and velocities in the model will be the same as in the prototype. Displacements and time will scale as λ (be 1/5.25th as large as full-scale values); model forces will be $(1/5.25)^2$ as large as full-scale values; and accelerations will be higher in the model than in full scale. With replica scaling, terms which contain gravity are not correctly scaled; thus, tube droop will not scale in the model, nor will gravitational accelerations which act on the tube and projectile. We expect these effects to be small, especially since we are principally concerned with the short time period from propellant ignition to projectile muzzle exit.

B. Model Features

For a 20mm bore size, a design study was performed to establish the model configuration. A weapon model evolved from the study which has the following general features:

- It closely replicates the M68 105mm tube and tube support in the 1/5.25th scale.
- The tube, constructed from heat-treated 4340 steel, has a 20mm smooth bore.

- Propellant is contained in 20mm cartridge cases which were modified to fit the scaled M68 cartridge chamber.

- The tube is supported by a cylindrical sleeve, which in turn is supported at its forward end as in the M68.

- The model breech and pressure-transducer assembly matches the mass and longitudinal C.G. location of the M68 breech.

- Vertical C.G. location of the total breech mass (breech block plus pressure-transducer assembly) is adjustable.

- Tube support stiffness is variable.

- Clearance between the tube and the tube support sleeve is easily changed.

A schematic of the weapon model is given in Figure 1. Variations in support stiffness are achieved by changing the diameter of the four small beams which attach the tube support sleeve to the mount. These beams have a high axial stiffness relative to their lateral stiffness. Interchangeable sleeves with different internal diameters give different clearances between the tube and sleeve. The sleeves are lined with a porous brass to reduce friction forces on the tube and to eliminate the possibility of scoring the tube and sleeve contacting surfaces. An undercut was made in the brass to give two distinct supporting surfaces.

Vertical adjustments in the total breech mass eccentricity are made by adjusting the position or size of the counterweight. The primary purpose of the counterweight is to balance the pressure transducer assembly, but it also affords small adjustments of the total breech mass as well. The counterweight is supported from the clamp which holds the pressure transducer. A clamp was required because the pressure transducer was too large to be threaded directly into the tube wall. Also, as will be discussed in Section IV, it was necessary to electrically isolate the transducer from the tube. This further enlarged the pressure transducer assembly.

Recoil of the tube is totally arrested by the recoil cushion; thus, no arresting forces act on the tube during recoil until it impacts the cushion. This occurs after projectile muzzle exit so that the tube is in "free" travel during the time period of primary interest.

C. Parameter Variations

Parameters that can be varied in tests conducted with the weapon model described above include:

- Tube support stiffness
- Clearance between the tube and the tube support sleeves
- Vertical breech eccentricity
- Lubrication between the tube and the tube support sleeve
- Projectile mass

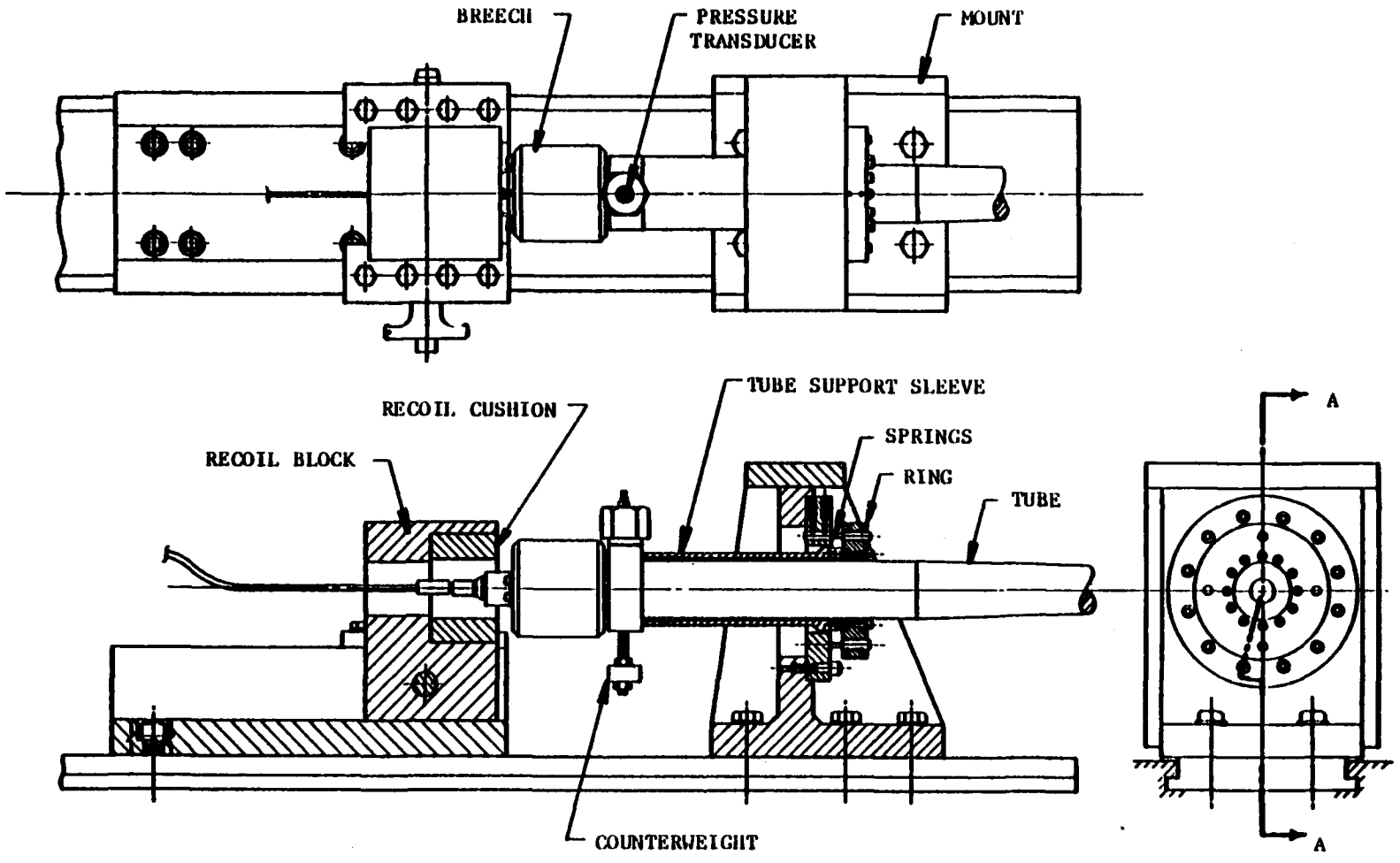

SECTION A-A

FIGURE 1. SCHEMATIC OF THE TEST FIXTURE

- Projectile unbalance
- Charge weight

The primary variables in the test program were the tube support stiffness and the clearance between the tube and the sleeve. Also varied in a limited series of tests were the breech mass vertical eccentricity and lubrication between the sleeve and the tube. A balanced projectile was fired in all tests, and the projectile and propellant weights were fixed after the initial checkout and evaluation tests.

Variations in the model parameters are given in Table 1. For comparison, these parameters are also given for the M68 gun. Actual stiffness values for the M68 are unknown. The values in Table 1 were taken from analytical studies performed in Reference 1. Stiffness variations in the model cover two orders of magnitude. Clearances in the M68 gun which are listed first give the range of values which can exist between the tube and the tube support sleeve. The values in parentheses include clearances between the tube support sleeve and the recoil piston and between the recoil piston and the cradle. These additional clearances are closed by seals and thus do not afford free travel. Clearances in the model weapon are nominal values and are characteristic of M68 scaled values. More exact values, measured at the forward and aft ends of the sleeve, are given in Section V.

Breech eccentricities do not match those of the M68 gun. A balanced breech (approximately) was chosen for a majority of the tests. A few were conducted with a large positive breech mass eccentricity for comparison purposes. Further description of the test setup is given in the next section. Section V describes the test program.

TABLE 1. RANGE OF VARIABLES

	M68 Gun	1/5.25 Scale	Model Weapon
Tube Support Stiffness, lb/in.	355 to 3.55 x 10^{8}*	67 to 6.7 x 10^{7}	6.748 x 10^{4} 6.746 x 10^{5} 6.746 x 10^{6}
Clearances, in.	0.008 to 0.015 (0.028 to 0.047)	0.0015 to 0.0029 (0.0053 to 0.0090)	0.0015 0.0030 0.0045
Breech Eccentricity, in.			
Vertical:	+0.40**	-0.076	0.014, 0.175
Horizontal:	+0.24**	-0.046	0

* Range used in analytical studies (reference 1).

** Positive directions are up and to the right, looking toward the muzzle.

III. TEST SETUP

A. Test Range and Mount

Tests were conducted at a covered firing range suitable for small-bore weapons. The model weapon was attached to a universal mount; the mount was solidly bolted to a test stand, which in turn was bolted to a concrete floor. Figure 2 shows an overall view of the test arrangement. Through vertical and horizontal adjustments in the universal mount, the tube was easily aligned with the displacement gages (described in Section IV) and was aligned for testing with the tube support sleeve horizontal. A view down range, showing the velocity screens, is given in Figure 3. In the experiments, projectiles were trapped by deflection screens and test data were recorded at a nearby instrumentation trailer.

B. Recoil Cushion

As noted in Section II, recoil was controlled by a crushable insert in the recoil block which was impacted by the breech. An initial series of tests was conducted to determine the required crushing strength of this insert, to select a suitable propellant, and to check out the instrumentation. An insert was needed which would limit recoil motions and prevent rebound of the tube into the tube support sleeve. Polyurethane foams caused excessive rebound, and so, a sodium-silicate foam was formulated at SwRI for the insert. The strength of the inserts was selected to arrest recoil in about 1.75 inches. This prevented the pressure-transducer assembly from interfering with the displacement gage used to measure breech vertical motions. Foam with a crushing strength of 100-120 psi was found to both limit recoil displacement to acceptable vaules and to prevent rebound. This strength level was used for the insert in all parameter studies.

C. Propellant and Projectile

WC 870, a standard 20mm propellant, was initially selected for the tests. With this propellant, pressures were found to be erratic and lower than expected. Also, unburned propellant was often found in the tube after the gun was fired. The addition of a black-powder boost and the use of an igniter mix of powdered aluminum and potassium perchlorate did not improve the burning. Other propellants, with higher relative quickness values (RQ), were then tried. A propellant with an RQ value of 100 was chosen for the tests. It was bagged inside the cartridge to reduce pressure fluctuations during the initial burning. The propellant charge was 24.65 gms in all parameter studies. It produced peak chamber pressures of about 30,000 psi when fired with a projectile with a nominal mass of 35.5 gms. Smooth cylindrical projectiles were used which could be seated into the bore by hand. The base of the projectile was undercut as shown in Figure 4 to improve the pressure seal.

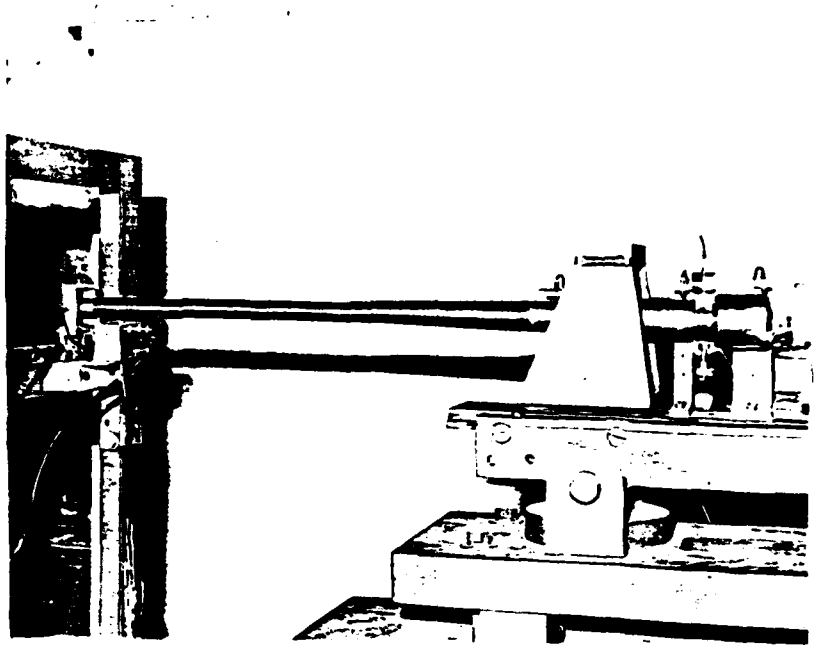

FIGURE 2. OVERALL VIEW OF THE TEST SETUP

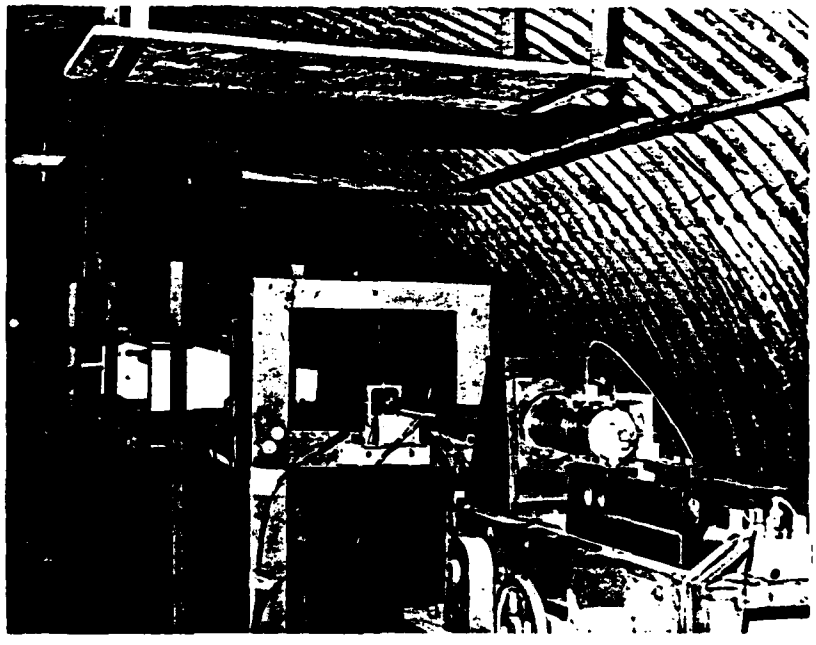

FIGURE 3. VIEW DOWN RANGE SHOWING VELOCITY SCREENS (RECOIL BLOCK REMOVED)

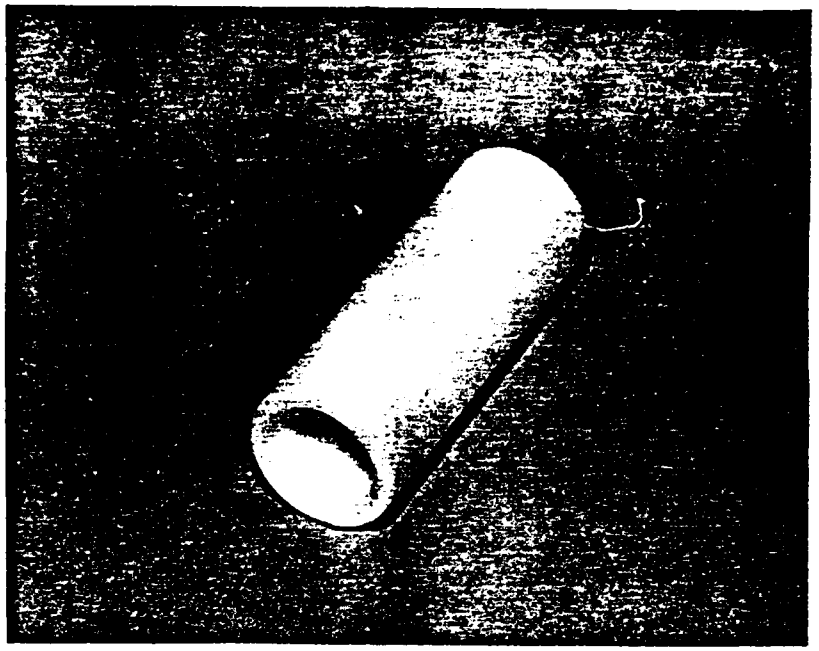

FIGURE 4. TEFLON PROJECTILE

The propellant was ignited with a high-intensity, short-duration firing pulse. This pulse was often picked up on other instrumentation channels, but when interference did occur, it was a spike of about 300 μs duration which occurred at the very beginning of the record. This interference usually had no noticeable influence on the remainder of the record. Other instrumentation problems occurred during the initial series of tests. These problems and their solutions are discussed in the following section.

IV. MEASUREMENT SYSTEMS

The model weapon was instrumented for chamber pressure, recoil, and out-of-plane displacements in two orthogonal planes on the breech, support sleeve, tube, and muzzle. Projectile exit velocity, ignition time (time zero), and projectile exit time were also recorded. A total of ten displacement locations were provided on the model, as shown in Figure 5. Half of these locations were for horizontal displacements (21, 22, 32, 42, and 62), and half were for vertical displacements (11, 12, 31, 41, and 61). Most of these displacement gage locations were instrumented during the parameter studies. Brief descriptions of the measurement systems used to obtain the test data are given in the following paragraphs.

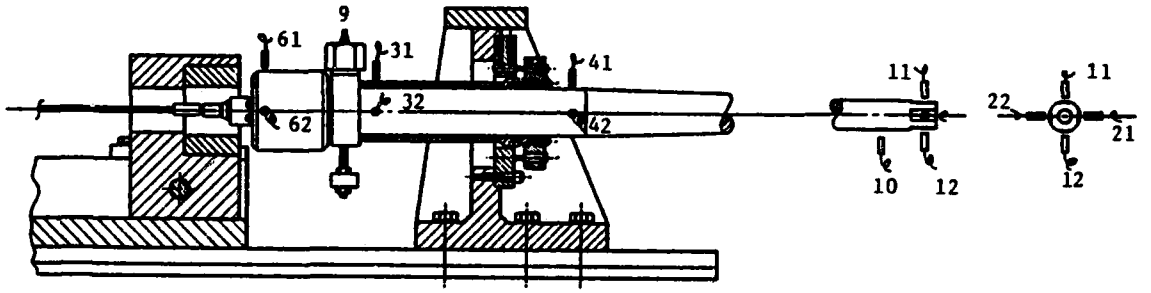

FIGURE 5. IDENTIFICATION NUMBERS AND LOCATIONS OF THE TRANSDUCERS

A. Pressure

Chamber pressure was measured with a PCB Piezetronics Model 109A transducer. This device is a miniature dynamic sensor specifically designed for measuring pressure when high frequency response is required. The transducer utilizes an acceleration-compensated, quartz piezoelectric pressure sensing element coupled to a miniature source follower within the body of the sensor. This micro-electronic amplifier converts the high-impedance output of the quartz element into a low-impedance, high-level output signal. The 109A sensor has a rise-time capability of 1 μs.

The transducer was powered, and its output was voltage conditioned and amplified, by one channel of a PCB Model 494A06 six-channel voltage amplifier. This amplifier has a frequency response (-3db) of 0.08 to 180,000 Hz. The coupling circuit time constant is two seconds, long enough to accurately measure the transient chamber pressure. The output of the amplifier was recorded on one channel of an Ampex Model 2230 14-track Wideband II FM tape recorder at a speed of 60 ips. The data bandwidth (-3db) at this speed is 0-250Khz.

The pressure sensor was installed in the model weapon system at location 9 in Figure 5. As shown in Figure 6, there is a tapered hole

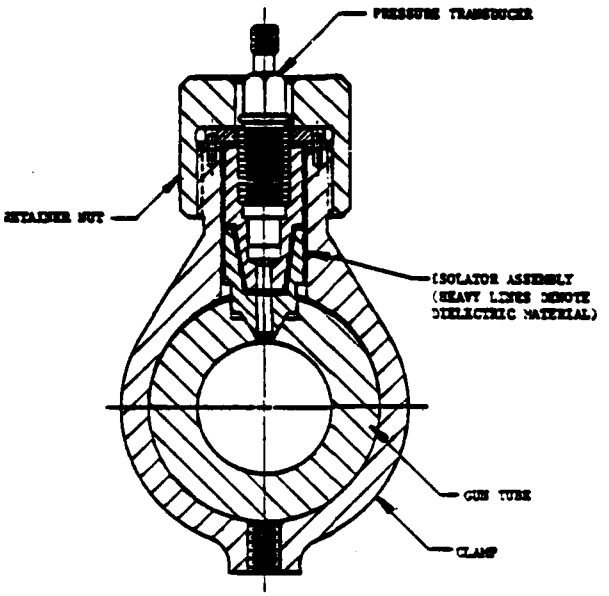

FIGURE 6. PRESSURE TRANSDUCER ASSEMBLY

in the gun tube at this location, which was lined up with a 0.25-in. hole in the brass shell casing. The transducer was mounted in an isolated adapter which has a tapered cone at one end which mates with the tapered hole in the tube to provide a pressure seal. The pressure developed by the burning propellant was transmitted through the holes in the case and gun tube and through a hole in the adapter leading to the sensing element of the transducer. Thermal protection for the transducer was provided by filling the cavity in the adapter with Dow Corning 4 Silicone Compound® and by an ablative coating over the diaphragm which was installed by the transducer manufacturer.

In the early experiments, an electrical interference signal was superimposed on most of the pressure and displacement signals. This interference was traced to the electrical firing system. Both the firing system and the pressure transducer were grounded to the weapon system. By redesigning the adapter to provide for electrical isolation of the transducer from the weapon (as shown in Figure 6), the electrical interference on the pressure and displacement signals was controlled.

B. Displacement

Tube lateral displacements were measured with the Kaman Sciences Model KD-2300 noncontacting linear proximity measurement system. The system consists of a model KD-2300-1SM sensor and a model KD-2300-1 modulator-demodulator. The sensor consists of a variable impedance bridge with an active and a reference coil. Variations in impedance result from the eddy currents induced in nearby conductive surfaces. The modulator-demodulator powers the sensor and converts detected variations in impedance into a voltage output which is linearly proportional to the distance between the sensor and the target.

The displacement system has a measurement range of 40 mils with a linearity of 1% of the measurement range (0.4 mils) and a resolution of 0.004 mils. Sensitivity is nominally 20mV/mil, and the frequency response (-3db) is 0-50Khz. Output of the displacement measurement system was recorded on the magnetic tape recorder. Because the sensitivity of this type of sensor varies with the type of target material, the displacement measurement system was calibrated at SwRI. The calibration consisted of varying the sensor-to-target distance with the aid of a micrometer and noting the output voltage on an accurate digital voltmeter. The target material in this case was a 1.0 x 0.5 x 0.25-in. piece of steel which simulated the gun tube. Typical calibration curves were essentially linear beyond the measurement range required in this study.

Displacement transducers were mounted in fixtures which were bolted to the gun mount at three locations and to a separate stand at the muzzle. These fixtures are shown in Figures 7, 8, and 9. They were designed to hold the face of the transducers parallel to the flats which had been machined on the gun tube forward of the mount (locations 41 and 42 in Figure 50 and at the muzzle (locations 11, 12, 21, and 22 in Figure 5). The diameters of the support sleeve (locations 31 and 32 in Figure 5) and the breech (locations 61 and 62 in Figure 5) were sufficiently large that no flats were required. Prior to each test, the sensors were adjusted so that the output of the probe was 0.5 volts, which corresponds to 25 mils between the target and sensor.

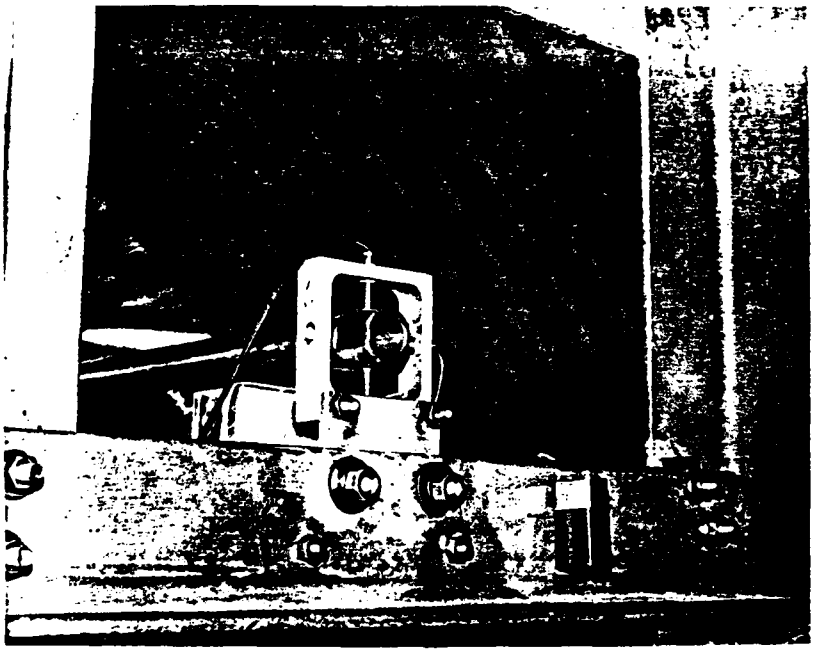

FIGURE 7. DISPLACEMENT GAGES AT THE MUZZLE

The sensors provided reasonable traces during the event, but problems also occurred. For example, electromagnetic signals are easily picked

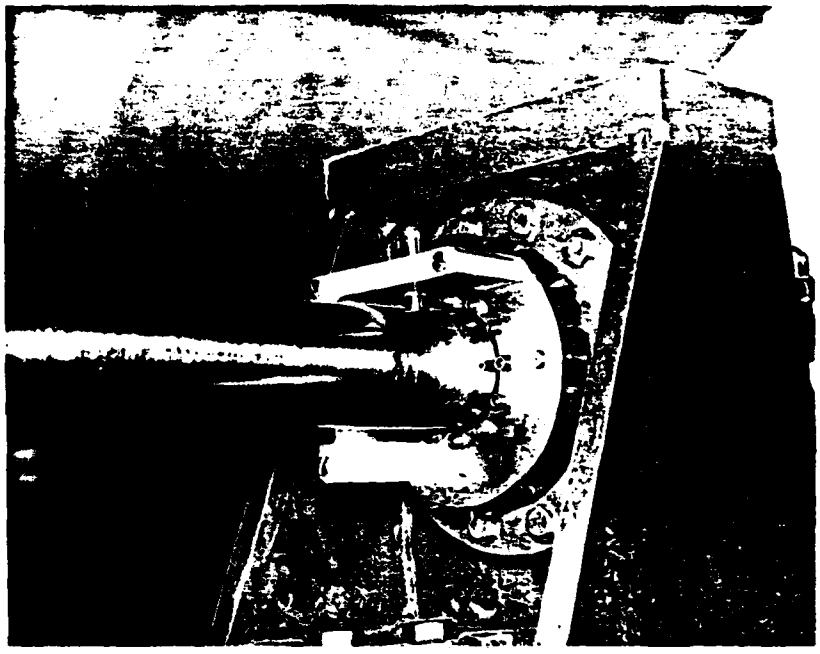

FIGURE 8. DISPLACEMENT GAGES FORWARD OF THE TUBE SUPPORT

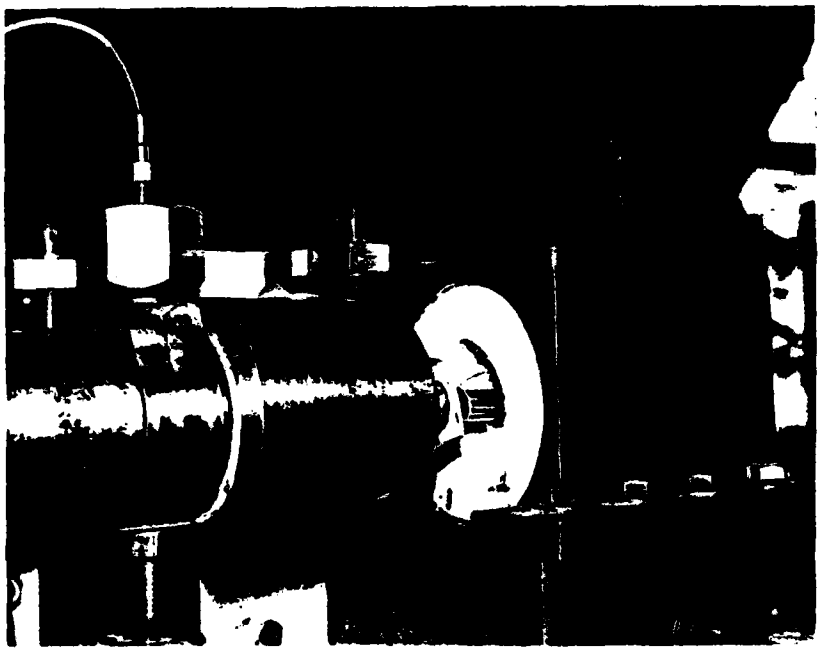

FIGURE 9. DISPLACEMENT GAGES ON THE SLEEVE AND THE BREECH

up by the sensors. Thus, the displacement measurement system was especially sensitive to noise from the firing signal, and careful placement of the firing lines and the firing module with respect to the displacement probes, cables, and modulator-demodulator was required. Even with proper precautions, the firing signal was often superimposed on the early portion of the displacement records. This is not a severe problem, since essentially no displacement was observed at any of the gage locations in this early time frame.

Transducers at the muzzle were installed in opposing directions, so they should provide equal, but opposite, signatures. In general, this was observed, but after muzzle exit the upper gage yielded a disporportionately larger signal than the lower gage. This apparently was caused by electromagnetic and possibly thermal energy in the hot gases leaving the muzzle. This effect was not a severe problem, since the time of interest was between ignition of the propellant and exit of the projectile from the gun tube.

One last problem with the displacement measurement system was that, over a period of a few days, the calibration sensitivity shifted so that frequent recalibration and alignment of the modulator-demodulator was required. During this program, the displacement measurement system was calibrated and aligned about once a week.

Figure 10 presents a typical set of muzzle vertical displacements. Part (a) is the response measured by the upper gage (number 11) [this trace was numerically inverted during plotting, *so all plots reflect* positive displacements when the muzzle moves up], and Part (b) is the response measured by the lower gage (number 12). Both signals were comprised of a true signal T_s and a noise contribution N. If the noise contribution is assumed to be exactly the same for both gages, then the true signal and the noise contribution can be determined from:

$$T_s = \frac{R_l - R_u}{2}$$

$$N = \frac{R_l + R_u}{2}$$

where R_l is the displacement measured at the lower gage, location 12, and R_u is the displacement measured at the upper gage, location 11.

The noise signal, N, and true displacement, T_s, derived from the responses in Figures 10 (a) and (b), are presented in Figures 10 (c) and (d), respectively. The true displacement signal is much cleaner than either of the original displacement signals, although the general character of the three displacement traces is similar. Note that there was essentially no net displacement at the muzzle until after 1 ms into the event, at which time the vertical motions increased dramatically. The vertical noise at the muzzle was generally a low amplitude signal which oscillated randomly about zero displacement until projectile exit.

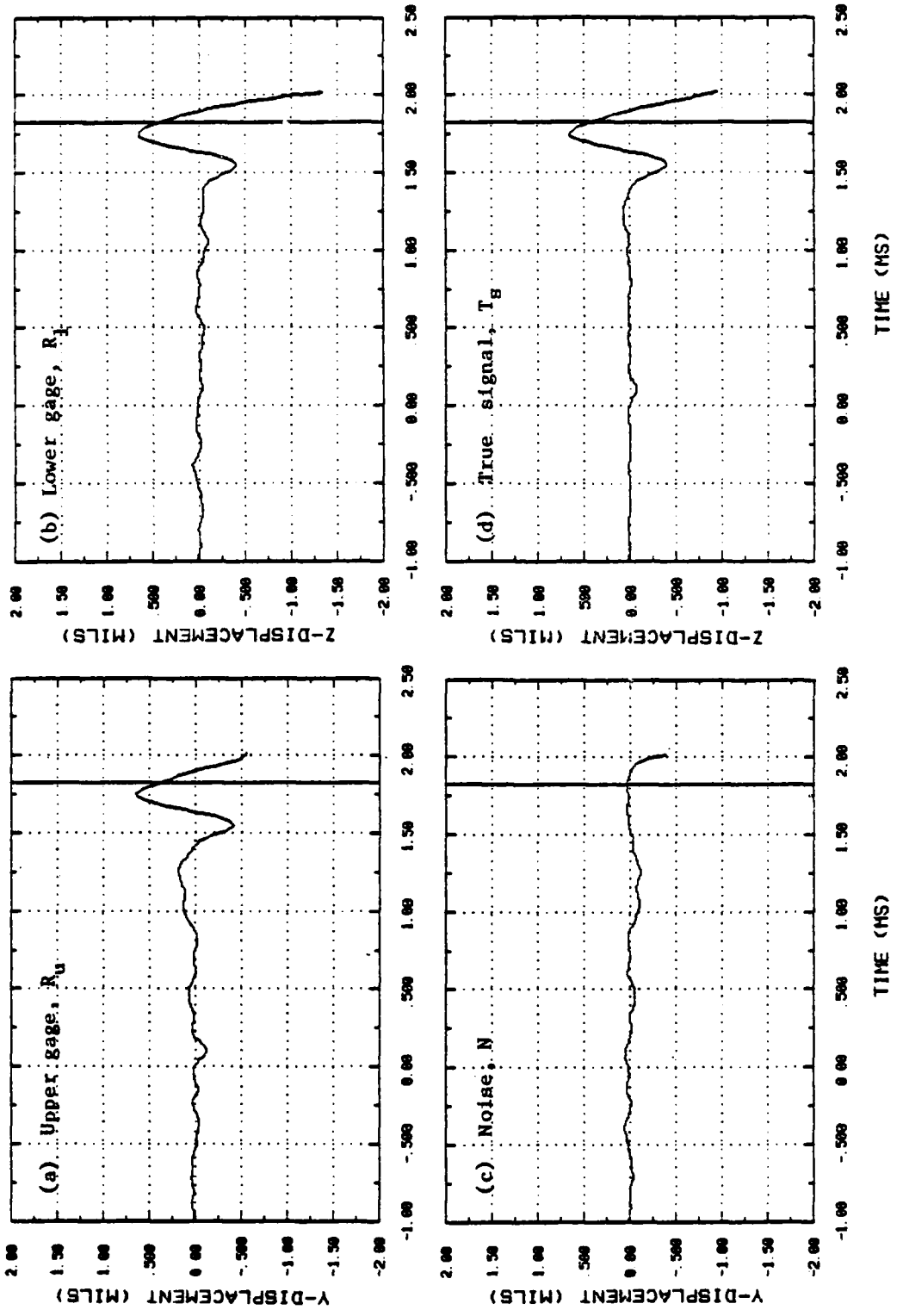

FIGURE 10. MEASURED MUZZLE DISPLACEMENTS, VERTICAL DIRECTION, TEST NO. 33

Thereafter, the noise signal generally increased rapidly in the negative displacement direction, presumably because hot gases escaping from the weapon excited (due to thermal or electromagnetic factors) the upper gage more dramatically than the lower gage. The amplitude of the noise signal prior to muzzle exit was generally on the order of 0.1 mils. This is about 25 times greater than the stated resolution of the transducer. Improvement in the noise levels obtained with the displacements transducer could probably have been achieved with additional shielding of the transducer, cables and firing lines, and by further amplification of the displacement signals prior to recording on the analog tape recorder.

C. Recoil

The recoil displacement was measured with a noncontacting probe designed at SwRI. The probe is based on a Hewlett-Packard HEDS-1000 High Resolution Optical Reflective Sensor. The transmitter portion of the circuit transmits a focused beam of red light which was reflected off the gun tube on which was placed an alternating pattern of 0.031-in.-wide black and white lines. The receiver portion of the circuit detects the reflected signal and outputs a high voltage when light is received (the sensor over a black line) and a low voltage when no light is received (the sensor over a white line). By counting the transitions between high and low signals, it was possible to plot the recoil replacement as a function of time with a resolution of ±0.016 inch. Since the sensor provided an output signal of 0 to 5 volts, no amplification was required, and the signal was recorded directly on the tape recorder.

D. Time

The time zero signal consisted of a 0 to 5 volt transition which occurred in parallel with the high voltage signal that fired the electric primers. The signal was directly recorded on one of the tape recorder channels. Projectile exit time was obtained from a breakwire which was secured over the muzzle. As the front edge of the projectile emerged from the gun tube, it severed the breakwire. The open circuit produced a sharp transition from 0 to 9 volts which was recorded directly on the tape recorder.

E. Muzzle Velocity

Projectile muzzle velocity was measured with accurately spaced paper velocity screens which can be seen in Figure 3. The screens have a reasonably dense conductive circuit printed on one side of the paper. When the projectile broke the paper, a large voltage transition occurred which was detected by a series of Hewlett-Packard 5315A counter/chronographs. Three screens were used on each test, which yielded three measurements of the projectile velocity over distances of 4 and 8 feet.

V. EXPERIMENTS

A. Test Program

Tests were conducted with three different support stiffnesses for the tube support sleeve and three different size sleeves (different internal diameters). This gave nine different support conditions. Three repeat tests were performed for each condition, giving a total of 27 tests. In these 27 tests, all other parameters were held constant as much as possible.

These tests are identified by Test Nos. 33-35 and 40-63 in Table 2. Note that the projectile mass changed slightly from test to test, and, of course, variations occurred in the chamber pressure, projectile velocities, etc. Four other tests were conducted, and they are identified by Test Nos. 64-67. For Tests 64 and 65, a heavy lubricant was used between the tube and the tube support sleeve, and for Tests 66 and 67, the breech mass eccentricity (in the vertical plane) was increased. In all tests except Nos. 64 and 65, the tube was sprayed with WD40 and wiped free of any excess prior to firing.

All tests in Table 2 were conducted with 24.65 gms of IMR 4350 propellant, bagged within a 20mm cartridge case. This propellant has a relative quickness, RQ, of 100 and produced a pressure-time history which is similar in shape to those measured for the M68 gun (2). The projectile weight varied slightly with each test, but was nominally 35.5 gms. In full scale, the corresponding propellant and projectile weights would be 7.86 lb and 11.32 lb, respectively.

Spring stiffness and sleeve tube clearance are designed by letters in Columns 3 and 4. These correspond to the following values:

Spring (Lateral Stiffness)	
S (Stiff)	6.746×10^6 lb/in.
F (Flexible)	6.746×10^5 lb/in.
VF (Very Flexible)	6.748×10^4 lb/in.

Sleeves (Diametral Clearance)	Aft	Fwd.
T (Tight)	0.0016 in.	0.0011 in.
I (Intermediate)	0.0029 in.	0.0026 in.
L (Loose)	0.0045 in.	0.0043 in.

The vertical breech eccentricity in Column 5 is the last item under test parameters. It is a calculated value which gives the position of the total breech mass (mass of the breech block, pressure-transducer assembly, and counterweight) above the tube centerline. The breech was balanced in the horizontal plane.

TABLE 2. SUMMARY OF TEST RESULTS

1	2	3	4	5	6	7	8	9	10	11	12	13	14	15	16
								Muzzle Lateral Displacements (mils)				Avg. of AMS Max. Before t_{ME} (mils)		Breech Max. Displacement t_{ME} (mils)	
								Vertical		Horizontal					
Test No.	Proj.* Weight (gm)	Springs	Sleeve	Vert. Breech. Ecc. (in.)	Time of Muzzle Exit t_{ME} (ms)	Peak Chamb. Press. (ksi)	Proj. Muzzle Veloc. (fps)	Max. before t_{ME}	At t_{ME}	Max. before t_{ME}	At t_{ME}	Vert.	Horiz.	Vert.	Horiz.
33	35.63	S	T	0.014	1.83	26.544	3380	0.640	0.403	0.258	0.049			NR	0.500
34	35.46				1.74	28.749	3479	0.553	0.407	0.149	0.112	0.627	0.244	NR	-0.490
35	35.44				1.90	27.650	3414	0.688	-0.596	0.324	0.085			0.117	NR
40	35.52	S	I		1.72	28.539	3447	0.594	0.445	-0.317	0.056			-0.737	0.417
41	35.57				1.73	29.108	3418	0.782	0.766	0.367	0.367	0.639	0.363	0.200	-0.525
42	35.55				1.84	27.546	3406	0.542	0.336	0.351 (-0.404)	0.351			0.467	0.583
43	35.15		L		1.75	29.399	3458	0.896	0.896	0.286	0.278			-0.450	-0.219
44	35.57				1.77	29.023	3463	0.815	0.742	0.277	0.269	0.810	0.277	0.592	-0.456
45	35.58				1.76	30.329	3502	0.720	0.712	0.267	0.092			-0.512	-0.429
46	35.54	VF	T		2.01	26.209	3354	1.596	-0.747	0.233	0.200			-2.115	0.433
47	35.62				2.05	22.341	3191	0.835	0.343	0.181	-0.208	1.067	0.192	-0.497	0.217
48	35.46				1.76	29.542	3460	0.626 (-0.769)	0.569	0.162	0.121			0.745	0.383
49	35.57		L		1.71	30.093	3449	0.772 (-0.594)	0.762	0.318	0.171			-0.317	-0.317
50	35.62				1.76	29.231	3472	0.366 (-0.716)	0.306	0.211 (-0.943)	0.122	0.789	1.08	1.410	0.700
51	35.52				1.80	31.353	3517	0.345 (-0.879)	-0.342	0.947 (-1.979)	-0.678			1.157	1.533
52	35.59		L		1.77	29.837	3476	0.677	0.496	0.216	0.114			0.458 (-0.383)	-0.292
53	35.49				1.78	30.653	3499	0.656	0.402	0.714 (-1.702)	0.084	0.678	0.774	0.517	0.967
54	35.53				1.65	33.473	3591	0.701	0.690	0.404	0.201			0.65 (-0.45)	-0.265
55	36.26	F	T		1.74	31.612	3507	0.676	0.572	0.271 (-0.433)	0.149			0.333	0.200
56	35.62				1.86	31.000	3460	0.807	-0.397	0.400	-0.372	0.774	0.402	-0.685	0.650
57	35.49				1.78	31.092	3507	0.838	0.332	0.372	0.169			-0.558	0.592
58	35.52		L		2.12	23.168	3253	0.303	-0.006	0.237 (-0.450)	-0.148			0.242	-0.328
59	36.18				1.99	27.185	3360	0.650	0.610	0.267	-0.073	0.633	0.324	0.483	0.433
60	35.62				1.69	32.672	3541	0.946	0.785	0.254	-0.086			0.383	-0.561
61	35.69		I		1.80	29.904	3464	0.572	0.541	0.493 (-0.919)	0.168			0.386	0.483
62	35.58				2.01	22.942	3218	0.555	0.221	0.157	-0.013	0.655	0.438	0.633	0.283
63	35.53				1.80	33.102	3537	0.838	-0.507	0.238	-0.046			-0.499	-0.284
64†	35.43				2.13	23.837	3288	0.459	0.099	0.213	-0.070	0.543	0.263	-0.608	0.333
65†	35.46				1.88	31.238	3499	0.626	-0.356	0.312	-0.101			-0.523	-0.800
66†	35.49			0.175	1.78	29.936	3450	0.733	0.228	0.295	-0.151			0.882	-0.267
67†	35.61			0.175	1.81	32.042	3535	0.720	-0.308	0.216 (-0.250)	-0.273	0.727	0.273	1.121	0.449

NOTES: * - All propellant was Type IMR4350 and HQ 100; weight was 24.65 grams.
† - Used a heavy lubricant between the tube and tube-support sleeve.
† - Removed counterbalance weight to increase breech mass eccentricity.

B. Test Results

Measured results are given in Table 2. Projectile muzzle exit time, given in the sixth column, is the time from the firing signal until the nose of the projectile severs the breakwire at the muzzle. These times are reasonably constant and relate well to the peak chamber pressure. High peak pressures generally produce lower muzzle exit times, but variations, which occurred in the shape of the p-t curve, also affected t_{ME}. The projectile muzzle velocity, measured independently of time, was calculated from velocity screens which were placed about 4 ft and 12 ft in front of the muzzle. Muzzle velocity also correlates reasonably well with the peak chamber pressure.

Vertical and horizontal displacements (in mils) at the muzzle are given next in Table 2. The maximum value before muzzle exit time (t_{ME}) can be either positive or negative, but, because most values were positive, the positive value is given first with any significant negative peak noted in parentheses. This is true for all cases except the horizontal displacement for Test 40. Here there was no significant positive displacement. The maximum values are considered a better measure of the influence of tube support conditions because muzzle displacements are changing rapidly at muzzle exit, and a small change in the exit time will significantly alter the corresponding displacement.

The absolute values of the maximum muzzle displacement from the three duplicate tests were averaged for each support condition, as shown in Columns 13 and 14. Variations of displacements within each group were sometimes large (particularly for the very flexible, VF, springs), and the average value was used as an indication of trends that might be present in the data. Finally, breech maximum displacements before projectile exit are given. Usually, these values were predominately positive or negative. In the two tests where positive and negative excursions were about equal, both values are given.

C. Comments on the Test Results

No strong trends, relating support conditions to muzzle motions, emerge from the data in Table 2. By comparing the average of the absolute maximum values before projectile exit we find:

- There is no consistent trend in the data associated with the clearances. For the stiff springs, increasing the clearances (T → I → L) increases the displacements slightly. For the flexible and very flexible springs, the reverse is true, and the greatest displacements occur with the smallest clearances. Overall there does not appear to be strong influence produced by the range of clearances used.

- If the absolute maximum values (in mils) are averaged for the three clearances, we have:

	Averaged Maximum Muzzle Displacements (mils)	
	Vertical	Horizontal
Stiff Springs, S	0.692	0.295
Flexible Springs, F	0.687	0.388
Very Flexible Spring, VF	0.845	0.682

Differences in muzzle motions for the stiff and flexible springs are slight. For the most flexible springs, an increase in displacements is noted. This is particularly evident for horizontal muzzle motions. Only with the most flexible springs did the magnitude of the horizontal motions start to equal those of the vertical motions.

- Motions of the breech tend to be opposite in direction to those at the muzzle when muzzle motions are large. This indicates that the tube is rotating in the support region. Motions of the sleeve (locations 31 and 32 of Figure 5) are smaller than those of the breech, indicating that the tube is moving within the sleeve. When muzzle motions are small, breech motions occur in the same or opposite directions. Note that the breech displacements (1-2 mils) are of about the same magnitude as the clearances at the aft end of the tight sleeve (1.6 mils).

- A heavy lubricant between the tube and the tube support sleeve has a slight attenuating effect on muzzle motion, whereas increasing the breech mass eccentricity increased both muzzle and breech displacements. These observations are made by comparing results for Tests 64 through 67 to Tests 61-63.

Additional observations on the data are made in Section VI.C. where the experimental data are compared to analytical predictions.

Typical data traces are given in Figure 11 for Test No. 33. Traces for other tests are given in Appendix A. The interference from the firing signal is very evident on many of the displacement channels just after time zero. The interference is greater on gages mounted near the breech and thus closest to the firing module. Displacements of the tube, parts (c) and (d), correspond to locations 41 and 42 in Figure 5. Significant displacements start to occur when the projectile reaches the measurement location, and these measurements reflect the tube radial expansion produced by chamber pressure plus some overall tube lateral motions. Radial displacements produced by the chamber pressure are 0.4 to 0.5 mils in this region of the tube.

The records for Test No. 33 are typical of many of the test results. However, some unusual displacement records occurred, as can be seen in Appendix A. Figure A-4 (Test 46) contains a trace of the largest muzzle motion measured in the tests. Its character is substantially different

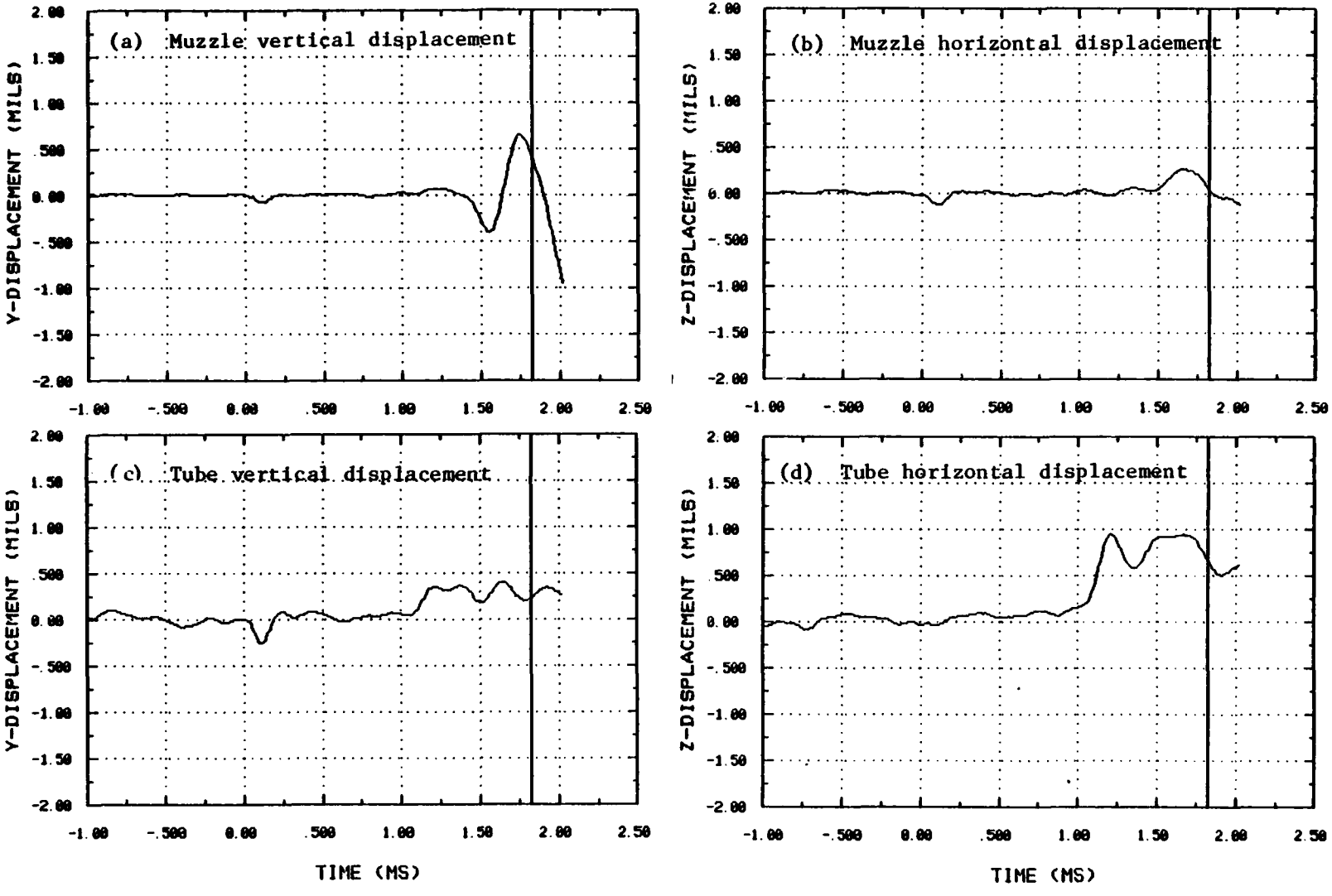

FIGURE 11. MEASURED DISPLACEMENTS AND CHAMBER PRESSURE FOR TEST NO. 33 (Cont'd.)

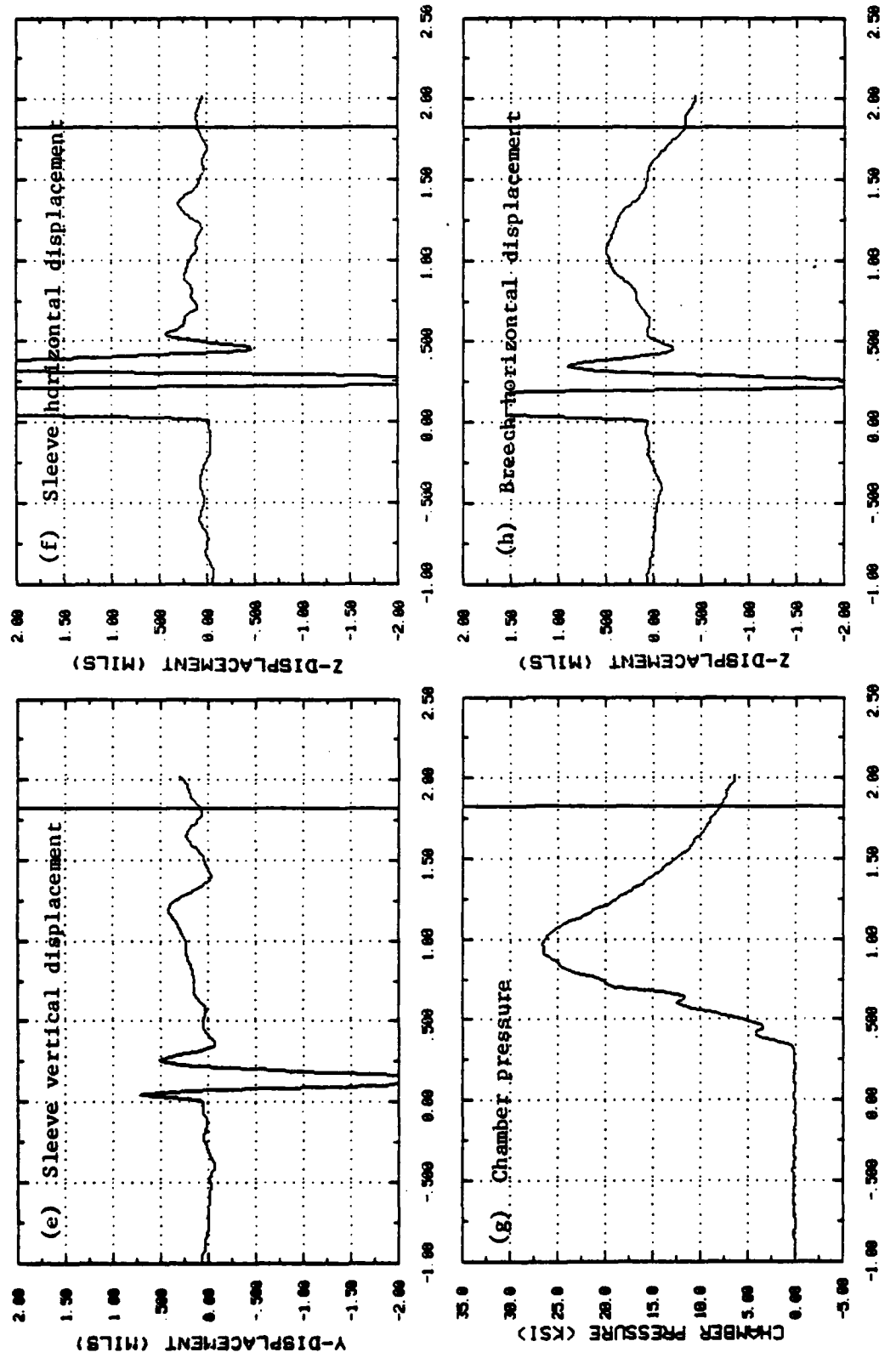

FIGURE 11. MEASURED DISPLACEMENTS AND CHAMBER PRESSURE FOR TEST NO. 33 (Concl'd.)

than those of the other traces, showing a lower frequency motion superimposed on the more typical trace as seen in Figure 11. The breech displacement for test 46 was also the largest value measured in any test; however, as noted on the data trace, the breech displacement is almost certainly a bad record and the muzzle displacement record is questionable. Figure A-8 (Test 53) shows vertical and horizontal muzzle displacements for a case in which the muzzle vertical displacements were mostly negative and where higher muzzle horizontal displacement occurred. Note that the motions are in phase and apparently coupled. These unusual tests and others were simulated analytically, and additional comments are given in the next section where analytical and experimental results are compared.

VI. ANALYTICAL MODEL

Motions of the test weapon in the horizontal and vertical planes were calculated using a two-dimensional computer program developed by Cox and Hokanson [1]. The basic program is described fully in Reference 1. Its principal features are:

- It formulates the system of equations for a plane two-dimensional framework of interconnected uniform beam elements.
- It computes the transient response of the framework to a system of in-plane time and motion dependent forces.
- The program has provisions for computing the time and motion dependent forcing functions produced by projectile tube interactions. These include axial friction and the forces produced by the moving projectile coupled with tube lateral motions (moving mass effects).
- It provides for tabular input of parameters such as breech pressure, torque on the breech computed from the torsional response of the tube, projectile axial motions, and friction functions.
- Inertia properties are lumped at the nodes and include rotary inertia.
- Beams can include the effects of shear deflections.
- Program output includes tabular summaries and computer generated plots.

The program was modified during this study to incorporate certain effects which were not treated in the study of Reference 1. These changes were made to:

1. calculate and apply to the tube the so-called "Bourdon" forces;
2. include the effects associated with high axial acceleration in the tube and tube lateral displacements;
3. treat clearances between the tube and its support;
4. treat contact forces and deformations between the tube and its support.

One other change was made to the program. The term which included projectile axial acceleration was eliminated from the expression for the projectile-tube interaction forces. In Reference 1, this change deleted the term containing A_p in Equation (B.18). The other changes are described in the following sections.

A. Bourdon Forces

The so-called Bourdon forces on a curved tube are those produced by the change in the internal surface area when the tube bends. If the tube is bent elastically, the surface area increases on the tension side and decreases on the compression side of the neutral axis. This change in area multiplied by the internal pressure gives a net lateral force.

A section from a curved tube is shown in Figure 12(a), and Figure 12(b) shows a differential element from the tube section. In the two-dimensional program, GUN2D, the tube bends in the X-Z plane and the net lateral force in the Z-direction is desired. This is the vertical component of the force F shown in Figure 12(b) and is given by

$$dF_z(x,t,R) = -p(x,t)\left(1 + \frac{a\sin\theta}{R}\right) a\sin\theta\, d\theta\, dx \qquad (1)$$

Substituting u" for 1/R (Note: $u'' = d^2u/dX^2$) and integrating θ over 2π we find

$$dF_z(x,t,u'') = -\pi a^2 p(x,t)\, u''dx \qquad (2)$$

Nodal forces on the element are obtained by solving for the virtual work of the Bourdon forces and recognizing that the virtual displacements cancel out of all equations. To evaluate the virtual work for an element, we assume a linear variation in pressure and use ξ to represent the non-dimensional position within the element. This gives

$$p(\xi,t) = p_1(t)(1-\xi) + p_2(t)\,\xi \qquad (3)$$

where p_1 and p_2 are the time dependent pressures at the ends of the element. The position within the element of length ℓ is

$$x = x_1 + \xi\ell \qquad (4)$$

and

$$dx = \ell\, d\xi \qquad (5)$$

The curvature, u", is written in terms of the interpolation functions defined in Reference 1 as

$$u'' = \frac{1}{\ell^2}\,[H^u_{\xi\xi}]\,\{u_n\} \qquad (6)$$

where $\{u_n\}$ is the vector of nodal displacements and $[H^u]$ is the second derivative with respect to ξ of the interpolation function for u. Substituting equations (3), (5) and (6) into Equation (2) gives the differential force as

$$dF_z(x,t,u_n) = -\pi a^2\left[p_1(t)(1-\xi) + p_2(t)\,\xi\right]\frac{1}{\ell^2}\,[H^u_{\xi\xi}]\,\{u_n\}\,\ell\, d\xi \qquad (7)$$

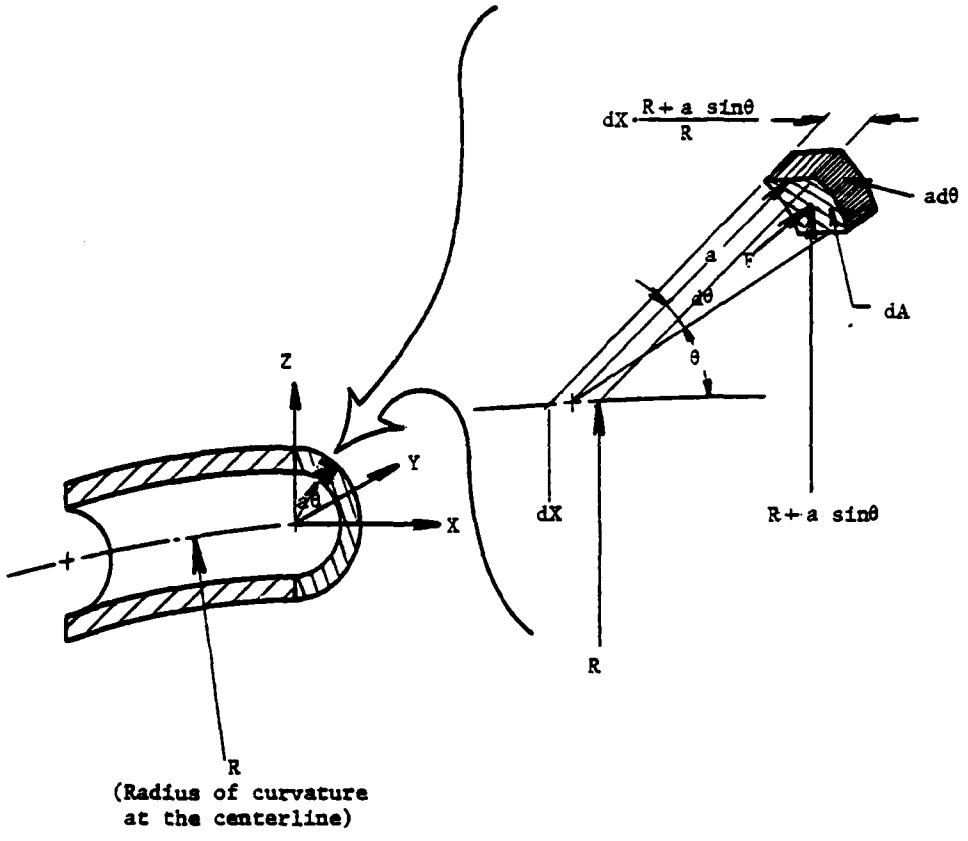

(a) Section of a Curved Tube

(b) Differential Element from the Tube Section

FIGURE 12. SECTION FROM A CURVED TUBE

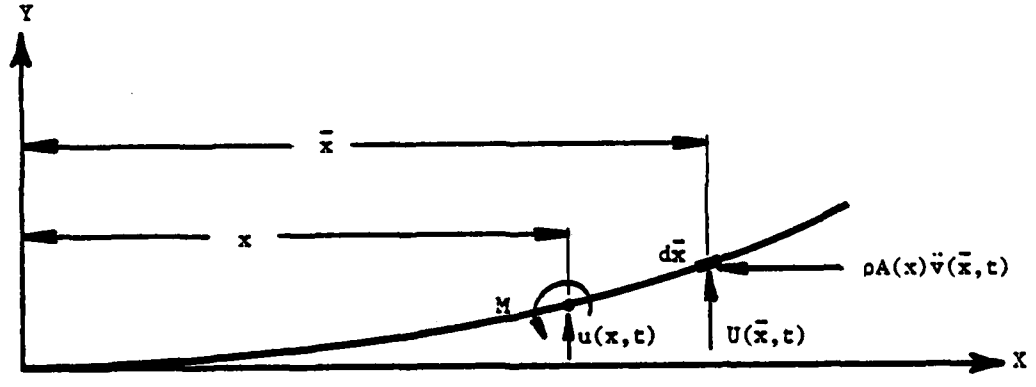

FIGURE 13. CURVED TUBE WITH AXIAL ACCELERATIONS

The virtual work of the Bourdon forces is given by

$$d(\delta W_B) = \delta u \, dF_z(x,t,u_n) \tag{8}$$

Noting that $u = [H^u]\, u = \{u_n\}^T [H^u]^T$, the virtual work is

$$\delta W_B = \{\delta u_n\}^T \left(\int_0^{\bar{\xi}} [H^u]^T (-\pi a^2) \, [\, p_1(t)\,(1-\xi) + p_2(t)\,\xi\,] \, \frac{1}{\ell} \, [H^u_{\xi\xi}] \, d\xi \right) \{u_n\} \tag{9}$$

Virtual displacements will cancel from the system of assembled equations and so the Bourdon forces at the nodes are given by

$$\{F_B\} = -\frac{\pi a^2}{\ell} \left(\int_0^{\bar{\xi}} [H^u]^T \, [\, p_1(t)\,(1-\xi) + p_2(t)\,\xi\,] \, [H^u_{\xi\xi}] \, d\xi \right) \{u_n\} \tag{10}$$

In the computer program, GUN2D, Equation (10) was evaluated using interpolation functions with shear effects given as Equation (A.51) in Reference 1. When the projectile is past the element, the integration limits are from 0 to 1 ($\bar{\xi} = 1$). When the projectile lies within the element, the integration is from 0 to the position of the base of the projectile within the element. The pressure is calculated at the base of the projectile as shown in Appendix C and is evaluated at the ends of the element by assuming linear decay from the breech face to the projectile.

B. Effect of Axial Accelerations

High axial accelerations produce forces which act to straighten a curved tube. These forces are illustrated in Figure 13. For a positive acceleration in the X-direction, v(x,t), the moment produced at any position x is positive and given by

$$M(x,) = \int_x^{\ell} \rho \, A(x) \, \ddot{v}(\bar{x},t) \, [\, u(\bar{x},t) - u(x,t) \,] \, d\bar{x} \tag{11}$$

where $\rho A(x)$ is the mass per unit length of the tube. Differentiation of M(x,t) gives the distributed lateral load. Applying Leibnitz's rule, and denoting differentiation with respect to x as prime quantities, we have

$$w(x,t,u',u'') = u'(x,t)\, \rho\, A(x)\, \ddot{v}(x,t) - u''(x,t) \int_x^{\ell} \rho\, A(\bar{x})\, \ddot{v}(x,t)\, d\bar{x} \tag{12}$$

Note that the integral is the axial force in the tube at x and can be written as

$$F_{AE} = \int_{x}^{\ell} \rho A(\bar{x}) \ddot{v}(\bar{x},t)\, d\bar{x} \tag{13}$$

To solve for the element nodal forces, evaluate the virtual work of $w(x,t,u', u")$ for the element. This is given by

$$\begin{aligned} \delta W_A &= \int_0^{\ell} \delta u\, w(x,t,u',u'')\, dx \\ &= \int_0^{\ell} \delta u \left[u'(x,t) \rho A(x) \ddot{v}(x,t) - u''(x,t) F_{AE}(x,t) \right] dx \end{aligned} \tag{14}$$

For a lumped parameter model as used in GUN2D, $F_A(x,t)$ is constant within the element. Thus

$$\delta W_A = \int_0^{\ell} \delta u \rho A(x)\, u'(x,t)\, \ddot{v}(x,t)\, dx - F_{AE} \int_0^{\ell} \delta u\, u''(x,t)\, dx \tag{15}$$

In terms of the nodal values and interpolation functions for the element we have

$$\delta u = \{\delta u_n\}^T [H^u]^T \tag{16}$$

$$u(x,t) = [H^u] \{u_n(t)\} \tag{17}$$

$$u'(x,t) = [H^u_\xi] \{u_n(t)\} \tag{18}$$

$$u''(x,t) = [H^u_{\xi\xi}] \{u_n(t)\} \tag{19}$$

$$\ddot{v}(x,t) = [H^v] \{\ddot{u}_n(t)\} \tag{20}$$

Substituting Equations (16) - (20) into Equation (15), the virtual work equation becomes

$$\begin{aligned} \delta W_A &= \{\delta u_n\}^T \int_0^1 \rho\, A(\xi) [H^u]^T [H^u_\xi] \{u_n\} [H^v] \{\ddot{u}_n\}\, d\xi \\ &- \{\delta u_n\}^T \frac{F_{AE}}{\ell} \int_0^1 [H^u]^T [H^u_{\xi\xi}]\, d\xi \{u_n\} \end{aligned} \tag{21}$$

Recognizing that the axial acceleration along the element is

$$[H^v] \{\ddot{u}_n\} = (1-\xi) \ddot{u}_1 + \xi \ddot{u}_4 \tag{22}$$

and that $\{u_n\}^T$ cancels from the system of equations, the nodal forces produced by the accelerations in a curved tube can be written

$$\{F_A\} = \left(\int_0^1 \rho A(\xi) [H^u]^T [H^u_\xi] (1 - \xi) \, d\xi \, \{u_n\} \ddot{u}_1 \right)$$

$$+ \left(\int_0^1 \rho A(\xi) [H^u]^T [H^u_\xi] \, d\xi \, \{u_n\} \ddot{u}_4 - \frac{F_{AE}}{\ell} \int_0^1 [H^u]^T [H^u_{\xi\xi}] \, d\xi \right) \{u_n\} \tag{23}$$

For a lumped mass formulation as used in GUN2D, $A(\xi)$ is zero except at the end points. Thus, the first two terms are evaluated only at the ends of the element. The forces F_A were evaluated in GUN2D using the element interpolation functions with shear effects as given by Equation (A.51) in Reference 1. Axial forces in the elements, F_{AE}, were calculated from the element axial deformations so that any axial frequencies in the tube also influenced the forces F_A. The basic equations derived here for both the Bourdon forces and the axial acceleration effects appear to agree with those presented by Simkins [4].

C. Tube Support Conditions

Conditions at the tube support were described by concentric cylinders of different diameters which were constrained to move in one plane. This is shown schematically, with an exaggerated clearance between the cylinders, in Figure 14. When in contact, the forces per unit length between the tube and the tube support sleeve were described by Hertzian contact forces for infinitely long parallel cylinders. When not in contact, small viscous forces were applied.

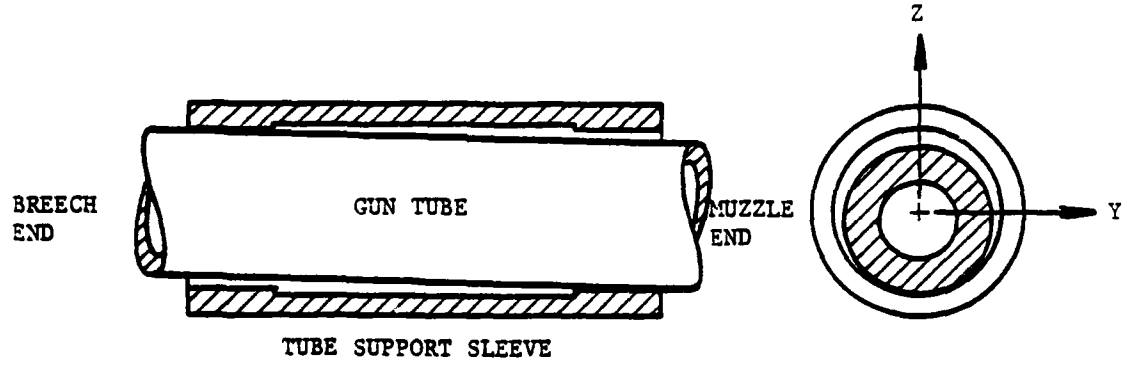

FIGURE 14. SCHEMATIC OF TUBE SUPPORT

4. Simkins, T. E., "Transverse Response of Gun Tubes to Curvature Induced Loads," Report No. ARLCB-SP-78013, Proceedings of the 2nd U.S. Army Symposium on Gun Dynamics, held at The Institute on Man and Science, Rensselaerville, NY, 19-22 September 1978.

The tube support sleeve was undercut in the center giving a well-defined bearing surface at each end. The resultant contact force on each surface was applied to the tube at a point one-third the length of the bearing surface from the sleeve ends. As the tube recoiled, this point of application of the support reaction changed (with respect to the tube).

Positive and negative clearances were defined at each end of the tube support sleeve. For the position of the tube in Figure 14, the positive clearance would be zero at the breech end, and the negative clearance would be zero at the muzzle end. Clearances were defined as a function of the internal pressure in the tube at the point of support to account for the tube radial expansion. The pressure was assumed to be zero ahead of the projectile, and pressures behind the projectile were calculated as described in Appendix C. Tube radial expansion was calculated for static conditions using the standard formula for thick-walled tubes.

Hertzian contact forces were calculated using Equations (24) through (27) given by Roark [5].

$$\Delta = \frac{P C_E}{\pi L}\left(\frac{2}{3} + \ell n \frac{2D_1}{b} + \ell n \frac{2D_2}{b}\right) \tag{24}$$

$$b = 1.60\sqrt{\frac{P K_D C_E}{L}} \tag{25}$$

$$K_D = \frac{D_1 D_2}{D_1 - D_2} \tag{26}$$

$$C_E = \frac{1 - \nu_1^2}{E_1} + \frac{1 - \nu_2^2}{E_2} \tag{27}$$

where

P = contact force between the two cylinders
Δ = radial change between centers of the cylinders
L = contact length
D_1 = outside diameter of the tube
D_2 = inside diameter of the sleeve

Note that a bearing length, L, is introduced to calculate the total contact force even though Equation (24) was derived to give the force per unit length for cylinders of infinite length.

For use in the calculations, Equation (24) was recast in a form to give the contact force as a function of contact deformation.

$$P = f(\Delta)$$

5. Roark, R. J., and Young, W. C., Formulas for Stress and Strain, 5th Edition, McGraw-Hill Book Co., New York, NY, 1975.

This was done by plotting the force-deformation relationships for the front and rear of each sleeve and curve fitting the results. Graphs of the contact forces are shown in Figure 15. In the computer program, the P-Δ relationship was approximated as log-linear out to 1000 lb. The highest calculated contact force was about 7000 lb, but most were less than 1000 lb. Above 1000 lb, the curve fit gives a progressively stiffer model than Equation (24).

In the program, equal and opposite contact and viscous forces were applied to the tube and to the tube support sleeve. Bending and shear deformations in the tube and sleeve were treated in the finite element model, but local deformations of the sleeve cross-section were ignored.

D. Finite Element Model

The finite element model of the test weapon is shown schematically in Figure 16. Part (a) shows the grid for the tube and part (b) shows the grid for the sleeve, ring and support beams. The models were constructed of rigidly connected beam elements with masses (including rotary inertia) lumped at the nodes. When assembled, nodes 15, 16 and 17 on the sleeve were initially coincident with, but not connected to, nodes 13, 12 and 11, respectively, on the tube. These nodes moved relative to each other as the tube recoiled. Forces were applied to the tube as described in Section VI.A.3. at nodes 15 and 17. These were the support reaction forces and were a function of the relative lateral position and velocity of the tube and the tube-support sleeve.

The model was attached to ground at the ends of the support beams. Flexibility of the mount (see Figure 1) was ignored. Three different beams and three different sleeves were used in the tests. These changes were accomplished in the model by changing the axial and bending stiffness of members 14, 15, 16, 19 and 20; clearances in the tube support model; and the contact stiffness between the tube and sleeve. Initial tube curvature was represented in the model by offsetting the nodes along the tube from the X-axis.

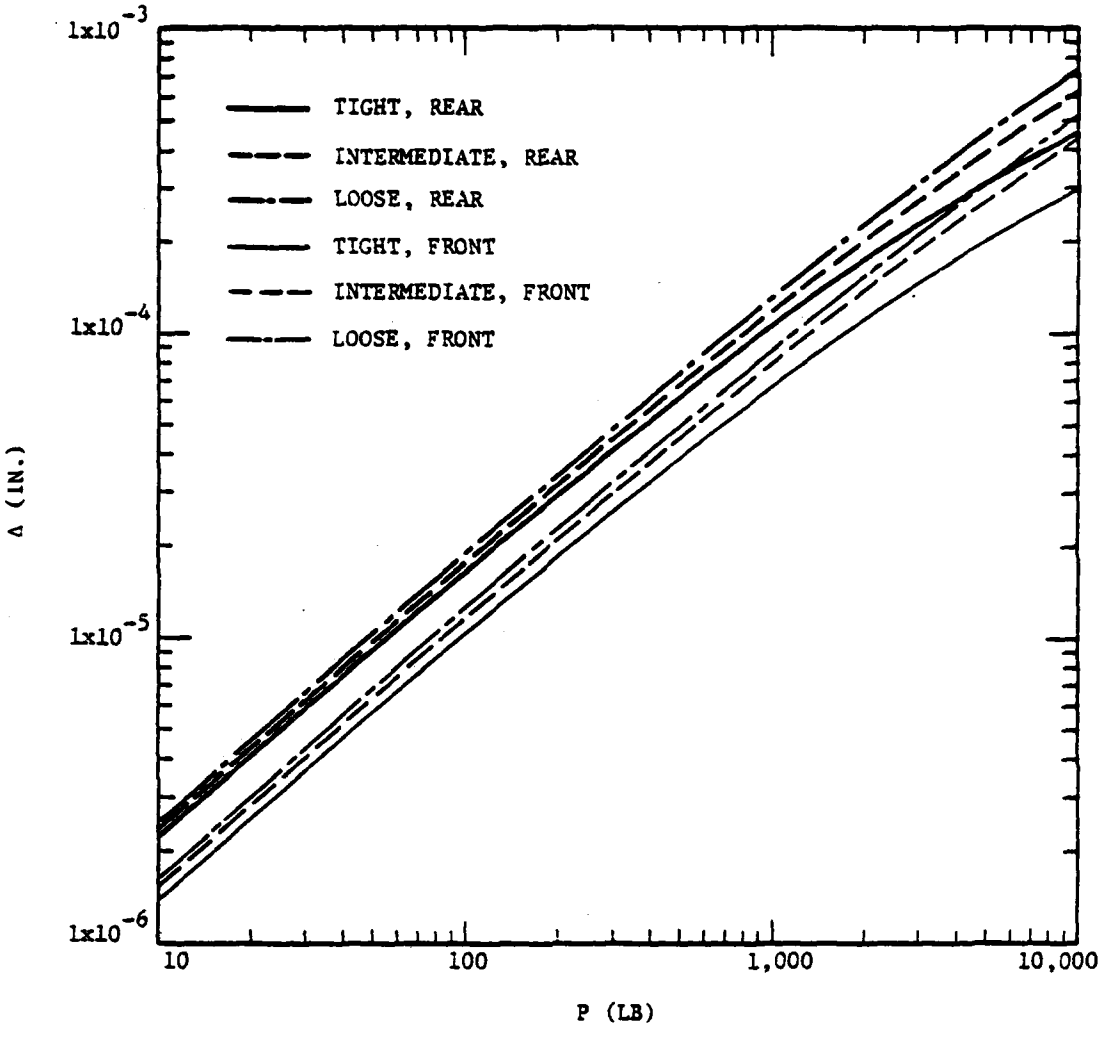

FIGURE 15. CONTACT FORCES BETWEEN THE TUBE AND SLEEVE

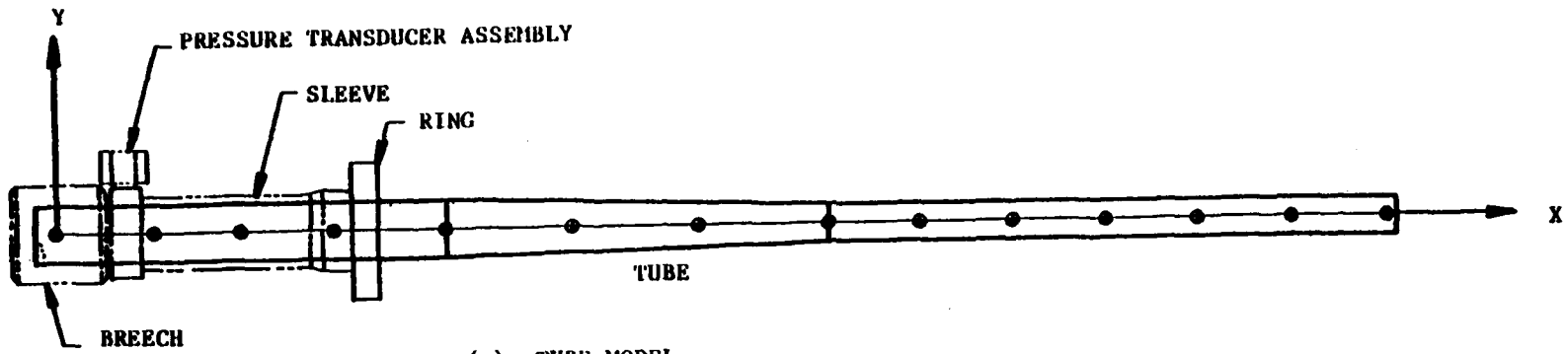

(a) TUBE MODEL

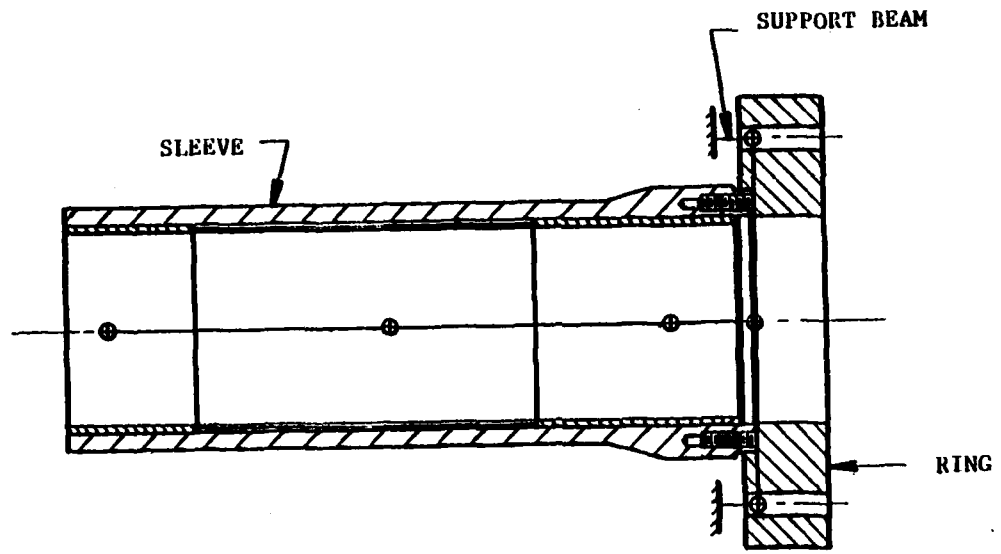

(b) MODEL OF SLEEVE, RING AND SUPPORT BEAMS

FIGURE 16. FINITE ELEMENT MODEL OF THE TEST WEAPON

VII. PARAMETER STUDIES

This section contains the results of a study to evaluate the influence on tube motions produced by several important parameters. The studies were based upon the first test listed in Table 2, Test 33. In this way the analytical model was tuned to the experimental results for this one test, and the parameters which have a major influence on tube motions were identified. The parameters investigated in this study were:

(1) initial tube curvature
(2) axial accelerations coupled with tube lateral displacements
(3) tube initial position
(4) tube radial expansion
(5) "Bourdon" forces

For the configuration of Test 33 the springs were stiff, the sleeve was tight, and the projectile mass was 35.63 gms. Measured chamber pressure (given in Appendix B) was used as the forcing function.

A. Initial Tube Curvature

The tube was initially curved in both the horizontal and vertical planes. Measured curvature is shown in Figure 17. The vertical scale is exaggerated by a factor of 500 relative to the horizontal scale. If plotted to the horizontal scale, the curvature would be very hard to distinguish. Note that some curvature is present in the sleeve region. This affects the initial position of the tube in the sleeve. It should also be noted that the curvature was determined by external measurements and that the bore of the tube may not be concentric with the exterior. The bore axis was not measured.

Calculations in the vertical plane were made for a straight tube and for one with the initial curvature of Figure 17. Other conditions for these calculations, identified by Run Nos. 33.03 and 33.05, are given in Table 3. Clearances are specified for the tube resting on the front support and against the top of the rear support. Thus, all of the clearance between the tube and the sleeve is negative (CN = 0.0016) at the rear support and positive (CP = 0.0011) at the front support. Tube radial expansion is treated in the calculations. The Bourdon forces and the effects produced by axial accelerations, coupled with the tube lateral displacements, are ignored.

Calculated vertical motions are given in Figure 18. Part (a) gives results for the straight tube and part (b) for the curved tube. The influence of tube curvature is to lift the muzzle and the breech. Comparing calculated results to the measurements for this test given in Figure 11, it is clear that the results for the straight tube are in better agreement with the measured data (particularly for the muzzle displacements) than are the results for the curved tube. This is surprising, since the tube is known to be curved. (When comparing analytical and experimental results, note that the time scale for the experimental data is compressed relative to the scale for the analytical results.)

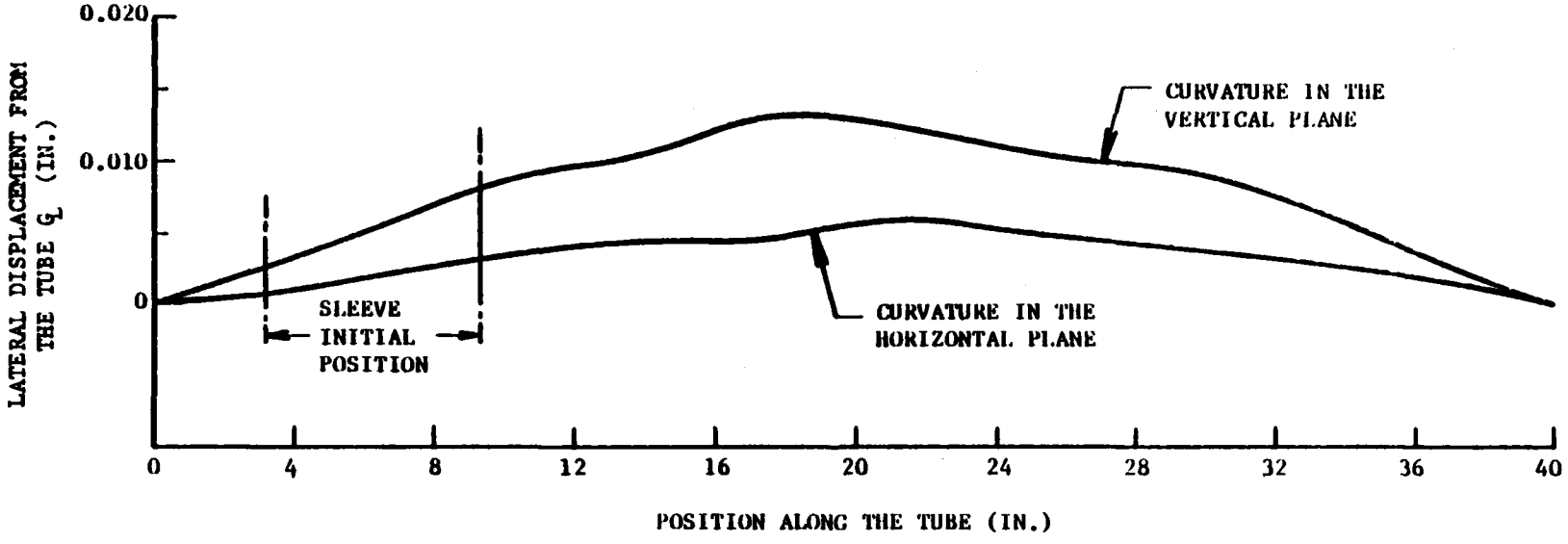

FIGURE 17. INITIAL TUBE CURVATURE

TABLE 3. SUMMARY OF PARAMETER VARIATIONS, TEST NO. 33, VERTICAL PLANE

Run No.	Springs	Sleeve	Proj. Mass	Chamb. Press.	Tube Initial Curvature	Tube Radial Expansion	Support Clearances (in.)				Bourdon Forces	Axial Acc. Effects
							Rear		Front			
							CP	CN	CP	CN		
33.01	Stiff	Tight	Test #33	Test #33	Yes	Yes	0.0004	0.0012	0.0009	0.0002	No	No
33.02	Stiff	Tight	Test #33	Test #33	Yes	Yes	0.0004	0.0012	0.0009	0.0002	No	Yes
33.03	Stiff	Tight	Test #33	Test #33	No	Yes	0.0	0.0016	0.0011	0.0	No	No
33.05	Stiff	Tight	Test #33	Test #33	Yes	Yes	0.0	0.0016	0.0011	0.0	No	No
33.07	Stiff	Tight	Test #33	Test #33	No	Yes	0.0004	0.0012	0.0011	0.0	No	No
33.08	Stiff	Tight	Test #33	Test #33	Yes	No	0.0	0.0016	0.0011	0.0	No	No
33.09	Stiff	Tight	Test #33	Test #33	Yes	Yes	0.0004	0.0012	0.0009	0.0002	Yes	No
33.11	Stiff	Tight	Test #33	Test #33	No	Yes	0.0008	0.0008	0.0005	0.0006	No	No
33.12	Stiff	Tight	Test #33	Test #33	No	Yes	0.0010	0.0004	0.0006	0.0002	No	No
33.13	Stiff	Tight	Test #33	Test #33	No	Yes	0.0004	0.0012	0.0008	0.0	No	No

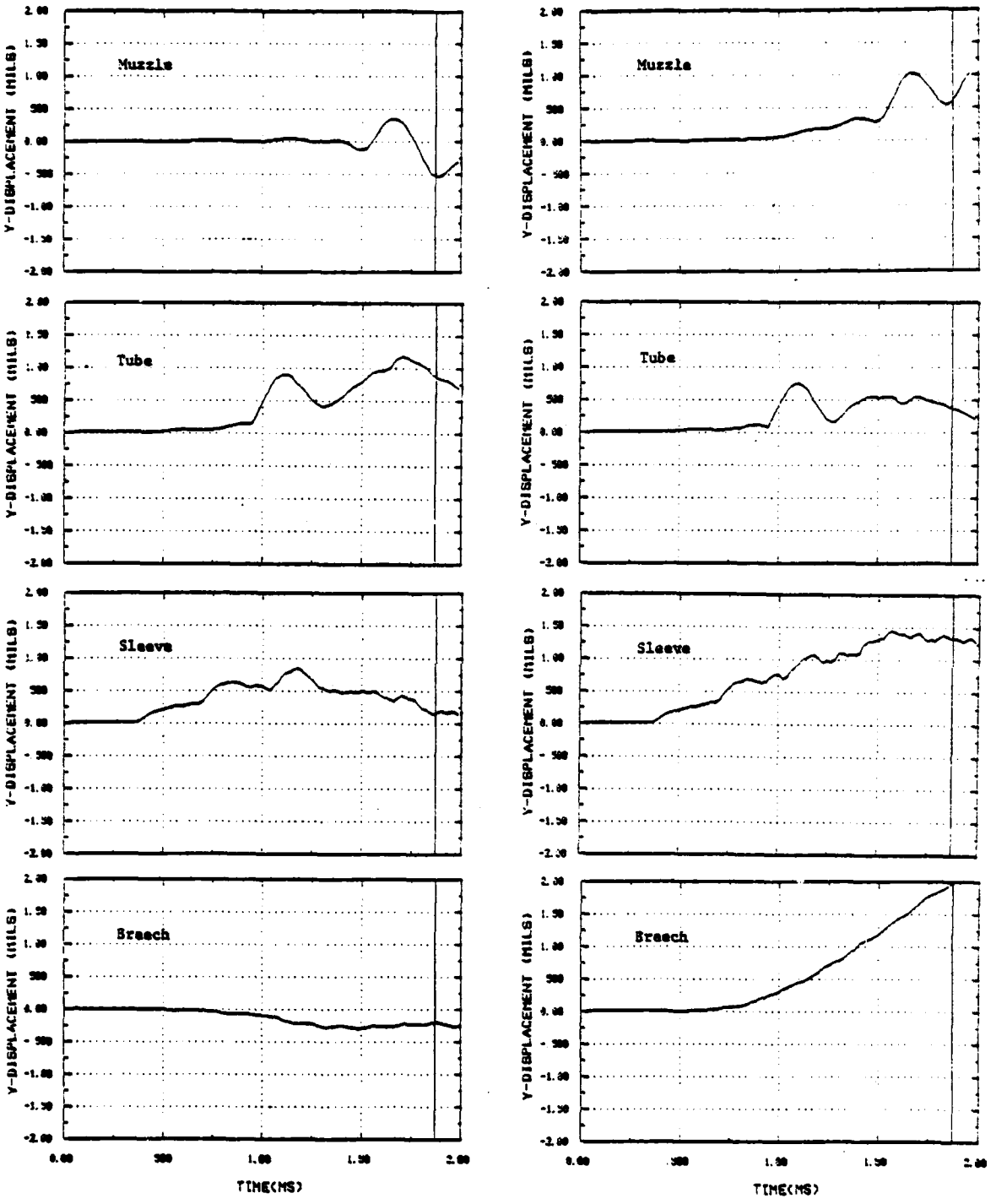

(a) Straight Tube (Run 33.03)

(b) Curved Tube (Run 33.05)

FIGURE 18. CALCULATED VERTICAL TUBE MOTIONS FOR STRAIGHT AND CURVED TUBES: STIFF SPRINGS, TIGHT SLEEVE, AND STANDARD POSITION

Profiles of the displacements along the tube are given for these calculations in Figure 19. Beginning at 1.25 ms, the curved tube starts to arch downward opposite the initial curvature. This is expected. The graphs give only displacements calculated from the tube initial position, not the actual curvature. Even at 1.75 ms, the tube curvature is still negative. Actual changes to the initial curvature are small at this time.

Tube initial curvature was accounted for by offsetting the tube initial coordinates from the X-axis in the model shown in Figure 16. Unless the geometry is continuously updated or unless the effect of the tube displacements on the forces produced by the tube axial accelerations are treated, the influence of the tube initial curvature is exaggerated. Thus, forces associated with tube lateral displacements and axial accelerations were calculated and applied to the tube.

B. Axial Acceleration Effects

As explained in Section VI.B., tube lateral displacements, coupled with tube axial accelerations, produce forces which act to straighten the tube (or to return it to some initial zero force position). As formulated in the program GUN2D, the forces act to return the tube to a zero reference position which is the initial tube position, whether straight or curved. Thus, for the initially curved tube, these forces will act to return the tube to the initially curved position. If the tube should become straight and aligned with the X-axis during the calculations, these forces should exactly balance the forces on the tube produced by its initial curvature.

These calculations are identified as Run Nos. 33.01 and 33.02 in Table 3. Note that initial tube curvature is included and that slightly different clearances have been used. The tube is still muzzle down, but small clearances have been inserted between the tube and the bottom of the front support, and between the tube and the top of the rear support. Opposing clearances were reduced accordingly.

Results of these calculations showed no appreciable change in the tube motions with and without the forces associated with tube lateral displacements and axial accelerations. Values of the muzzle lateral displacement, velocity, and acceleration are given below for comparison.

Run	Displacement (mils)		Velocity (in/sec)		Acceleration (in/sec^2)	
No.	Max.	@ Exit	Max.	@ Exit	Max.	@ Exit
33.01	1.9708	1.2201	8.6947	3.5830	120,780	85,789
33.02	1.9468	1.2111	8.6393	3.5330	118,950	84,653

The differences between the two cases are quite small. Thus, the forces produced by the coupling of the axial acceleration with the lateral tube

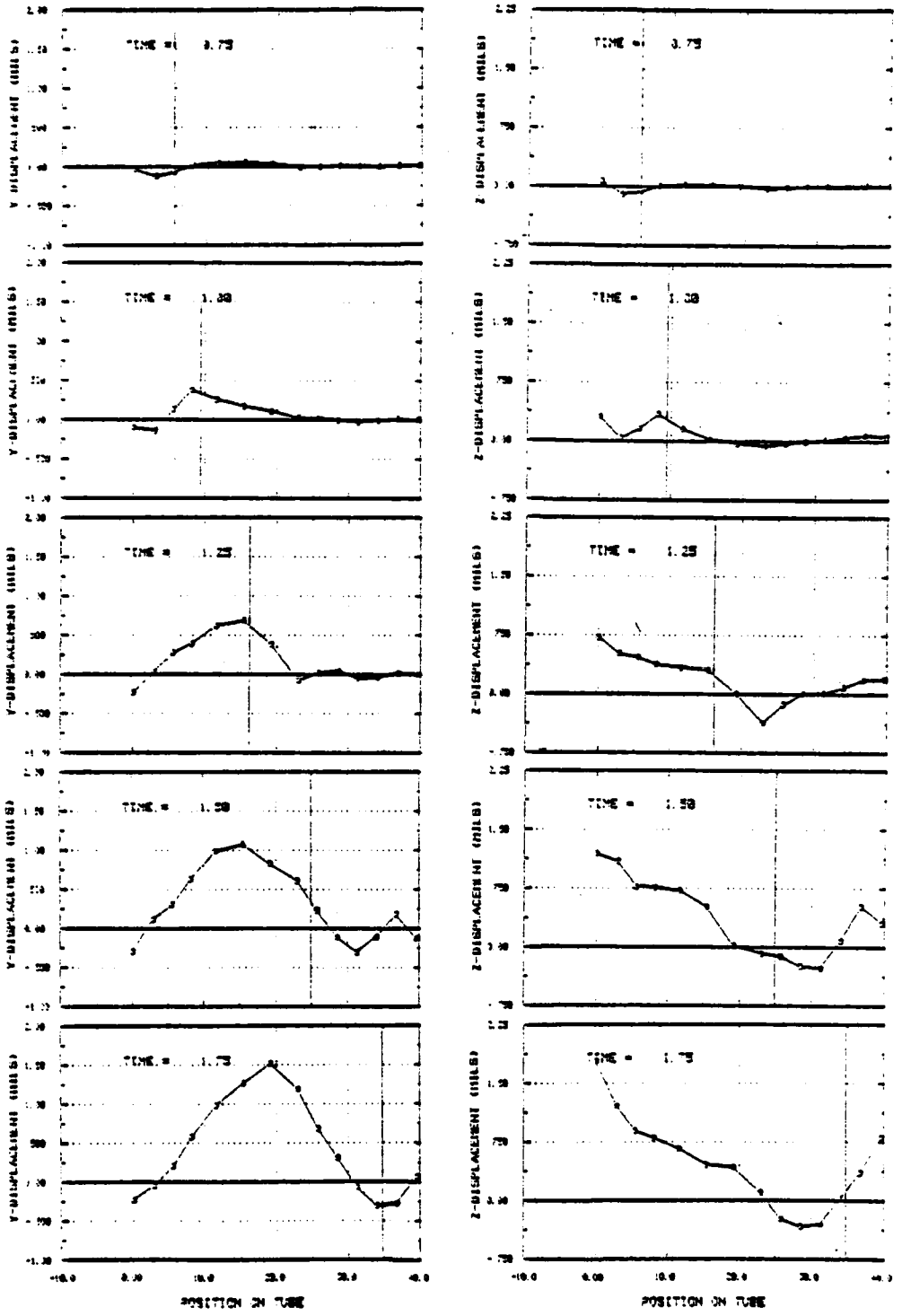

(a) Straight Tube (b) Curved Tube

FIGURE 19. SEQUENTIAL BARREL PROFILES FOR TEST NO. 33: STIFF SPRINGS, TIGHT SLEEVE, AND STANDARD POSITION

displacement are either small in magnitude or act in inconsistent directions.

To study the nature of the forces, profiles along the tube were plotted at five times. The graph was obtained by subtracting the nodal lateral forces for Run 33.01 from Run 33.02 to eliminate the lateral loads associated with projectile-tube interactions and support reactions. The values are plotted in Figure 20. Because even small changes in the support reactions would mask the axial acceleration effects, the forces were omitted in this region (0 to 15 in.) of the tube. Notice that the forces do oscillate between positive and negative values. This indicates that the axial accelerations are varying, because of axial vibrations in the tube, or that the curvature, relative to the initial position, is oscillating between negative and positive values. The magnitudes of these forces are also quite small.

In the remainder of this study, these forces were omitted from the calculations because of their negligible effect (as formulated) on the tube motions. Further investigation of the effects produced by axial accelerations is warranted, particularly in view of the fact that the calculated results for a straight tube give a better approximation to measured tube motions than do the results for a curved tube.

C. Tube Initial Position

The tube initial position refers to the position of the tube relative to the support points. For the tight sleeve, the total diametral clearance at the rear support is 0.0016 in., and at the front support it is 0.0011 inch. The diametral expansion of the tube under the maximum chamber pressure is approximately 0.0008 in., so that the free travel at maximum pressure is only 0.0008 in. at the aft support and 0.0003 in. at the front support.

Because the tube must be supported by the sleeve and is "muzzle heavy," the tube should always be in contact with the front support (CN = 0.0). The breech end of the tube may or may not be in contact unless the tube is forced into contact before firing. Since this was not done in the experiments, the initial position may vary.

Three calculations were made for comparison with the results of Run 33.03. In Run 33.07 the front support is in contact (CN = 0.0), and the aft support has a positive clearance (CP = 0.0004 in.) between the top of the tube and the breech. In Run 33.11 the tube is approximately centered between the supports, and for Run 33.12 the clearances are reduced at both the front and aft supports and the tube is almost straight in the sleeves. Table 3 gives the clearances which were specified in the model.

Results for Run 33.07 are given in Figure 21. Although results are given for both the vertical and horizontal motions, here we are comparing the vertical motions only. Comparing the results of Run 30.07 with those of Run 30.03 in Figure 18, it is seen that the positive displacement of the muzzle is slightly larger for Run 30.07, but that the negative displacement is reduced. Also, the positive clearance at the rear support allowed the breech to move up rather than be forced down as in Run 33.03.

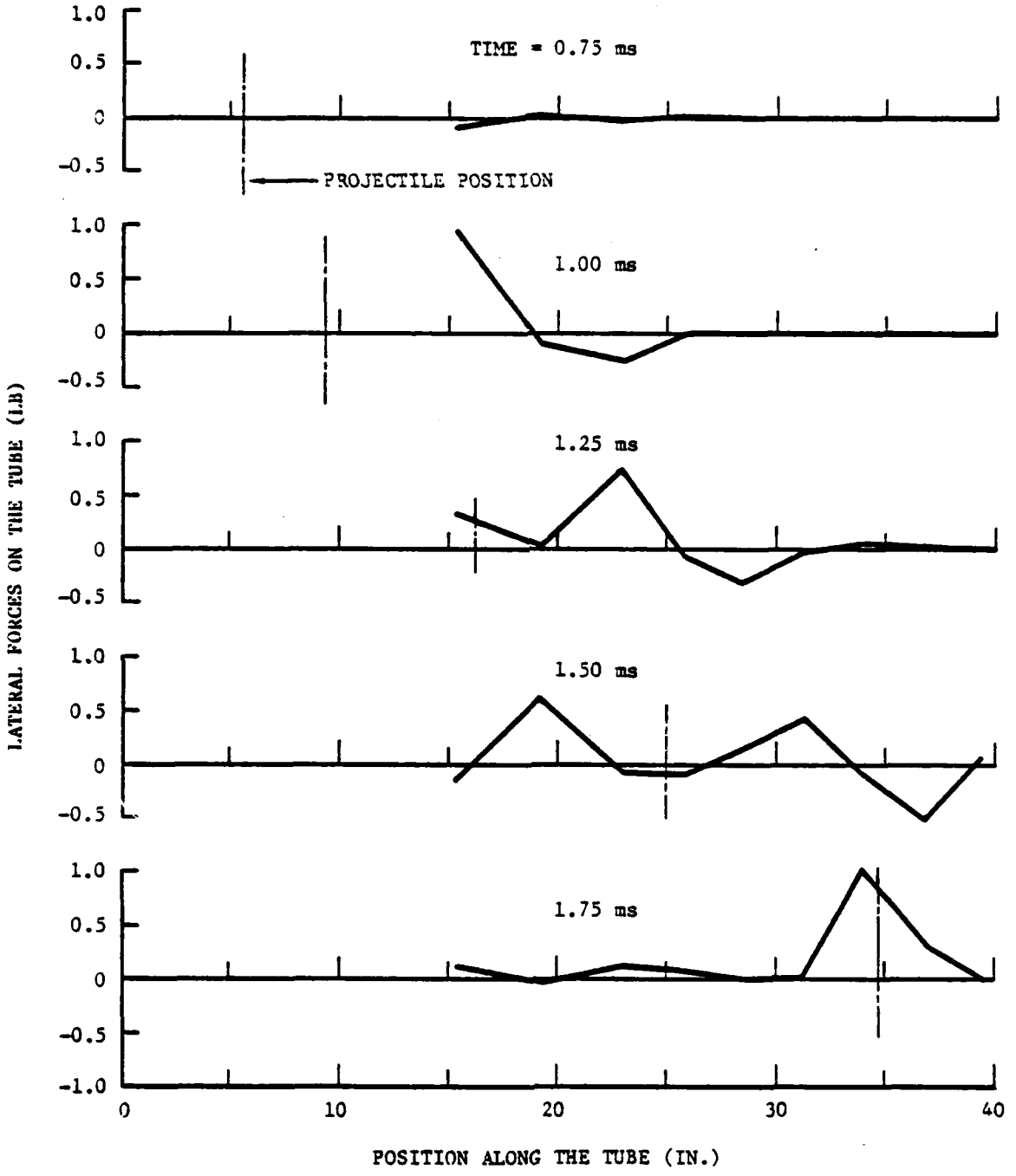

FIGURE 20. PROFILES OF THE FORCES PRODUCED BY AXIAL ACCELERATIONS AND TUBE LATERAL DISPLACEMENTS, RUN 33.02

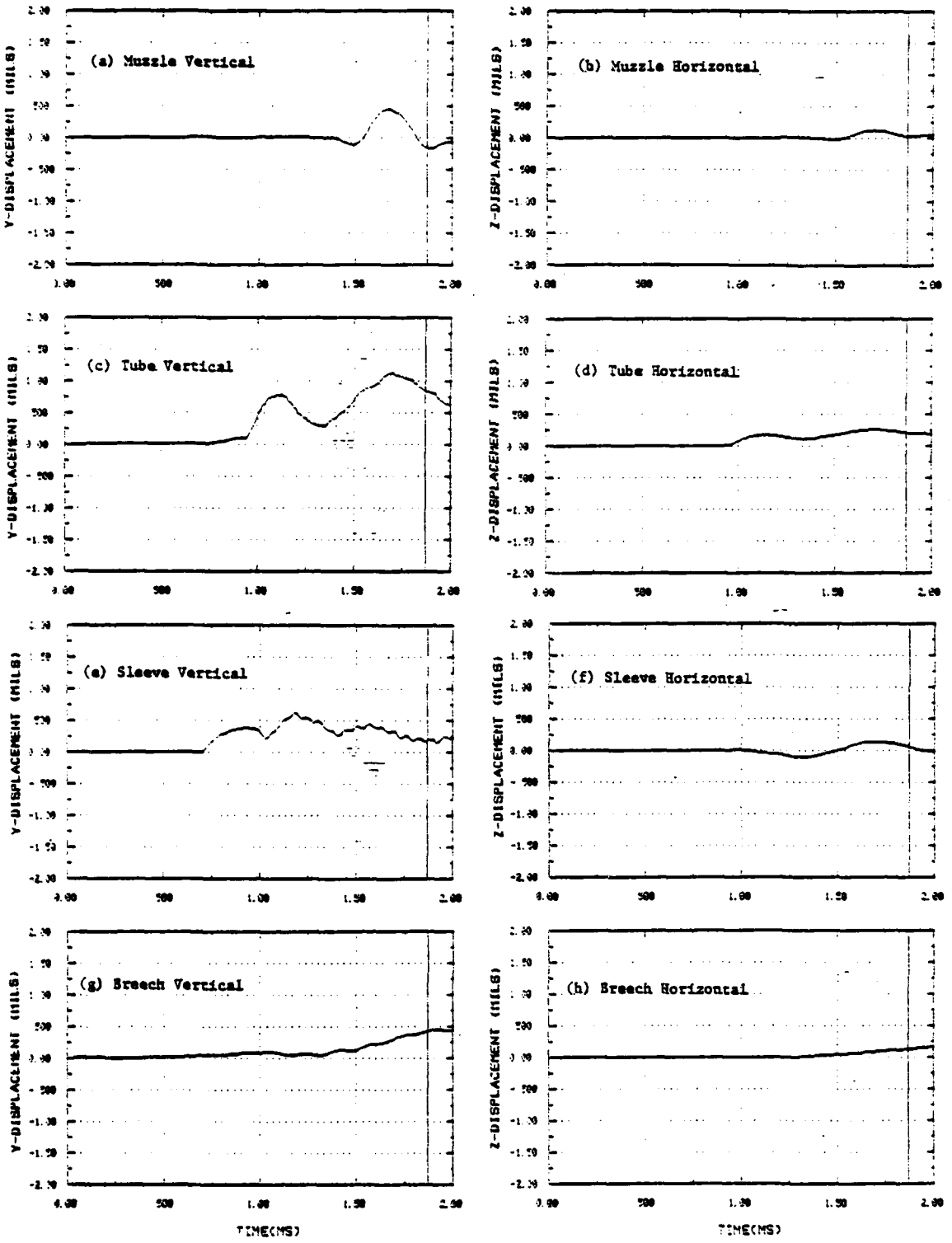

FIGURE 21. CALCULATED TUBE MOTIONS FOR TEST NO. 33: STIFF SPRINGS, TIGHT SLEEVE, AND STRAIGHT TUBE

Tube displacements for Runs 33.11 and 33.12 are given in Figure 22. Muzzle amplitudes and signatures are much different than those for Runs 33.03 and 33.07. Further, comparing to the experimental data for Test No. 33 (Figure 11), it is clear that the muzzle displacements for Runs 33.11 and 33.12 do not match the measured values. Runs 33.03 and 33.07 provide much better experimental-analytical correlation.

The strong interaction of the tube and the mount at the front support, missing in Run 33.11 because of the clearances, appears to be a very important contributor to the muzzle signature obtained. This interaction is caused by the initial position of the tube in the sleeve and by the tube radial expansion.

D. Tube Radial Expansion

The tube radial expansion is a function of the internal pressure and the position of the projectile. Tube expansion is assumed to be zero ahead of the projectile and to reach the static value behind it. This imparts a sharp impulse to the tube as the projectile passes the front support. A more gradually increasing force is applied to the tube at the rear support, which is always exposed to the chamber pressure.

Calculations of tube response without radial expansion, Run 33.08, were made for comparison with Run 33.05. Results are given in Figure 23. Without radial expansion, a completely different signature is obtained [compare to Figures 18(b) and 19(b)]. The sudden reversal in direction of the muzzle near projectile exit is missing, and higher frequency modes are missing from the tube profiles given in Figure 23(b). Thus, radial expansion appears to make a very important contribution to the muzzle motions of the test weapon.

The tube-support interaction forces, the motions of the support points, and the motions of adjacent tube nodes are given in Figures 24 and 25 for Runs 33.07 and 33.08, respectively. The projectile reaches the front support at about 0.9 ms and produces the large reaction shown in Figure 24(b) for Run 33.07. No such reaction is observed without radial expansion [Figure 25(b)]. In fact, the peak reaction force is only about 100 lb. With radial expansion, reaction forces at the front support can be large, reaching approximately 6700 lb for Run 33.07. Reaction forces at the rear support, where the support sleeve is more flexible, are only one-tenth as large. The high forces at the front support might be attenuated somewhat by local distortions of the sleeve cross-section and by accounting for the radial expansion of the tube ahead of the pressure pulse. These effects were not included in the model.

E. Bourdon Forces

The Bourdon forces were calculated in GUN2D as described in Section VI.A. They produce lateral forces on a curved tube which act to straighten it. Calculations were made with the Bourdon forces added (Run 33.09) for comparison with Run 33.01. The effects on tube motions were hardly detectable from displacement plots. Muzzle displacements, velocities, and acceleration for the two calculations are given below.

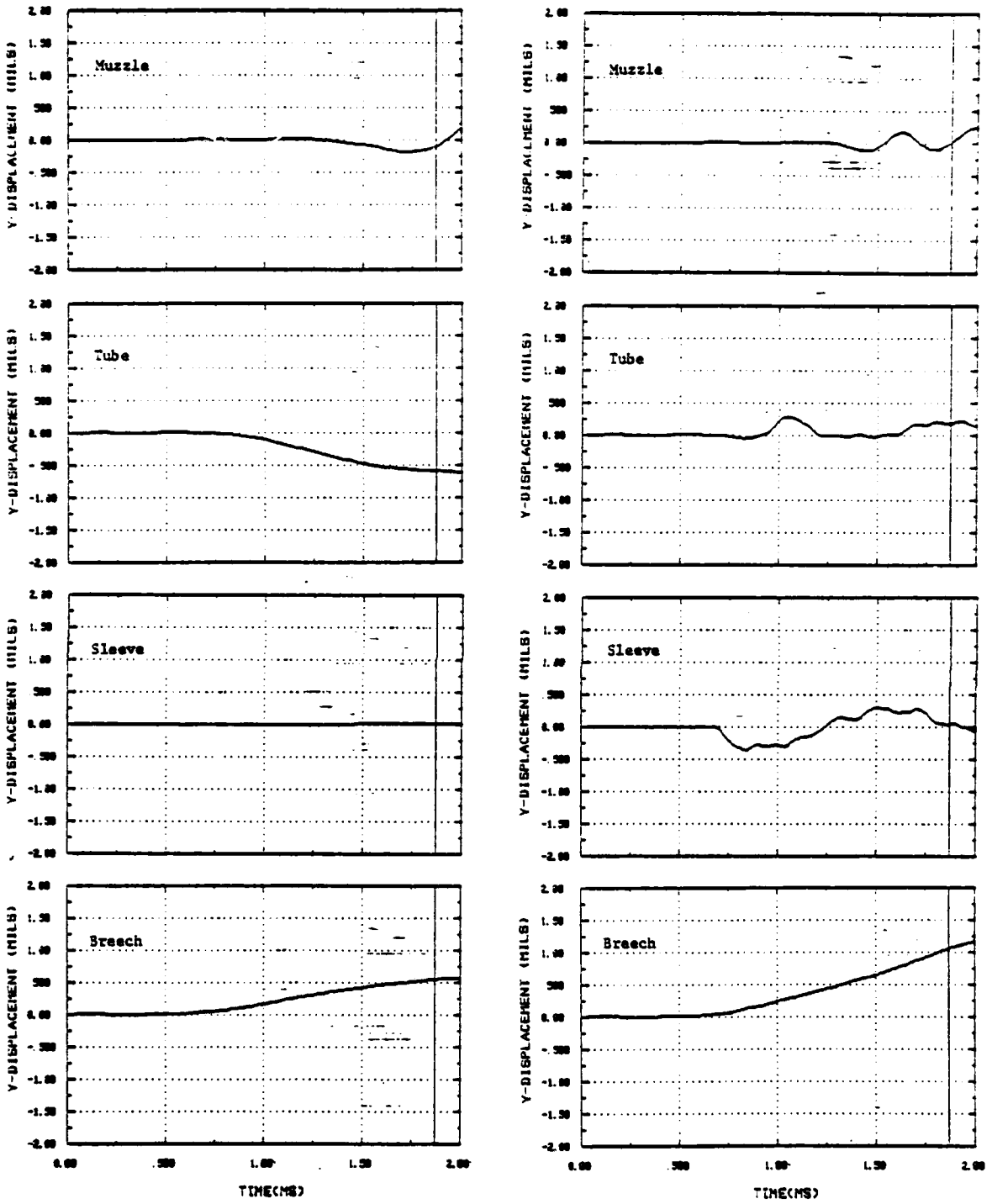

(a) Run 33.11

(b) Run 33.12

FIGURE 22. CALCULATED VERTICAL TUBE MOTIONS FOR DIFFERENT INITIAL TUBE POSITIONS: STIFF SPRINGS, TIGHT SLEEVE, AND STRAIGHT TUBE

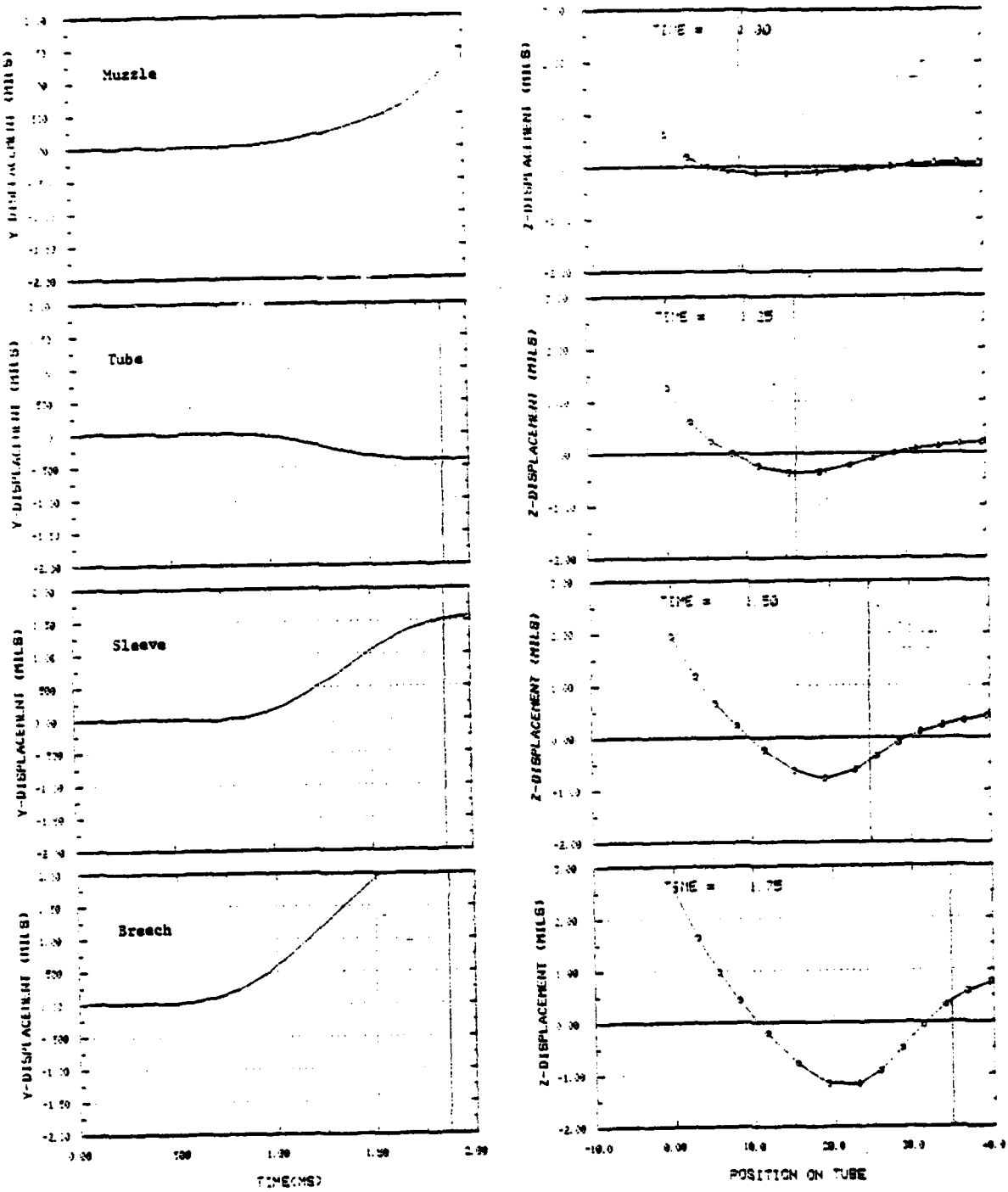

(a) Displacement Histories

(b) Displacement Profiles

FIGURE 23. CALCULATED RESULTS FOR RUN 33.08,
NO RADIAL EXPANSION, CURVED TUBE

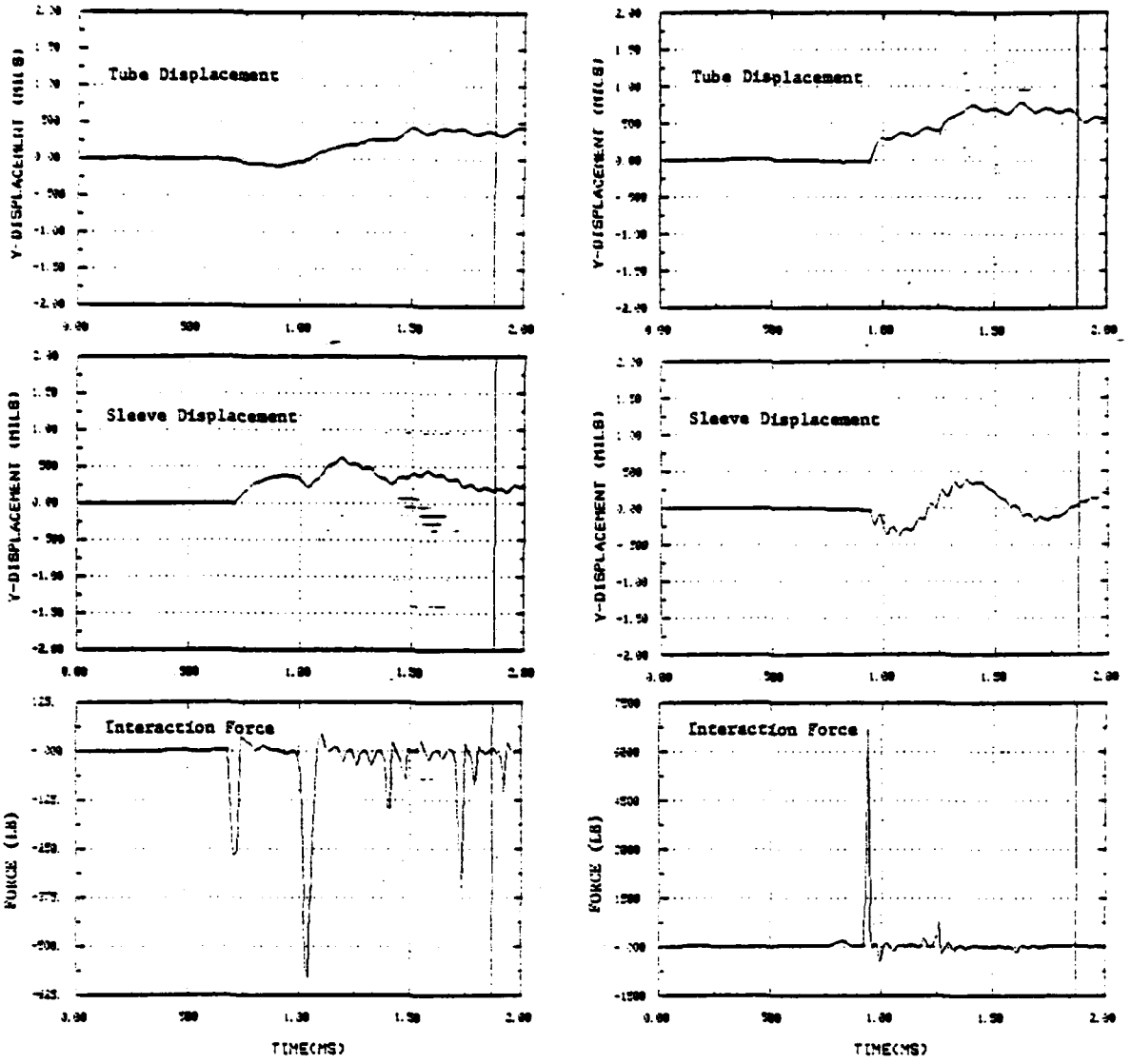

(a) Rear Support

(b) Front Support

FIGURE 24. DISPLACEMENTS AND FORCES AT THE SUPPORTS FOR RUN 33.07, WITH RADIAL EXPANSION

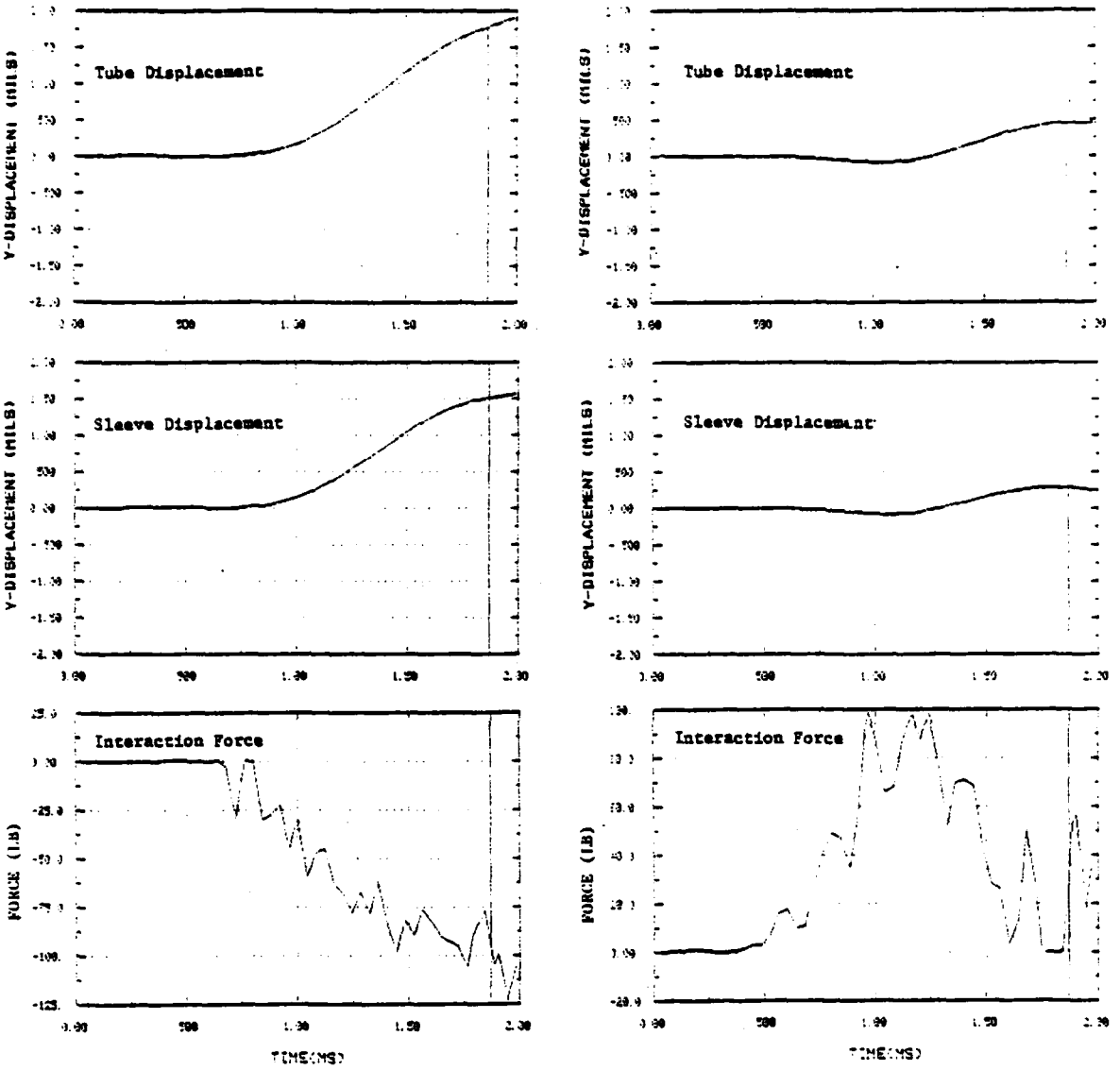

(a) Rear Support

(b) Front Support

FIGURE 25. DISPLACEMENTS AND FORCES AT THE SUPPORTS FOR RUN 33.08, NO RADIAL EXPANSION

Run	Displacement (mils)		Velocity (in/sec)		Acceleration (in/sec^2)	
No.	Max.	@ Exit	Max.	@ Exit	Max.	@ Exit
33.01	1.9708	1.2201	8.6947	3.5830	120,780	85,789
33.09	1.9755	1.2136	8.6989	3.6017	123,190	84,770

The differences in these values are also very small.

Profile plots of the lateral Bourdon forces at discrete times are given in Figure 26. Forces on the tube from 0 to 15 in. were omitted from the plots because they were masked by the high support reaction forces which occur in this region. Comparing Figures 26 and 20, the Bourdon forces are seen to be smaller and generally in opposition to the forces associated with the axial accelerations. Note also that the forces are zero ahead of the projectile. (In the model they are zero ahead of the element in which the projectile lies.) Projectile position is noted by the vertical line in each graph. Because of their negligible effect on the tube motions, Bourdon forces were omitted from the remainder of the calculations.

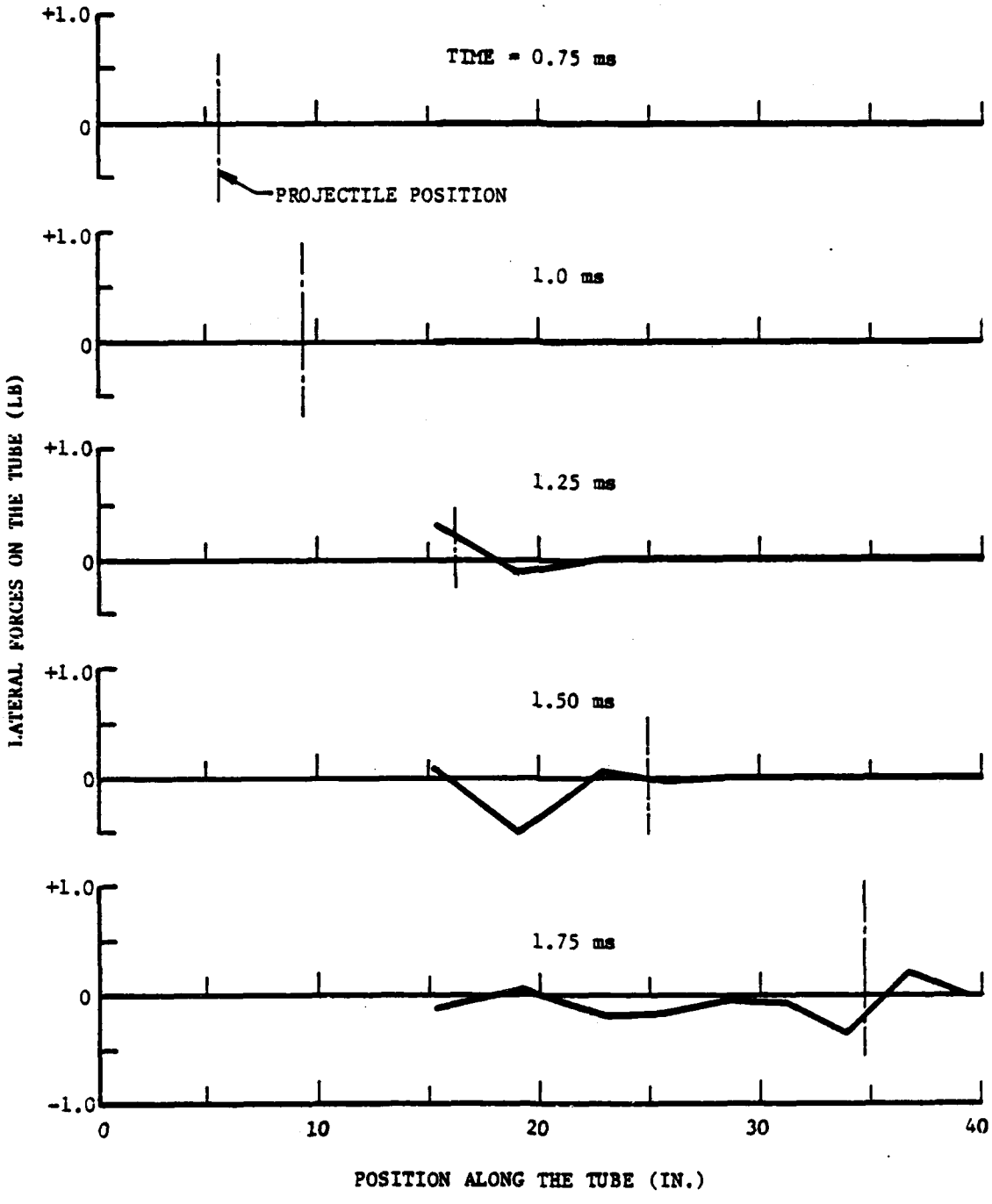

FIGURE 26. PROFILES OF THE BOURDON FORCES FOR RUN 33.09

VIII. ANALYTICAL-EXPERIMENTAL COMPARISONS

Based on the parameters investigated for Test No. 33 and described in the previous section, a standard analytical model was selected with which to make calculations for other tests. For the vertical plane this model is characterized by Run 33.07 in Table 3. The tube is straight; radial expansion is included; the tube is resting on the front support (CN = 0.0); and a small clearance exists between the top of the tube and the rear support (CP = 0.0004 in.). Bourdon forces and the forces produced by axial acceleration coupled with tube lateral displacements are ignored.

The horizontal model is similar to the vertical model except that there are no gravitational acceleration effects on the projectile, the tube is centered at the aft support, and the tube rests 0.0003 in. from the left side of the front support. This placement of the tube at the front support was chosen to provide some excitation to the tube from the radial expansion and because the displacements of the tube just ahead of the front support and at the muzzle were almost always positive (to the right looking down the tube) in the experiments. This is seen in part (d) of the measured data given in Appendix A.

Table 4 gives the parameters which were included in the models for the other tests analyzed. Notice that for the vertical plane, CP at the rear support is always 0.0004 and CN at the front support is always 0.0. This is the muzzle-down position chosen from the parameter studies. For the horizontal plane, CP and CN are equal at the aft support and CN is always 0.0003 at the front support. Results of the calculations are included in Appendix D. Comments on the similarities and differences between experimental and analytical results for these tests are given below. The influence of the support conditions is discussed more fully in the next section.

A. Test 33 (Figure 11 Versus Figure 21, Run 33.07)

Muzzle Displacements - Comparisons of analytical to experimental results were made for Test 33 in the parameter studies. The signatures of the muzzle displacements were made to match reasonably well, but the magnitudes of the calculated displacements are lower (about 31% lower for the maximum vertical displacements) than the measured data. Time correlation is also reasonably good, but the projectile exits the tube in the experiments when the muzzle is up and in the calculations when the muzzle is down. Note also that no reversal of the muzzle displacement occurs after projectile exit in the experiments, whereas it does in the calculations. The experimental data is suspect after projectile exit because of the influence of the exhaust gases. After projectile exit, the analytical results are more reliable.

Tube Displacements - These are the displacements of the tube relative to the ring (Figures 1 and 16) and correspond to a point on the tube just ahead of the ring. (See Figure 5 for the measurement locations.) Measured displacements include the tube radial expansion produced by the internal pressure, whereas calculated displacements include only lateral motions of the tube centerline. Note that except for some high frequency content

TABLE 4. PARAMETERS USED IN THE CALCULATIONS FOR SELECTED TESTS

Run No.	Plane*	Springs	Sleeve	Proj. Mass	Chamb. Press.	Tube Initial Curvature	Tube Radial Expansion	Support Clearances (in.) Rear CP	Rear CN	Front CP	Front CN	Bourdon Forces	Axial Acc. Effects	Breech Ecc. (in.)
33.07	V	Stiff	Tight	Test #33	Test #33	No	No	0.0004	0.0012	0.0011	0.0	No	No	0.014
(repeated)	H	Stiff	Tight	Test #33	Test #33	No	No	0.0008	0.0008	0.0008	0.0003	No	No	0.0
44.01	V	Stiff	Loose	Test #44	Test #44	No	No	0.0004	0.0041	0.0043	0.0	No	No	0.014
	H	Stiff	Loose	Test #44	Test #44	No	No	0.00225	0.00225	0.0040	0.0003	No	No	0.0
45.01	V	Stiff	Loose	Test #45	Test #45	No	No	0.0004	0.0041	0.0043	0.0	No	No	0.014
	H	Stiff	Loose	Test #45	Test #45	No	No	0.00225	0.00225	0.0040	0.0003	No	No	0.0
46.02	V	Very Flexible	Tight	Test #46	Test #46	No	No	0.0004	0.0012	0.0011	0.0	No	No	0.0014
	H	Very Flexible	Tight	Test #46	Test #46	No	No	0.0008	0.0008	0.0008	0.0003	No	No	0.0
53.01	V	Very Flexible	Loose	Test #53	Test #53	No	No	0.0004	0.0041	0.0043	0.0	No	No	0.0014
	H	Very Flexible	Loose	Test #53	Test #53	No	No	0.00225	0.00225	0.0040	0.0003	No	No	0.0
66.01	V	Flexible	Interm.	Test #66	Test #66	No	No	0.0004	0.0025	0.0026	0.0	No	No	0.1752
	H	Flexible	Interm.	Test #66	Test #66	No	No	0.00145	0.00145	0.0023	0.0003	No	No	0.0

*V denotes vertical and H denotes horizontal.

in the measured data, the calculated results for the vertical motions match the measured horizontal motions and vice versa. A switch in the measurement channels could have occurred, but we were unable to verify that it did after the experiments were completed.

The vertical measurement appears to contain only the radial expansion component (~0.0004 in.), whereas the horizontal measurement contains substantial tube lateral displacement. Motions of the tube at this location are produced by the radial expansion of the tube pressing against the front of the tube support sleeve. Placing the tube against the left side of the sleeve (looking toward the muzzle) would produce horizontal tube displacements which match the experiments, but then the muzzle displacements would be much too large. On the basis of the analytical results, we suspect that the two channels were inadvertently reversed.

Sleeve Displacements - Measured and calculated sleeve displacements have about the same magnitudes, and there are similarities in the signatures. Calculated horizontal displacements are smooth because very little tube sleeve interaction occurred in the horizontal model.

Breech Displacements - Vertical breech displacements were not measured in Test 33. Horizontal displacements do not match in either magnitude or signature. In fact, breech measurements do not correlate well with calculated motions in any of the tests. This discrepancy could be caused by several factors. The most likely factors are breech motions relative to the tube and transducer mount motions.

B. Tests 44 and 45 (Figures A-2 and A-3 Versus Figures D-2 and D-3)

Muzzle Displacements - Tests 44 and 45 were duplicate tests, and the experimental results for the two tests are very similar. The calculations gave very similar results also, so the tests have been grouped together for comparison. The discussion for Test 33 applies to these comparisons as well. Both tests had the stiff support springs, and it is apparent that the tube sleeve clearance (tight for Test 33 and loose for Tests 44 and 45) made very little difference in the results.

Tube Displacements - The comments made for Test 33 apply here also; however, for these tests the measured vertical tube displacements are slightly larger than for Test 33 and have signatures which more closely match the calculated signatures. In these tests some lateral tube motion is obviously added to the radial expansion in both the horizontal and vertical directions. This lateral tube motion produced by tube sleeve interactions is characterized by the initial bump in the displacement (for stiff support springs).

Sleeve Displacements - Measured vertical sleeve displacements closely match calculated values for Test 44. For Test 45 the displacements are similar to those for Test 33. Measured horizontal sleeve displacements are essentially zero, which implies that very little tube-sleeve interaction occurred in the horizontal plane.

Breech Displacements - Measured breech displacements are consistent for Tests 44 and 45; however, they do not match calculated values. Consistently small positive breech displacements were obtained in the calculations except for Test 66, in which the breech mass eccentricity was increased by about one order of magnitude. A negative breech mass eccentricity might have produced negative breech displacements as observed in these tests, but this was not investigated. We assume that the calculated breech C.G. location of +0.014 in. is correct.

C. Test 46 (Figure A-4 Versus Figure D-4)

Muzzle Displacements - Measured vertical displacements for Test 46 are an anomaly relative to all of the other measurements. The magnitude of the displacement is larger than for any other test and the signature is totally different. Calculated muzzle motions are similar to those for Tests 33, 45, and 46 except that the negative excursion is greater for the vertical motions. Measured horizontal displacements are similar to the previous tests. We cannot explain satisfactorily the large and unusual vertical displacement. As will be discussed for the breech displacements, the breech measurement record is bad. The muzzle displacement record may have also been bad for this test.

Tube Displacements - As for Test 33, the calculated vertical displacement agrees reasonably well with the horizontal measurements and vice versa. Further, the measured data are similar to those for Tests 33, 44, and 45.

Sleeve Displacements - Measured and calculated sleeve displacements match reasonably well in magnitude. Similarities exist in the vertical signatures late in time but with some time shift.

Breech Displacements - Large negative vertical displacements occur in the measured data, opposite to the sleeve displacements. Unless the breech moved relative to the tube, it is unlikely that these motions could have occurred. Negative breech displacements imply negative tube displacements just ahead of the breech (in the sleeve). If even 1.6 mil negative displacements of the tube occurred ahead of the breech, then the sleeve could not have displaced upward as seen in part (e) of Figure A-4. Thus, these measurements appear to be inconsistent and imply a bad record for the breech displacement. Measured horizontal breech displacements are small, but greater than calculated values; however the displacement directions (both positive) do agree.

D. Test 53 (Figure A-8 Versus Figure D-5)

Muzzle Displacements - Test 53 is one test in which substantial horizontal as well as vertical muzzle motions occurred. Notice that there is a definite time correlation between the vertical and horizontal muzzle displacements, indicating that the motions were indeed coupled. Calculated muzzle motions for this test are similar to those for the earlier tests except that the vertical amplitudes are lower. Tests 46 and 53 both had the very flexible springs and Test 53 had a higher chamber pressure. Lower displacement amplitudes for Test 53 may have been caused by the shorter projectile exit time. The coupled motions measured for this test could

not be duplicated with the two-dimensional model used for the calculations. These results emphasize the need for a three-dimensional analysis of the motions.

Tube Displacements - Calculated vertical tube displacements are larger than measured values; however, if we again compare the measured horizontal displacements to the calculated vertical displacements and vice versa, the agreement is improved. The measured data does have higher frequency components than the calculated results, but this is not unusual. It is interesting to note that the signature and magnitudes of the measured tube motions are similar for the stiff and very flexible springs (e.g., Tests 33, 45 and 46 versus Tests 46 and 53), whereas for the calculated motions they are not. The calculated tube motions for the stiff springs match the measured motions reasonably well. This implies that the support springs are stiffer in the test weapon than in the analytical model. In the analytical model the stiffness of the support springs is calculated as though all four springs are parallel. Misalignment would make the net stiffness higher than the calculated values.

Sleeve Displacements - Calculated sleeve vertical displacements are higher in magnitude, but are similar in signature to the measured values up to projectile exit. Horizontal displacements agree well in magnitude and direction, but the signatures are very different.

Breech Displacements - Directions of the breech displacements are the same, but otherwise measured and calculated values do not agree. Measured horizontal breech displacements are much higher than calculated values for this test. This is consistent with the other horizontal displacements, which were higher also. As noted in the discussion of muzzle displacements, higher excitations occurred in the horizontal plane than were simulated in the model for this test. The coupled motions which occurred were probably produced by an off-centered initial position of the tube.

E. Test 66 (Figure A-14 Versus D-6)

Muzzle Displacements - In this test and in Test 67, the balance weight (see Figure 1) was removed from the pressure transducer assembly to produce a larger mass unbalance at the breech (0.1752 in. versus 0.0145 in.). This breech unbalance caused a large difference in the calculated vertical muzzle displacements. They are predominately negative, and their magnitude has more than doubled relative to the calculations for other tests. In contrast, it is surprising to note that the measured muzzle displacement was not markedly different from the other tests. Comparing Test 66 (Figure A-14) to Test 61 (Figure A-11), which also had the flexible springs and intermediate sleeves, shows that the muzzle motions are very similar. Thus, breech eccentricity made a significant change to the calculated muzzle motions, but not to the measured motions.

Tube Displacements - As for the muzzle displacements, the breech eccentricity made a large difference in the calculated motions but not in the measured motions. In the calculations an initial positive displacement occurred at about 1.00 ms, caused by the tube radial expansion

(the tube rests on the front support), and then subsequently negative displacements occurred, caused by the negative breech moment. Measured motions showed little changes from previous tests. They are very similar to the results for stiff springs which were measured for Tests 33, 44 and 45. The reasons why the breech eccentricity did not affect tube motions are unknown.

Sleeve Displacements - Calculated displacements show a sharp increase in sleeve positive displacements, which exceeded 2.0 mils at approximately 1.45 ms and reached 4.0 mils at muzzle exit. They correspond to the breech motions which were high positive values, i.e., the tube moved up and pushed the back of the sleeve up with it. Again, measured motions were similar to earlier tests with a balanced breech.

Breech Displacements - The positive breech eccentricity produced a sharp increase in positive breech vertical motions in the calculated results. Breech displacements were 7.0 mils at projectile exit. This can be seen in the tube profile given in Figure 27. Note in the figure that the vertical scales are different for different tests and that the vertical scales are greatly exaggerated relative to the horizontal scale. In Figure A-14 some increase in measured breech displacements is noted just before projectile exit. Compared to the calculated values, it occurs later in time and is much lower in amplitude.

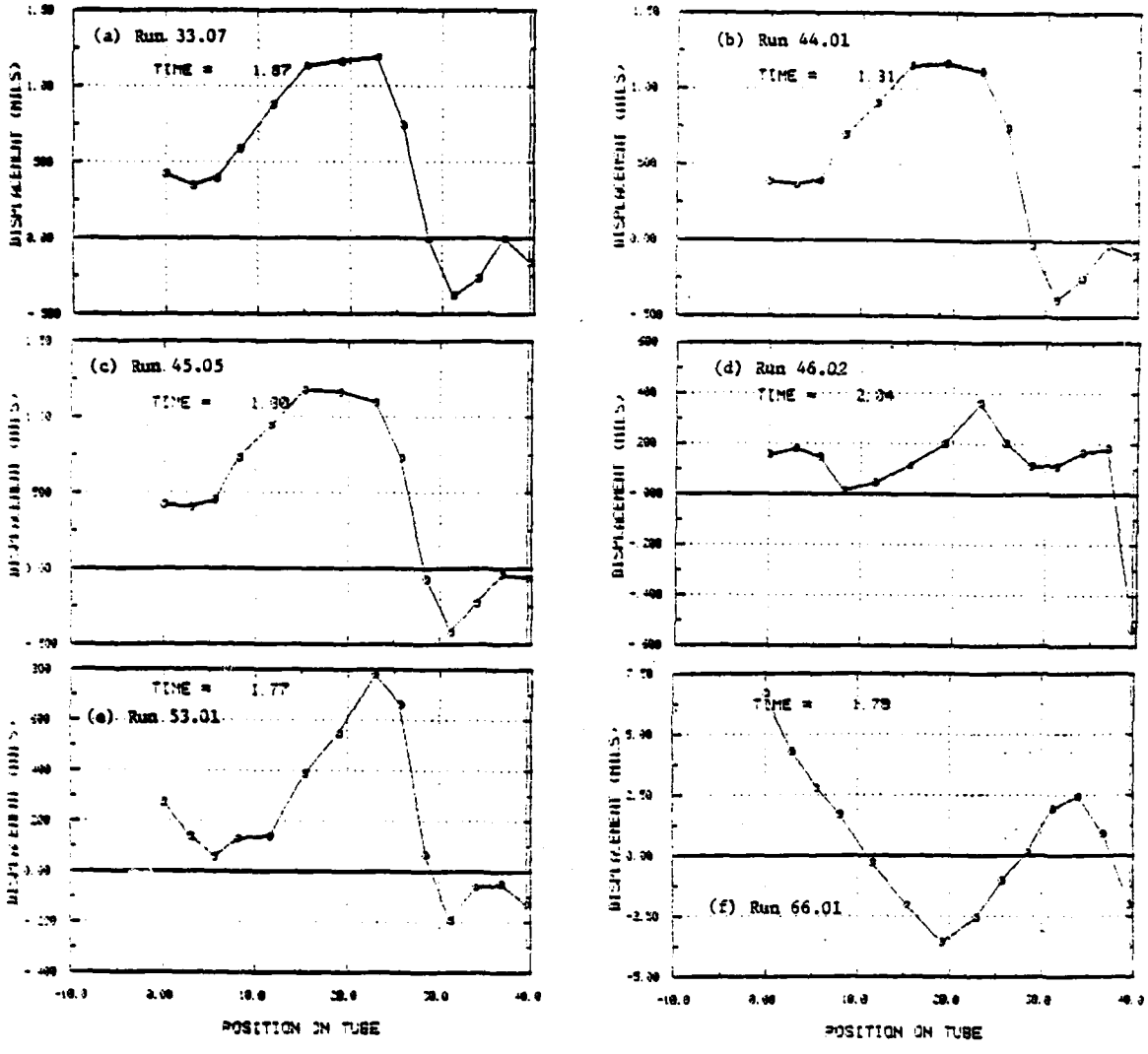

FIGURE 27. CALCULATED TUBE PROFILES OF VERTICAL DISPLACEMENTS AT PROJECTILE MUZZLE EXIT

IX. INFLUENCE OF TUBE SUPPORT CONDITIONS

A. Clearances

As was observed from the experiments, Section V.C., no significant change in muzzle motions occurred when clearances were changed. These observations were confirmed by the calculations, as discussed in the experimental-analytical comparisons. When calculated results for the tight sleeve (Test 33, Figure 21) and for the loose sleeve (Test 44, Figure D-2) are compared, the displacements are seen to be almost identical. Test 45 (Figure D-3) is a repeat of Test 44, and again, the results are almost identical. Note that these comparisons of tight (Test 33) and loose (Tests 44 and 45) sleeves are for the stiff springs. Calculations for Tests 46 (Figure D-4) and 53 (Figure D-5) can be compared for the most flexible springs; however, for these two tests the results are distorted by the fact that the projectile exit times and the horizontal scales are different. These differences were caused by differences in chamber pressures for the two tests. Experimental results for Tests 46 and 53 cannot be compared because of the questionable records for Test 46; however, Tests 47 and 48 are repeats of Test 46. These duplicate test results agree well with Test 53.

The small influence which the clearances had on tube motions is explained by the fact that, even for the tighest sleeve, the clearances were large enough so that when the tube was forced away from the nearest surface it had very little interaction with the opposing surface. This observation is supported by the data in Figure 24, which give the displacements and forces at the support points for Run 33.07. Note that the interaction forces at the rear support are predominately negative, indicating that the tube is repeatedly interacting with the top of the sleeve, and at the front support they are predominately positive, indicating that the tube is interacting predominately with the lower surface of the sleeve.

To illustrate that clearances can make a difference in the tube motions, Run 33.13 (Table 3) was made with reduced clearances at the front support. Otherwise the calculation was identical to Run 33.07. For Run 33.13, the clearances were reduced so that the tube contacted both sides of the sleeve at maximum pressure. Comparing the results for Run 33.07 (Figure 21) and Run 33.13 (Figure 28) reveals that very different muzzle motions were produced by reducing the clearance at the front support. Thus, a tight fit between the tube and the sleeve can drastically alter muzzle motions; however, above a value which precludes (or substantially limits) interaction of the tube with both opposing support surfaces, increasing the clearance will produce minimal effect. This was the case in the experiments reported in Section V.

It should also be noted that clearances used in this study were scaled from the M68 105-mm tank gun, so clearances for that gun should not significantly affect its tube motions.

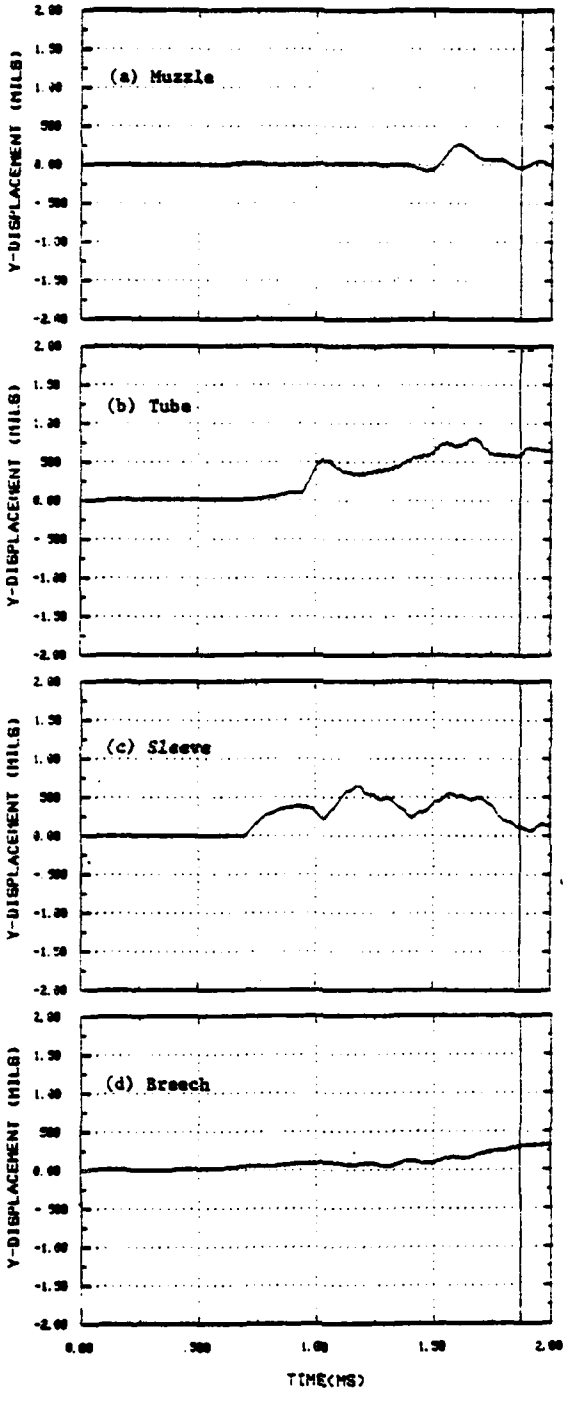

FIGURE 28. CALCULATED TUBE VERTICAL DISPLACEMENTS FOR RUN 33.13, REDUCED CLEARANCES AT THE FRONT SUPPORT

B. Tube Support Stiffness

The effect of changes in support stiffness are shown analytically by comparing the following results:

	Stiff	Very Flexible
Tight Sleeve:	Run 33.07 (Figure 21)	to Run 46.02 (Figure D-4)
Loose Sleeve:	Run 44.01 (Figure D-2) & Run 45.01 (Figure D-3)	to Run 53.0 (Figure D-5)

For the tight sleeve, the most pronounced differences occur for the tube displacement (just ahead of the front support) and for the sleeve (at the rear support point). Muzzle signatures, while different, are not changed substantially. Tube displacement profiles show the pronounced differences which occur. Profiles at projectile muzzle exit, for all of the runs included in Appendix D, are given in Figure 27. Notice that the profiles for Run 33.07 in part (a) and for Run 46.02 in part (d) are very different. As already noted in Section VII.C., the analytical and experimental results do not match for Test 46. It is an anomaly among the test results and must be discounted as valid data or attributed to randomness in the experiments which is as yet unexplained. Experimental results for Tests 47 and 48 (Figures A-5 and A-6, respectively), which are repeats of Test 46, give results which more closely match Test 33.

For the loose sleeve (Figures D-2 and D-5), a more pronounced difference in muzzle motion is produced by stiffness changes. The signature is very similar, but the magnitude of the displacement is less with the more flexible springs. Again, the differences are more pronounced at other locations on the tube and also show up clearly in the displacement profiles of Figure 27. Experimentally (Figures A-2 and A-5), the differences were even less pronounced than for the calculated results. Notice that muzzle motions in the vertical plane are similar except for more pronounced oscillations in Test 53 between 1.0 and 1.6 ms. In the horizontal plane the muzzle motions are entirely different. It is clear that coupling occurred between the horizontal and vertical muzzle motions in Test 53. This effect could not be duplicated in the two-dimensional analysis performed. Again, horizontal motions for Test 53 were very different from most other tests; however, because of its phasing with the vertical motions it appears to be valid data.

These comparisons have shown that support stiffness can have a pronounced effect on tube displacements. The effects are most obvious at loations along the tube other than the muzzle and show up most clearly in the tube displacement profiles.

X. CONCLUSIONS AND RECOMMENDATIONS

A. Conclusions

The most significant conclusions from this study are:

- The initial position of the tube relative to its support is the primary variable in the tube-support parameters which affects tube motions.
- Above some minimum value, changing clearances between the tube and its support does not significantly alter tube motions. For the model test weapon used in these experiments, the minimum value was about three times the maximum tube radial expansion.
- Changing support stiffness noticeably alters tube motions in the tube support region, but it may have only a small effect on muzzle motions.

Other important observations are:

- Tube radial expansion, produced by the internal pressure, is the primary cause for interaction between the tube and its support.
- Initial tube curvature produced effects in the analytical model which were not observed in the experiments.
- Breech mass eccentricity produced effects in the analytical model which were not observed in the experiments.
- Noncontacting displacement transducers are suitable instrumentation for measuring tube motions.

B. Recommendations

Based upon the findings in this research project, several studies have been identified which should be conducted to forward the analytical modeling capability in gun dynamics. These are:

- Develop a three-dimensional model of the tube and the tube-support system.
- Reevaluate the analytical formulation of axial acceleration effects.
- Further develop an instrumentation system using the noncontacting inductance probe, to eliminate all interferences.
- Include dynamic effects in the calculation of tube radial expansion.
- Perform additional experiments in which the tube initial position is carefully controlled.
- Perform additional experiments in which the tube-to-sleeve clearances are reduced to a point which produces interference between the tube and the sleeve at maximum pressure.

REFERENCES

1. Cox, P. A., and Hokanson, J. C., "Muzzle Motions of the M68 105mm Tank Gun," Contract Report ARBRL-CR-00418, Prepared by Southwest Research Institute, San Antonio, Texas, March 1980.

2. Cox, P. A., and Hokanson, J. C., "Muzzle Motions of the M68 105mm Gun," Proceedings of the 2nd U. S. Army Symposium on Gun Dynamics, held at The Institute on Man and Science, Rensselaerville, NY, 19-22 September 1978.

3. Cox, P. A., and Hokanson, J. C., "The Influence of Tube Support Conditions on Muzzle Motions," Report No. ARLCB-SP-82005, Proceedings of the 3rd U. S. Army Symposium on Gun Dynamics, Vol. II of II, held at The Institute on Man and Science, Rensselaerville, NY, 11-14 May 1982.

4. Simkins, T. E., "Transverse Response of Gun Tubes to Curvature Induced Loads," Report No. ARLCB-SP-78013, Proceedings of the 2nd U. S. Army Symposium on Gun Dynamics, held at The Institute on Man and Science, Rensselaerville, NY, 19-22 September 1978.

5. Roark, R. J., and Young, W. C., Formulas for Stress and Strain, 5th Edition, McGraw-Hill Book Co., New York, NY, 1975.

APPENDIX A

GRAPHS OF MEASURED TUBE MOTIONS FOR TESTS

33
44
45
46
47
48
49
53
55
58
61
64
65
66
67

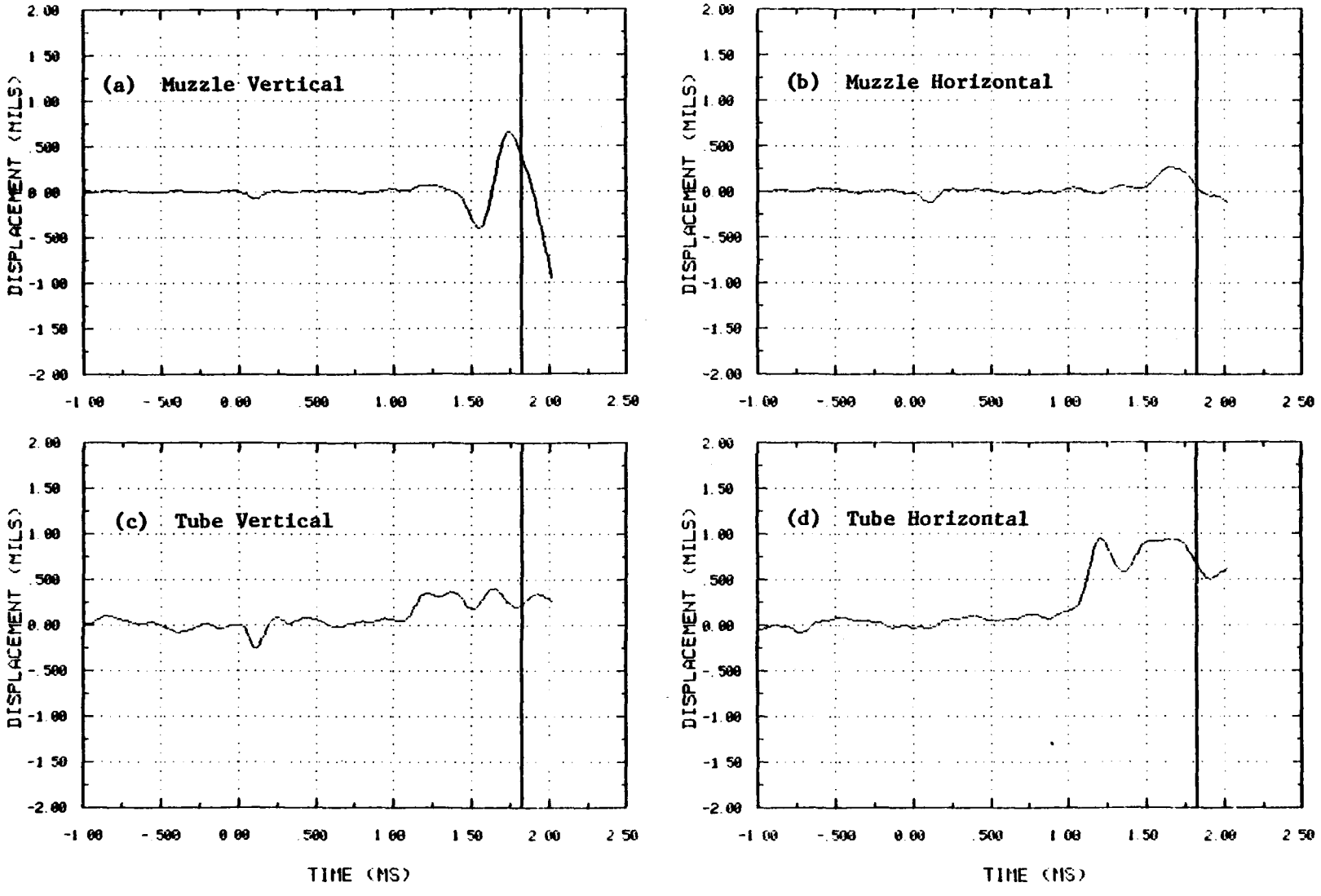

FIGURE A-1 MEASURED DISPLACEMENTS FOR TEST NO. 33 (Continued)

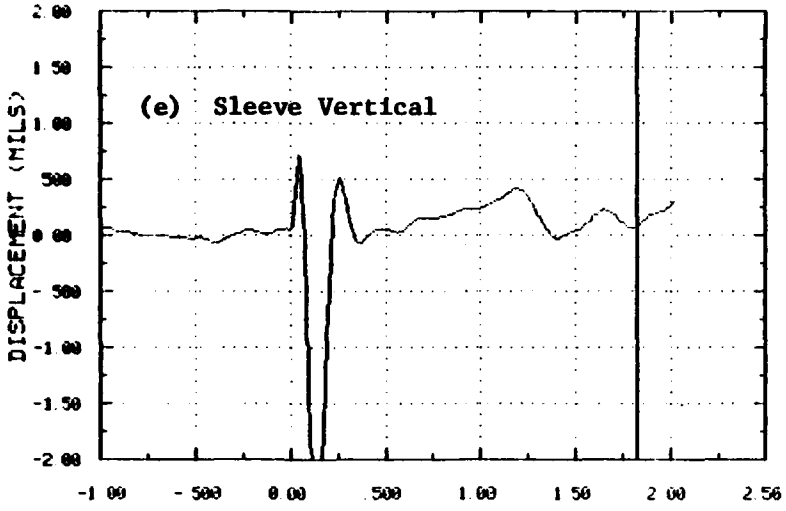

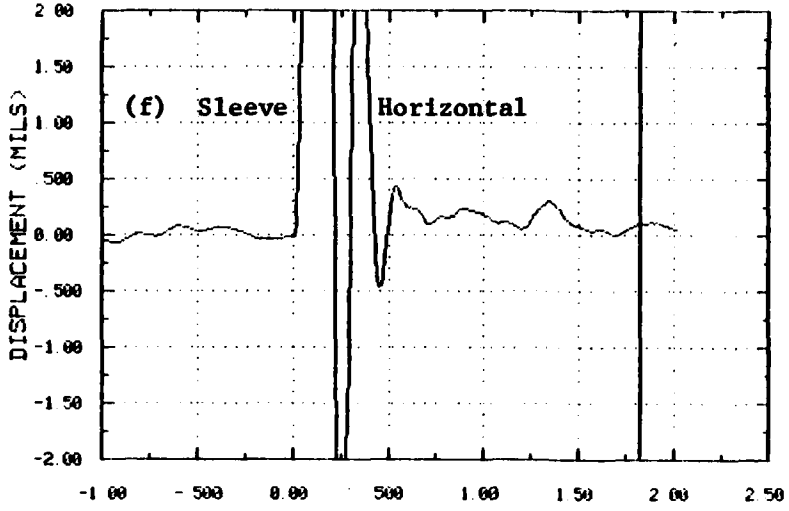

(g) Breech Vertical - not recorded for this test

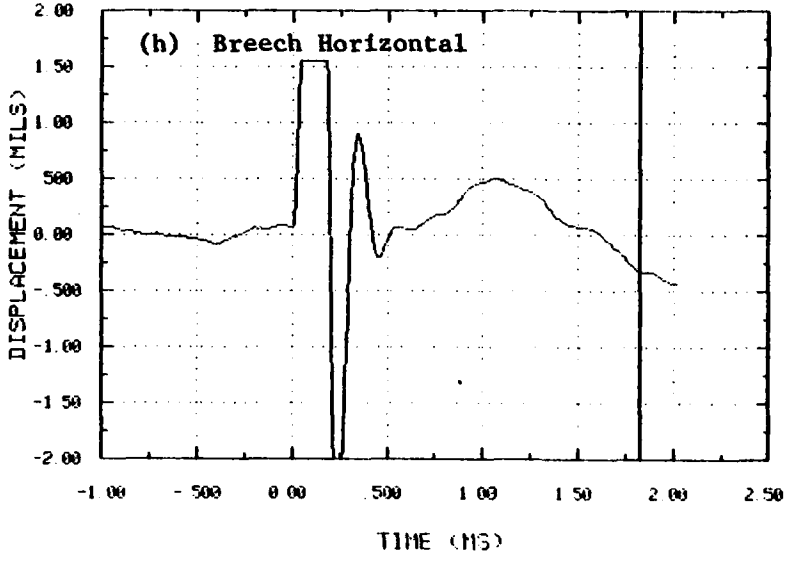

FIGURE A-1 MEASURED DISPLACEMENTS FOR TEST NO. 33 (Concluded)

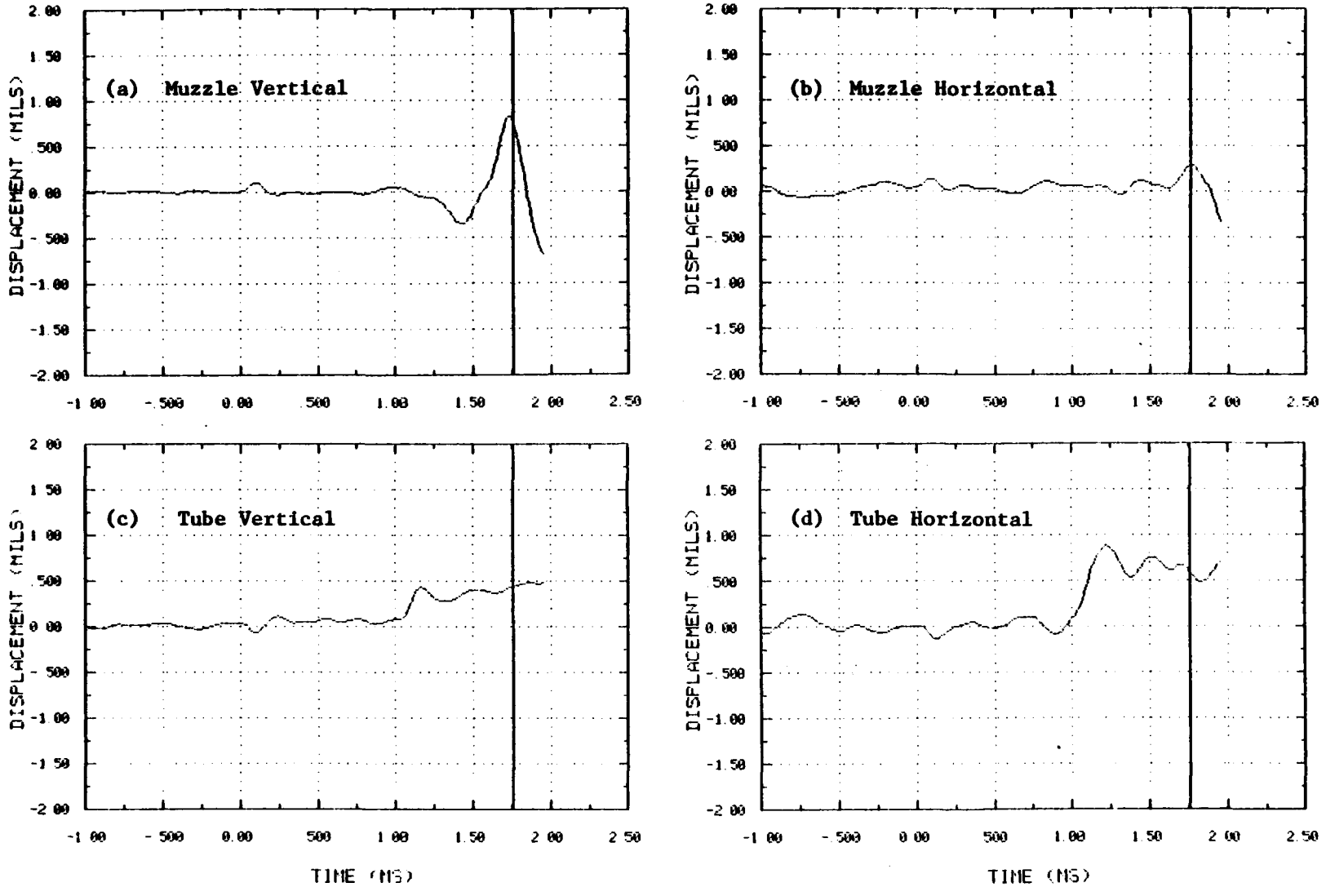

FIGURE A-2 MEASURED DISPLACEMENTS FOR TEST NO. 44 (Continued)

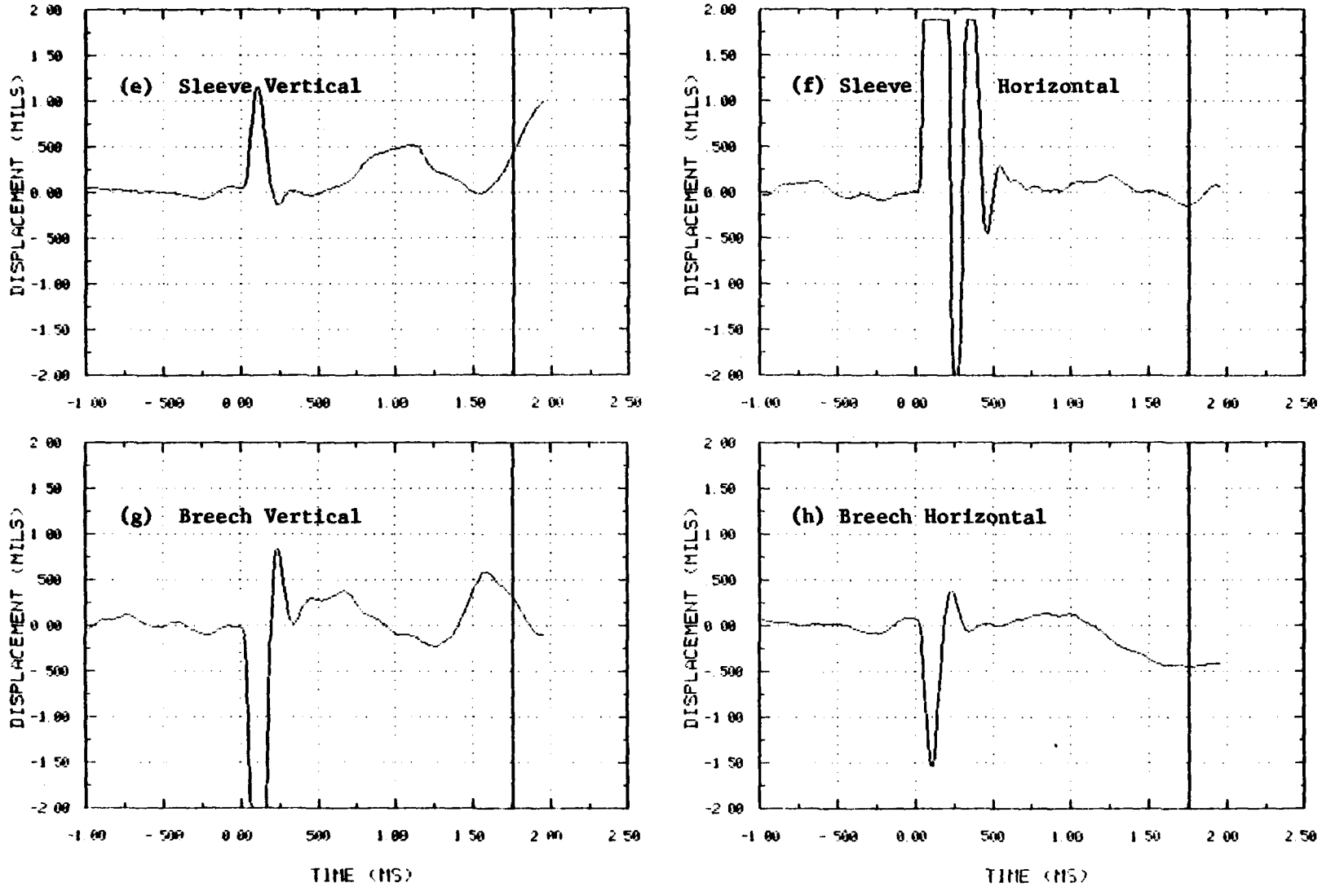

FIGURE A-2 MEASURED DISPLACEMENTS FOR TEST NO. 44 (Concluded)

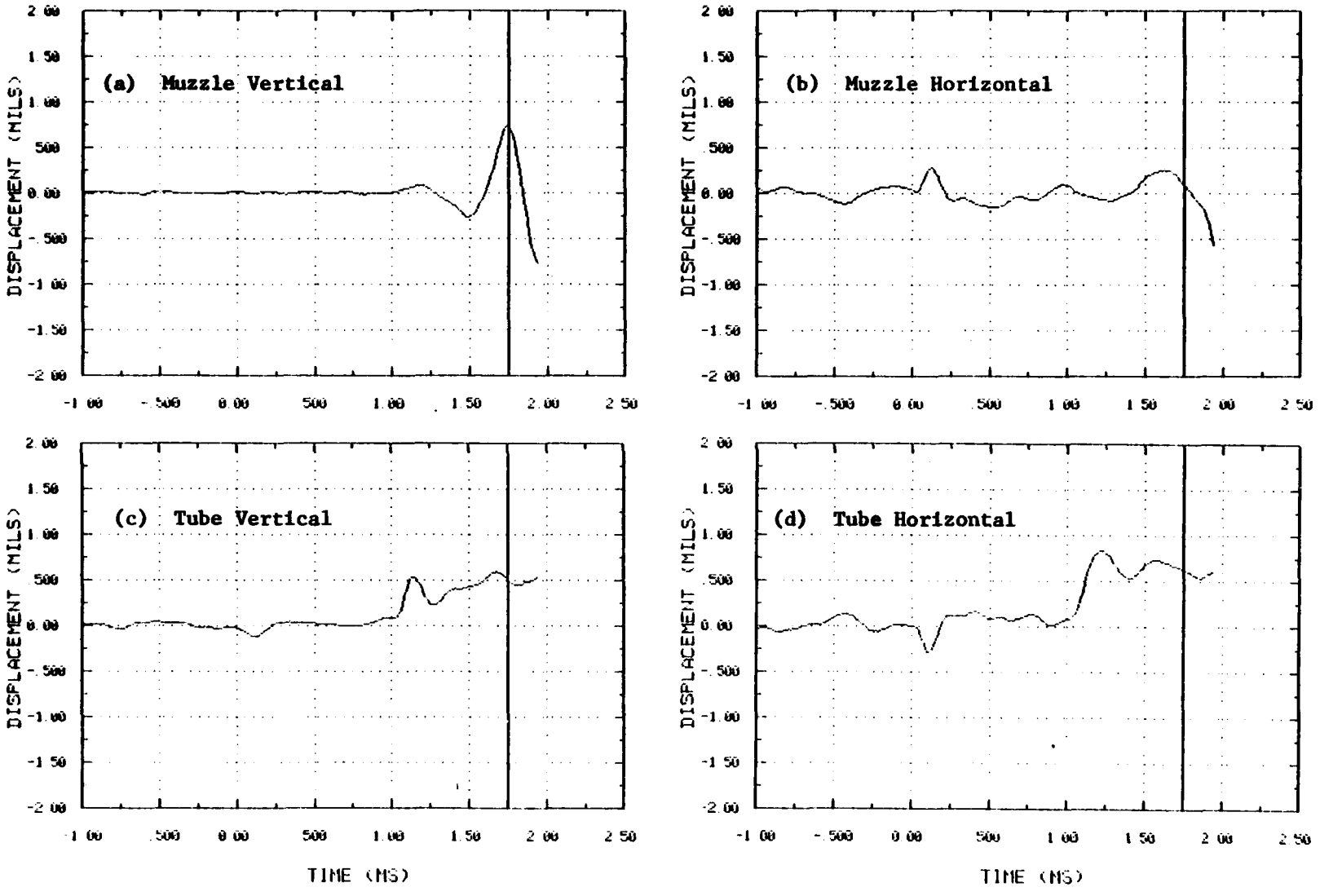

FIGURE A-3 MEASURED DISPLACEMENTS FOR TEST NO. 45 (Continued)

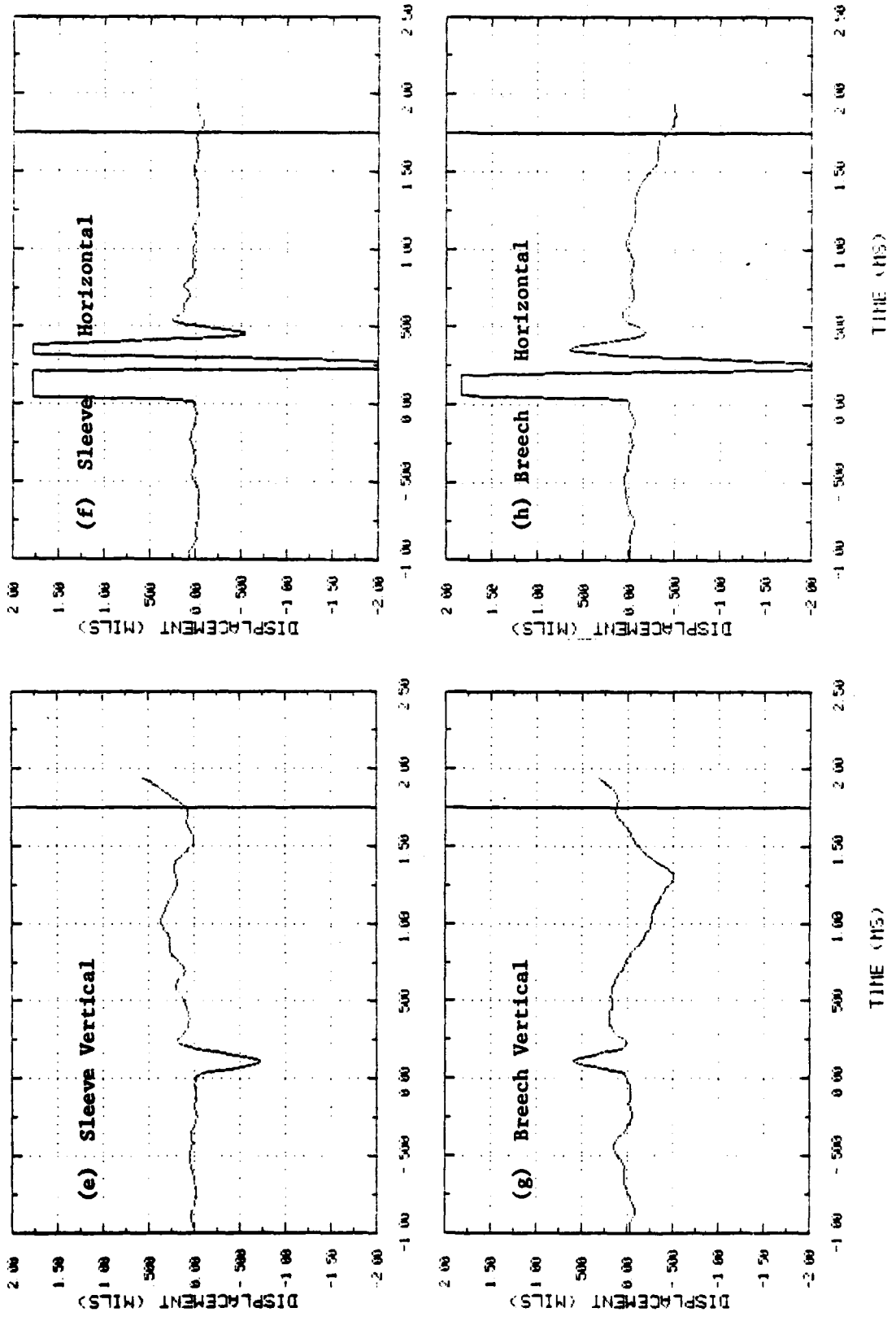

FIGURE A-3 MEASURED DISPLACEMENTS FOR TEST NO. 45 (Concluded)

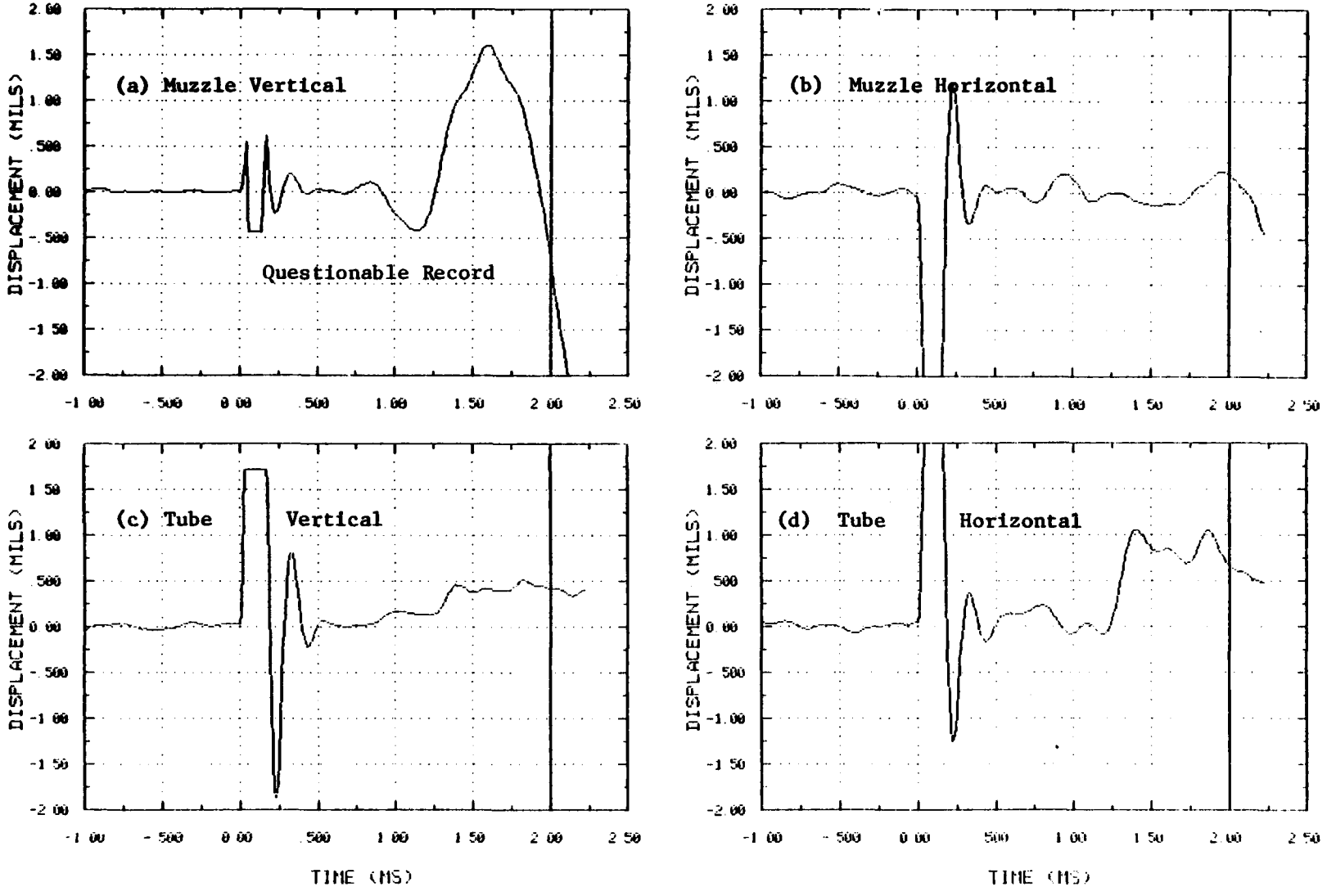

FIGURE A-4 MEASURED DISPLACEMENTS FOR TEST NO. 46 (Continued)

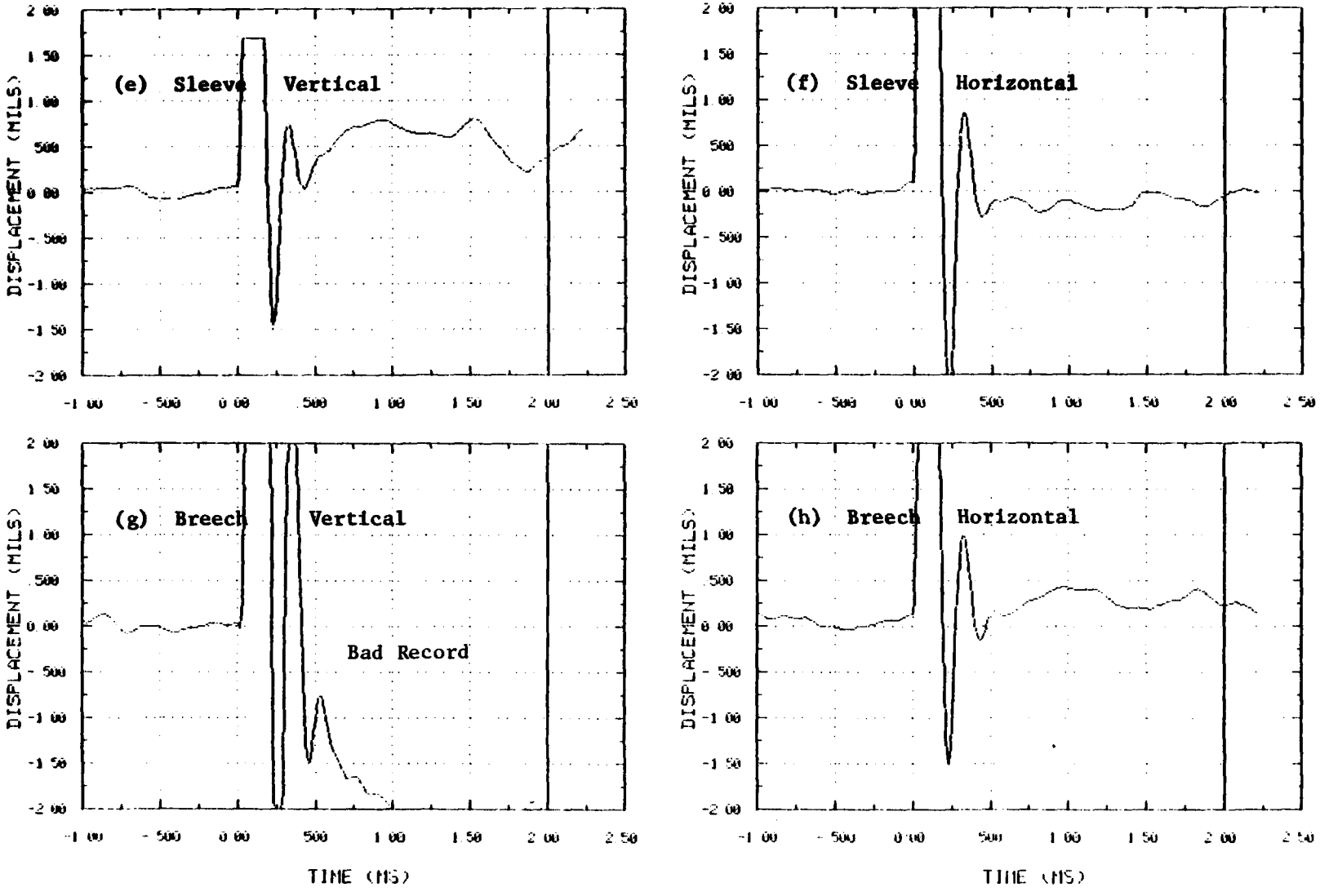

FIGURE A-4 MEASURED DISPLACEMENTS FOR TEST NO. 46 (Concluded)

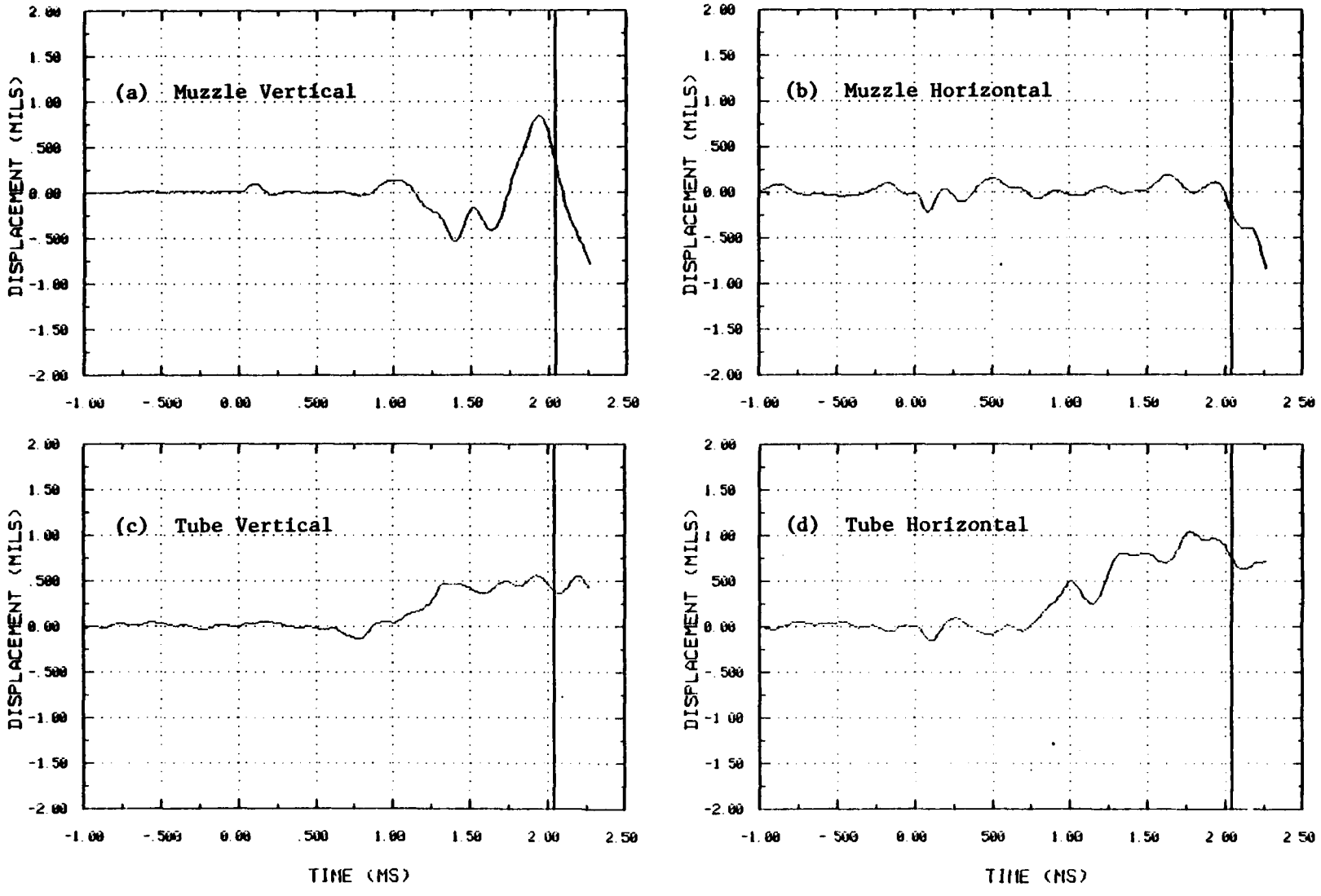

FIGURE A-5 MEASURED DISPLACEMENTS FOR TEST NO. 47 (Continued)

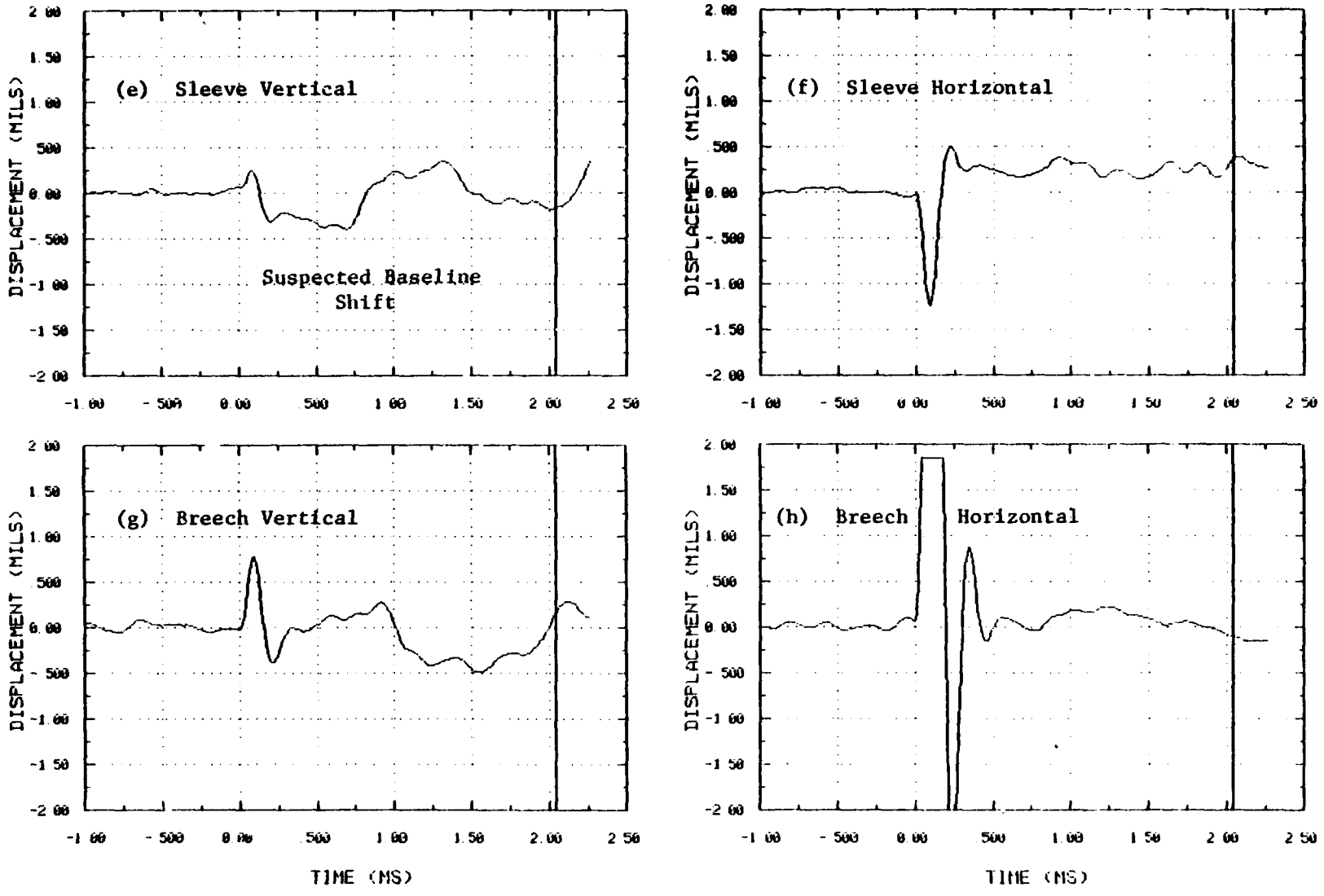

FIGURE A-5 MEASURED DISPLACEMENTS FOR TEST NO. 47 (Concluded)

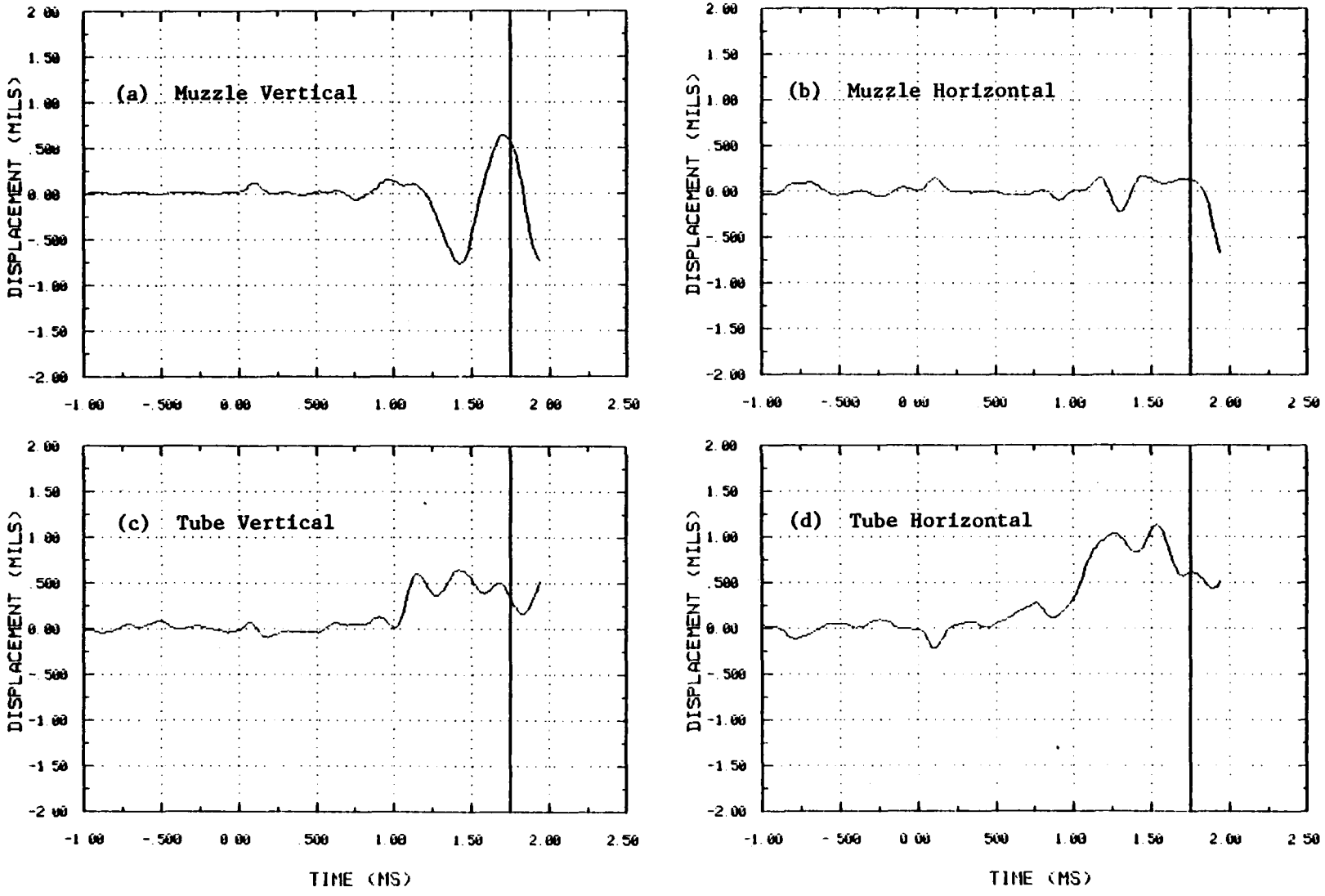

FIGURE A-6 MEASURED DISPLACEMENTS FOR TEST NO. 48 (Continued)

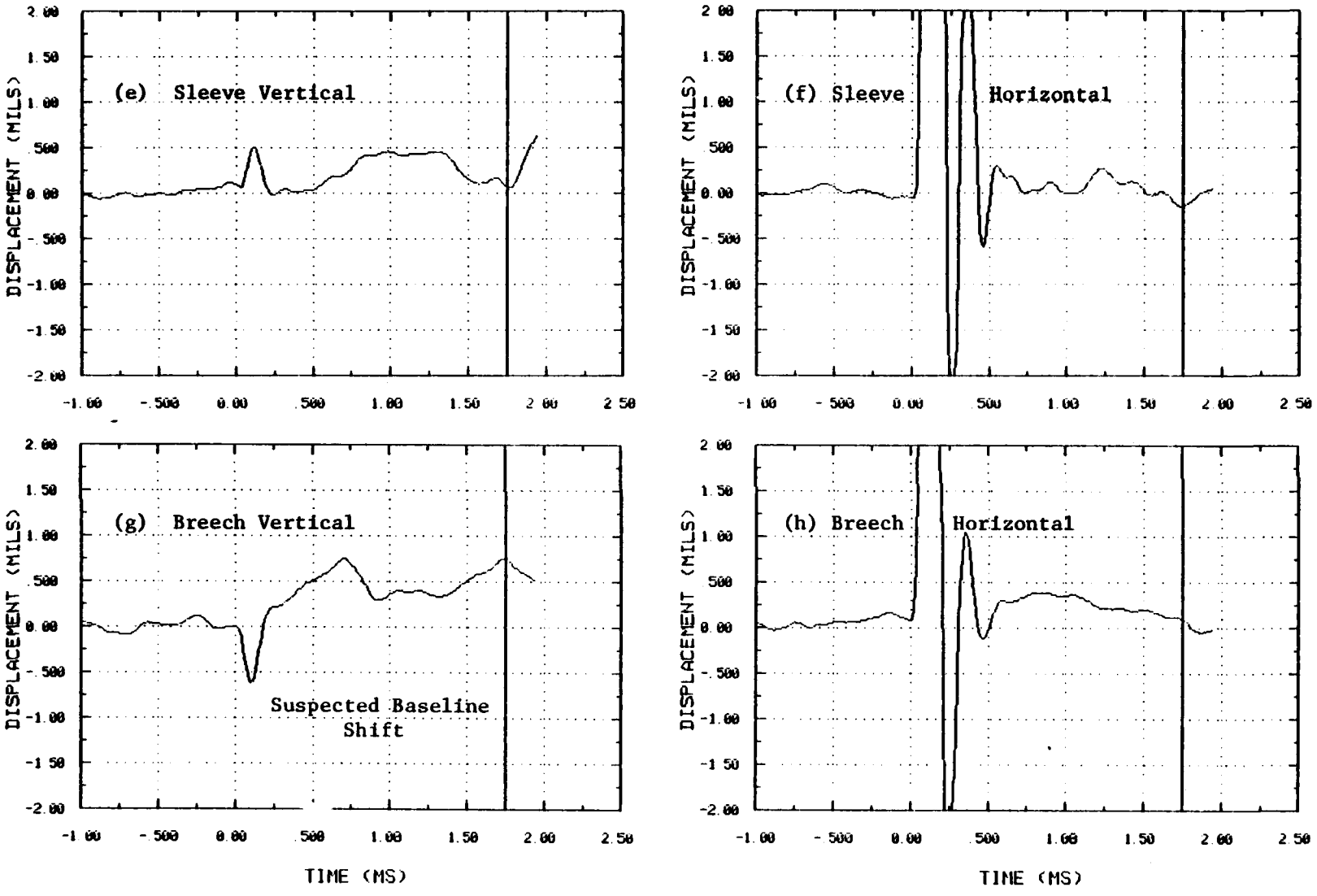

FIGURE A-6 MEASURED DISPLACEMENT FOR TEST NO. 48 (Concluded)

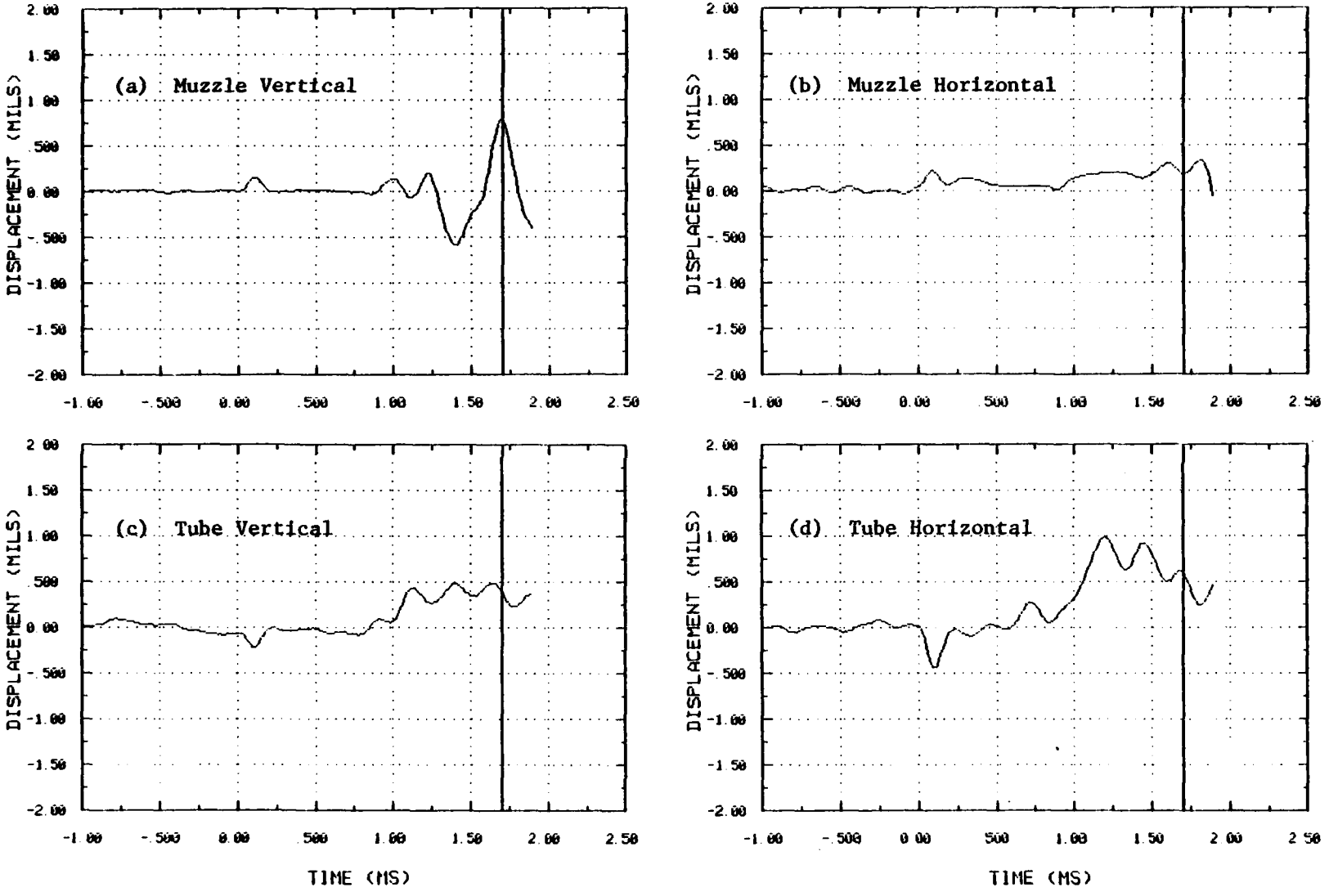

FIGURE A-7 MEASURED DISPLACEMENTS FOR TEST NO. 49 (Continued)

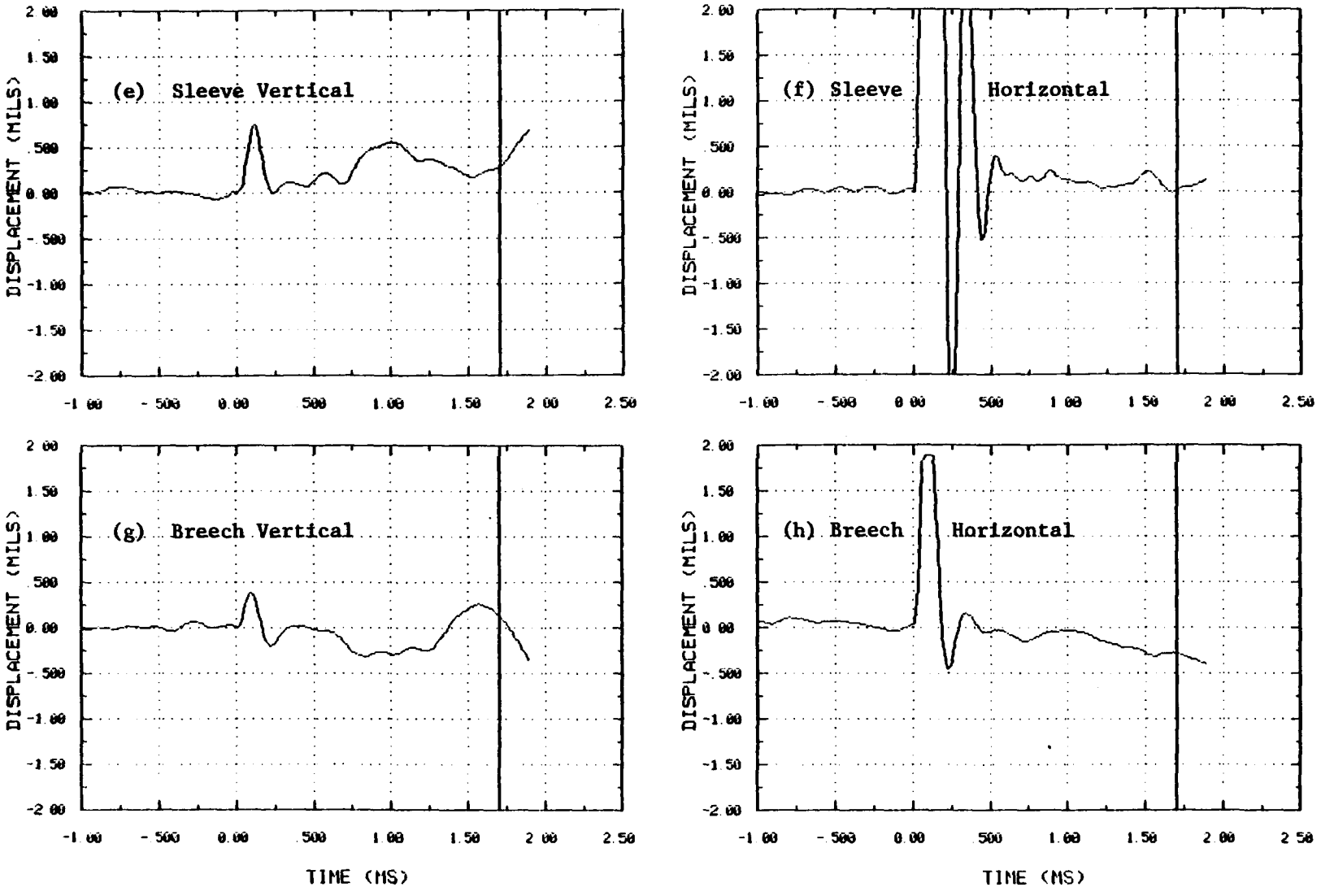

FIGURE A-7 MEASURED DISPLACEMENTS FOR TEST NO. 49 (Concluded)

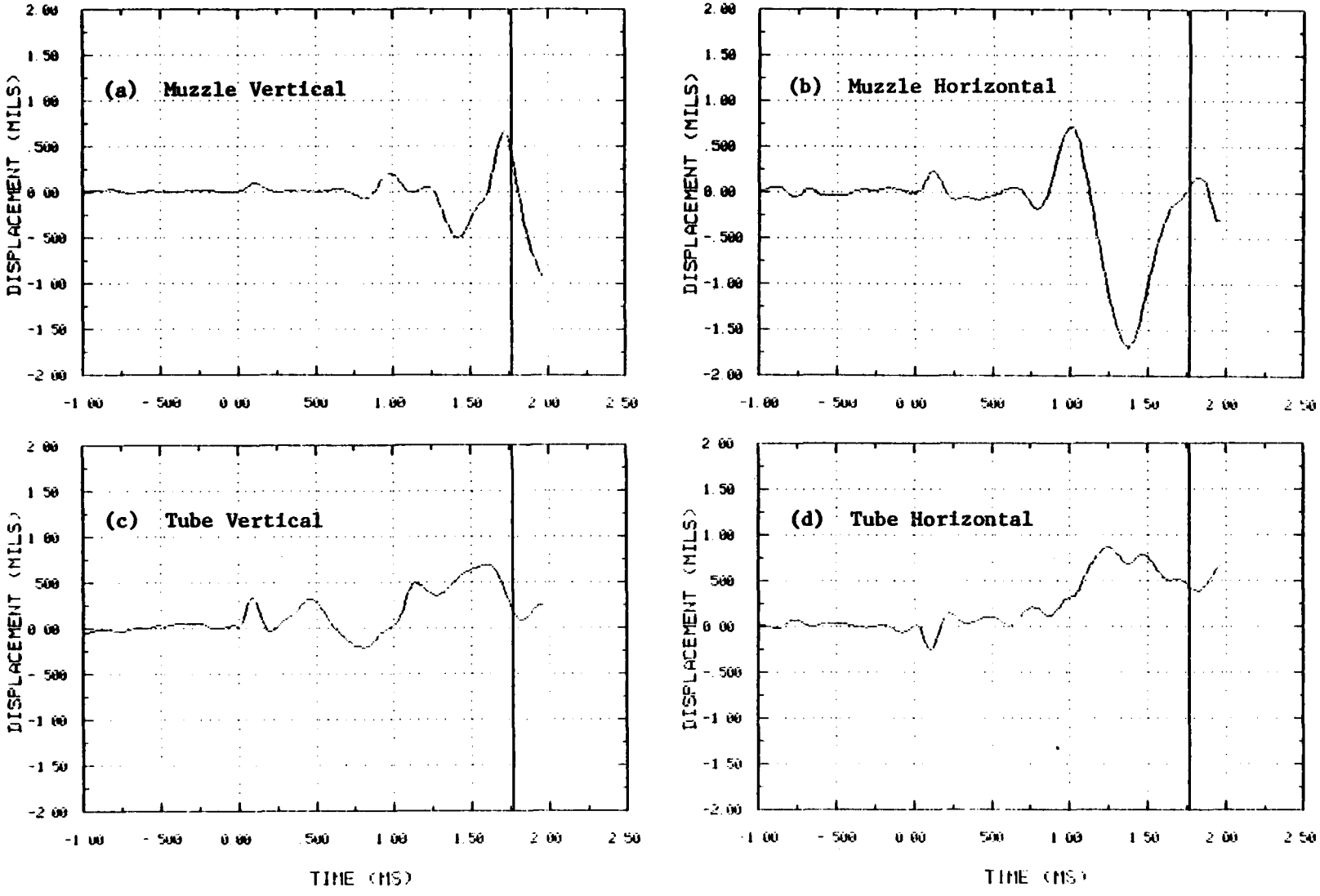

FIGURE A-8 MEASURED DISPLACEMENTS FOR TEST NO. 53 (Continued)

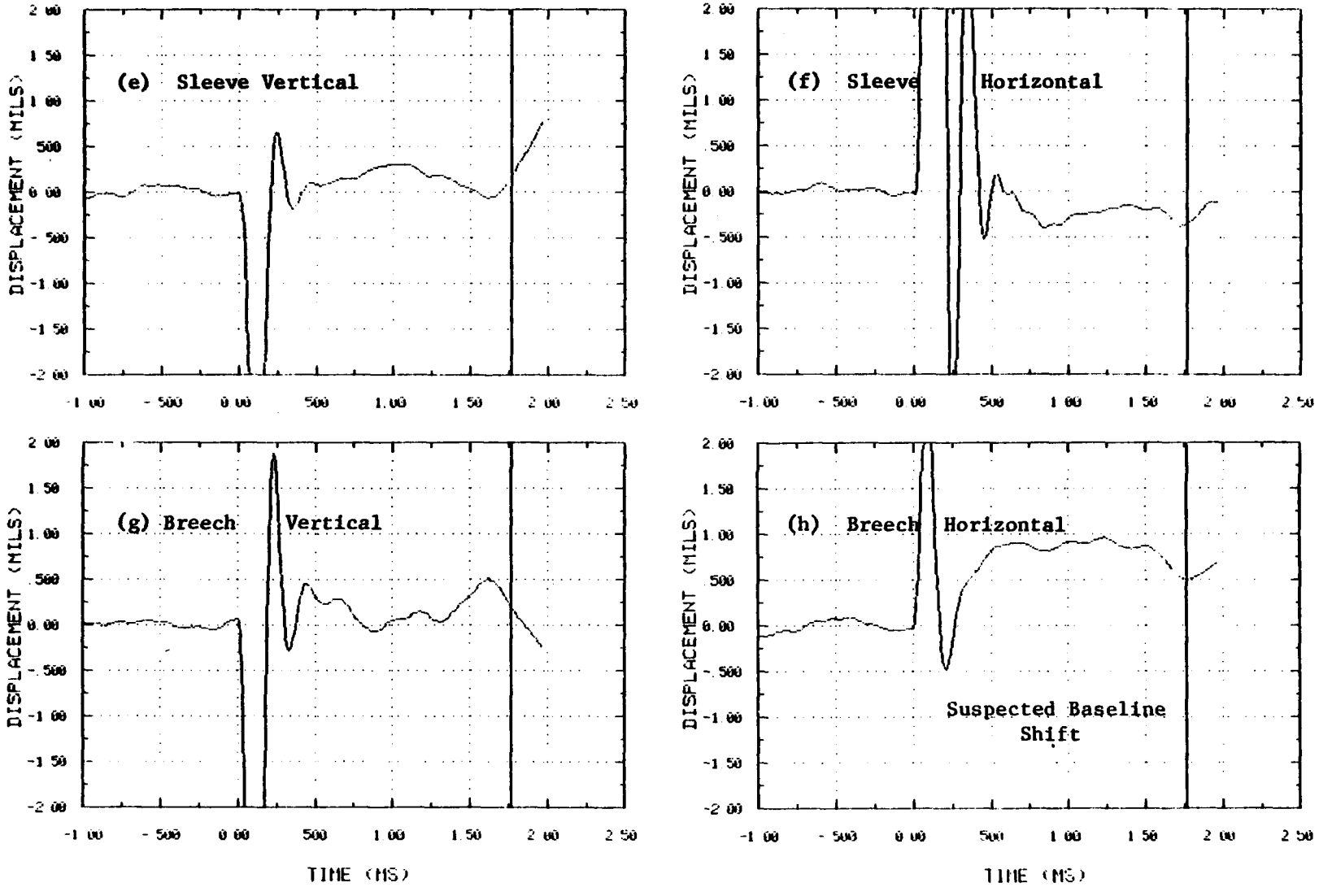

FIGURE A-8 MEASURED DISPLACEMENTS FOR TEST NO. 53 (Concluded)

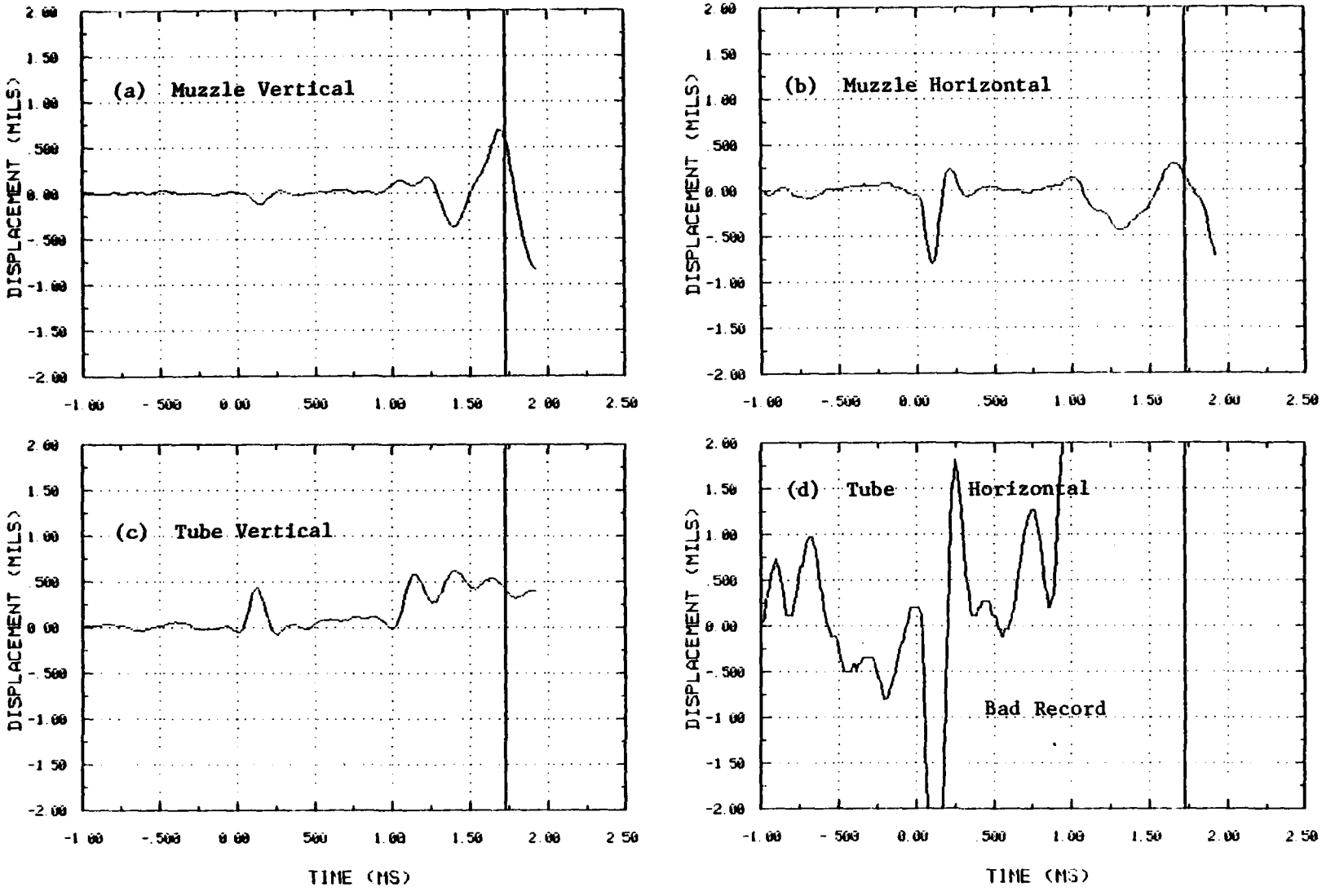

FIGURE A-9 MEASURED DISPLACEMENTS FOR TEST NO. 55 (Continued)

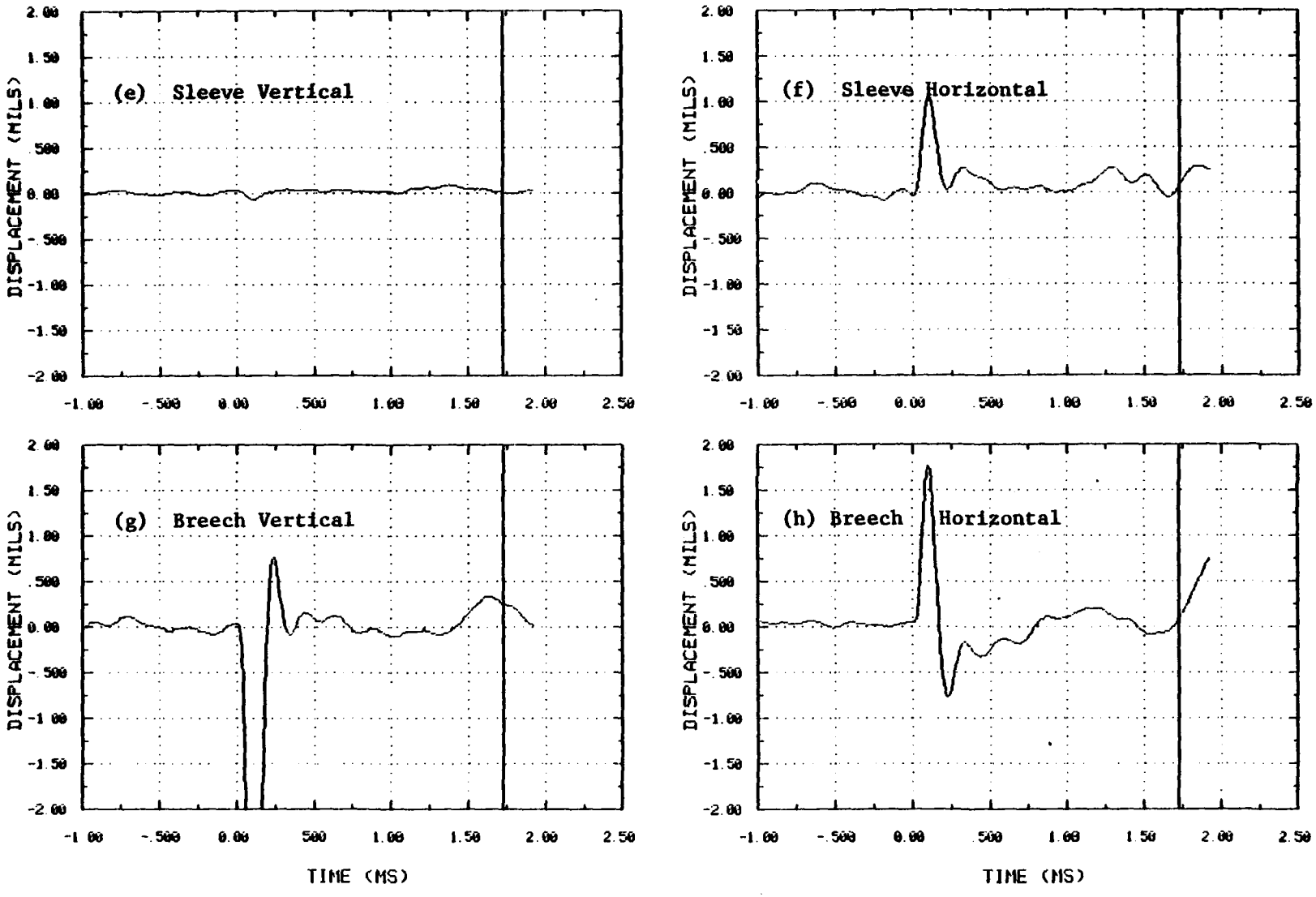

FIGULE NO. A-9 MEASURED DISPLACEMENTS FOR TEST NO. 55 (Concluded)

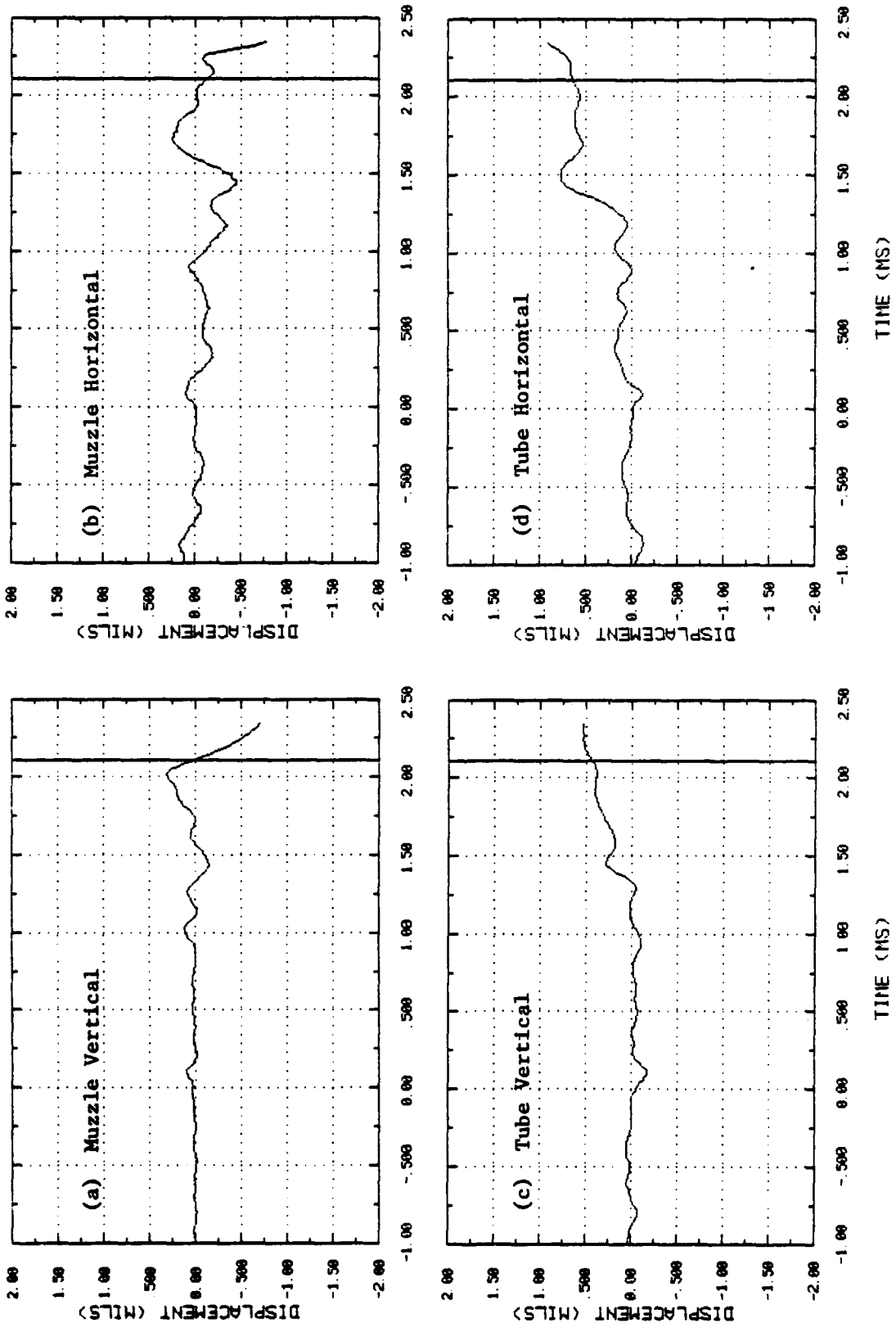

FIGURE A-10 MEASURED DISPLACEMENTS FOR TEST NO. 58 (Continued)

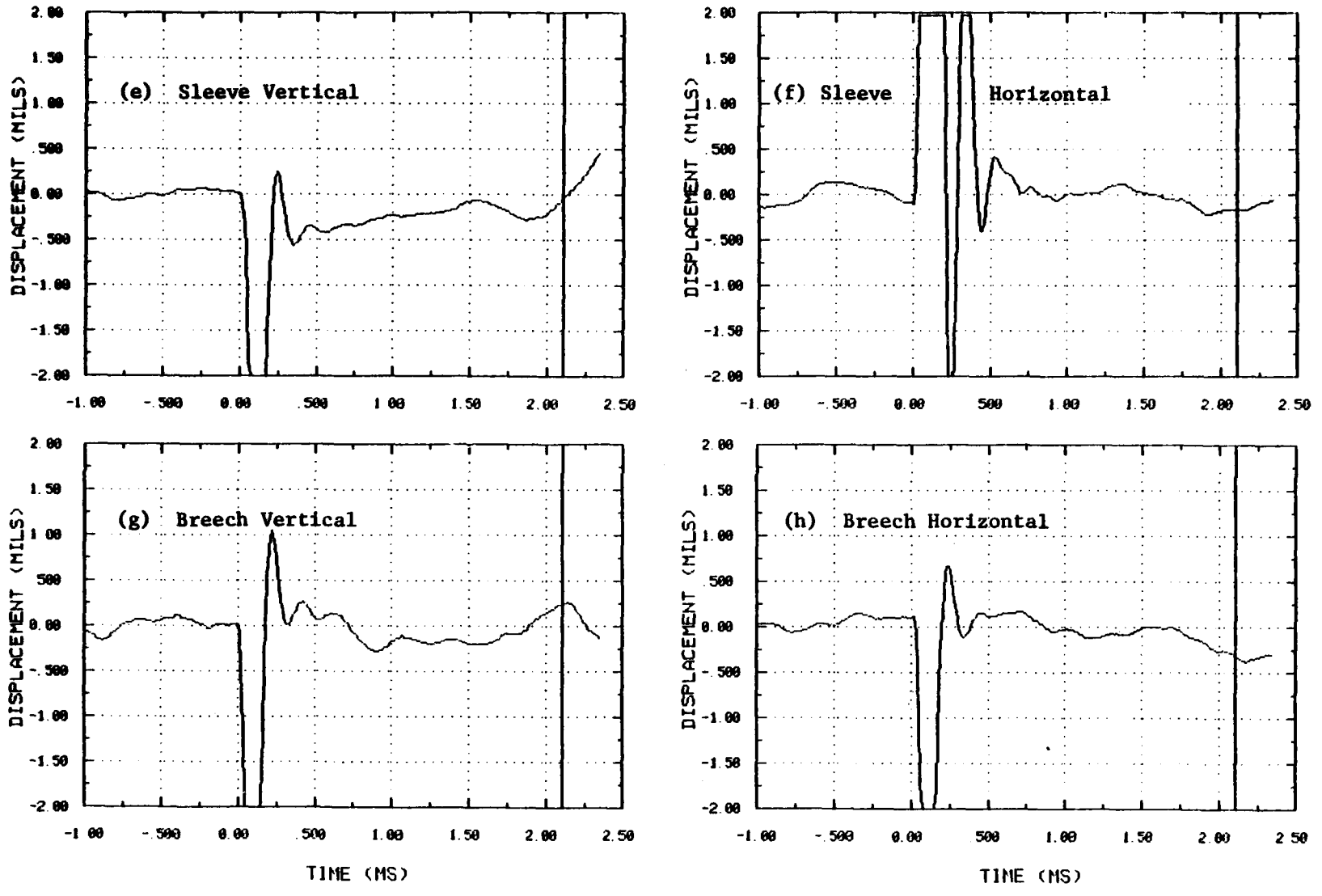

FIGURE A-10 MEASURED DISPLACEMENTS FOR TEST NO. 58 (Concluded)

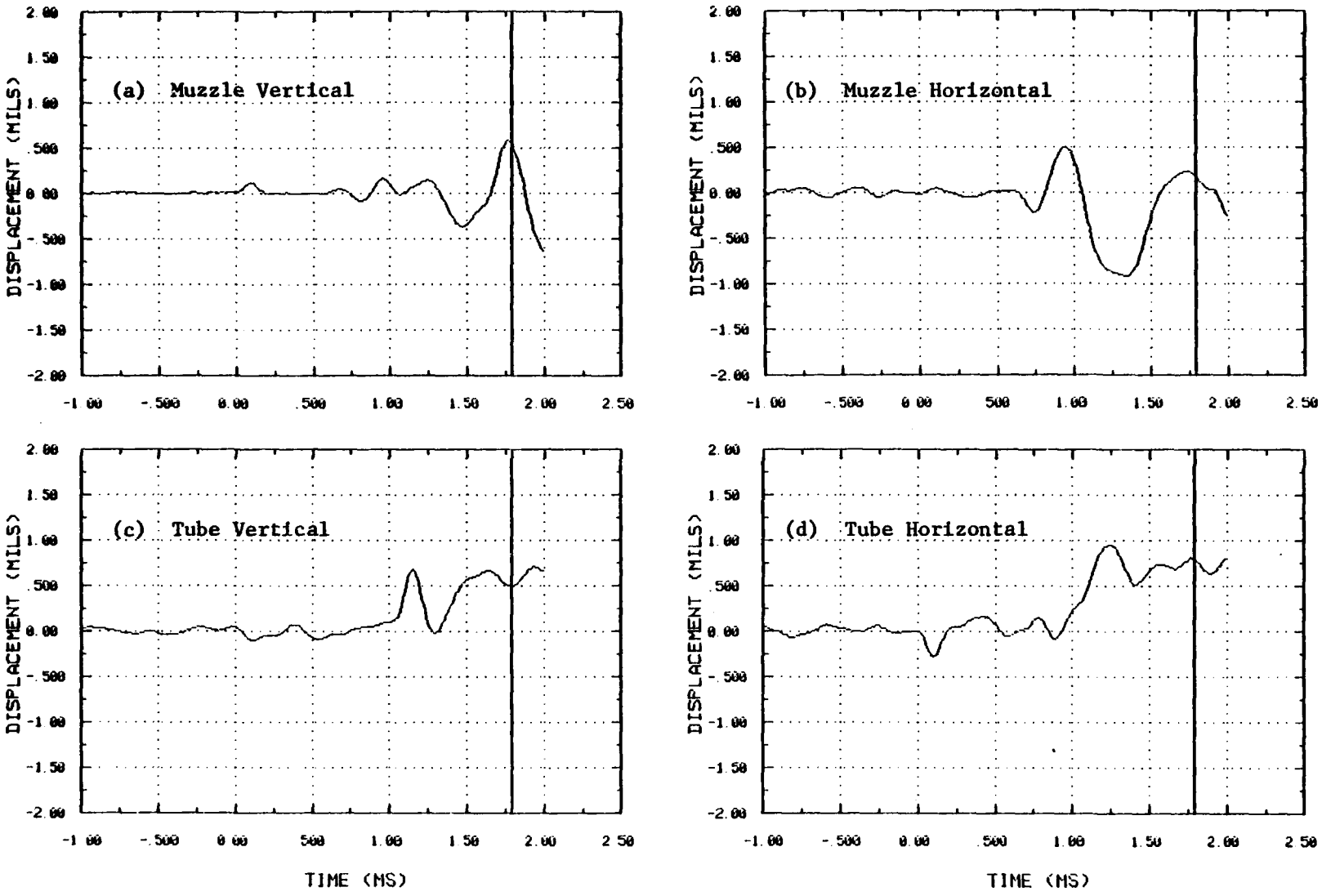

FIGURE A-11 MEASURED DISPLACEMENTS FOR TEST NO. 61 (Continued)

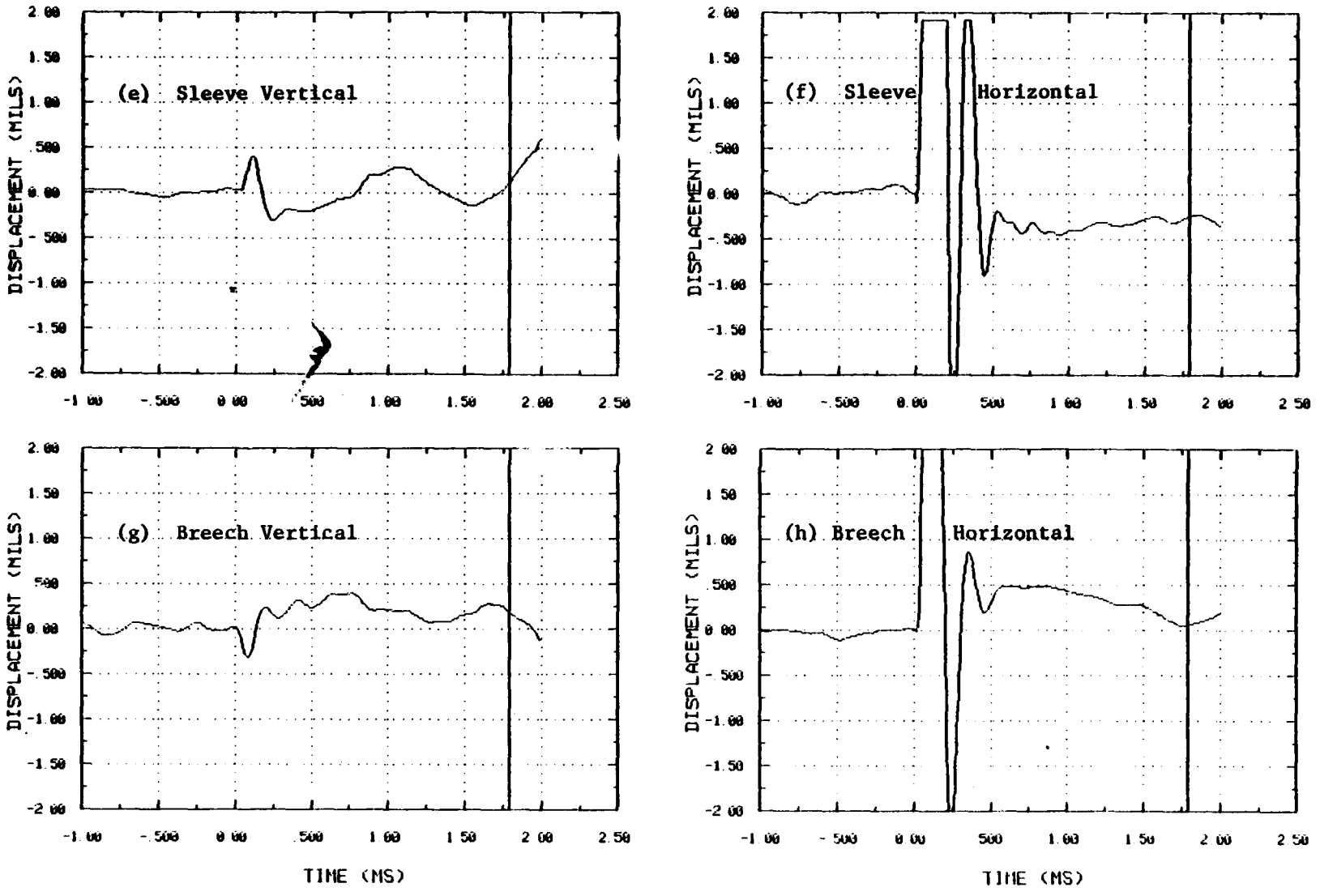

FIGURE A-11 MEASURED DISPLACEMENTS FOR TEST NO. 61 (Concluded)

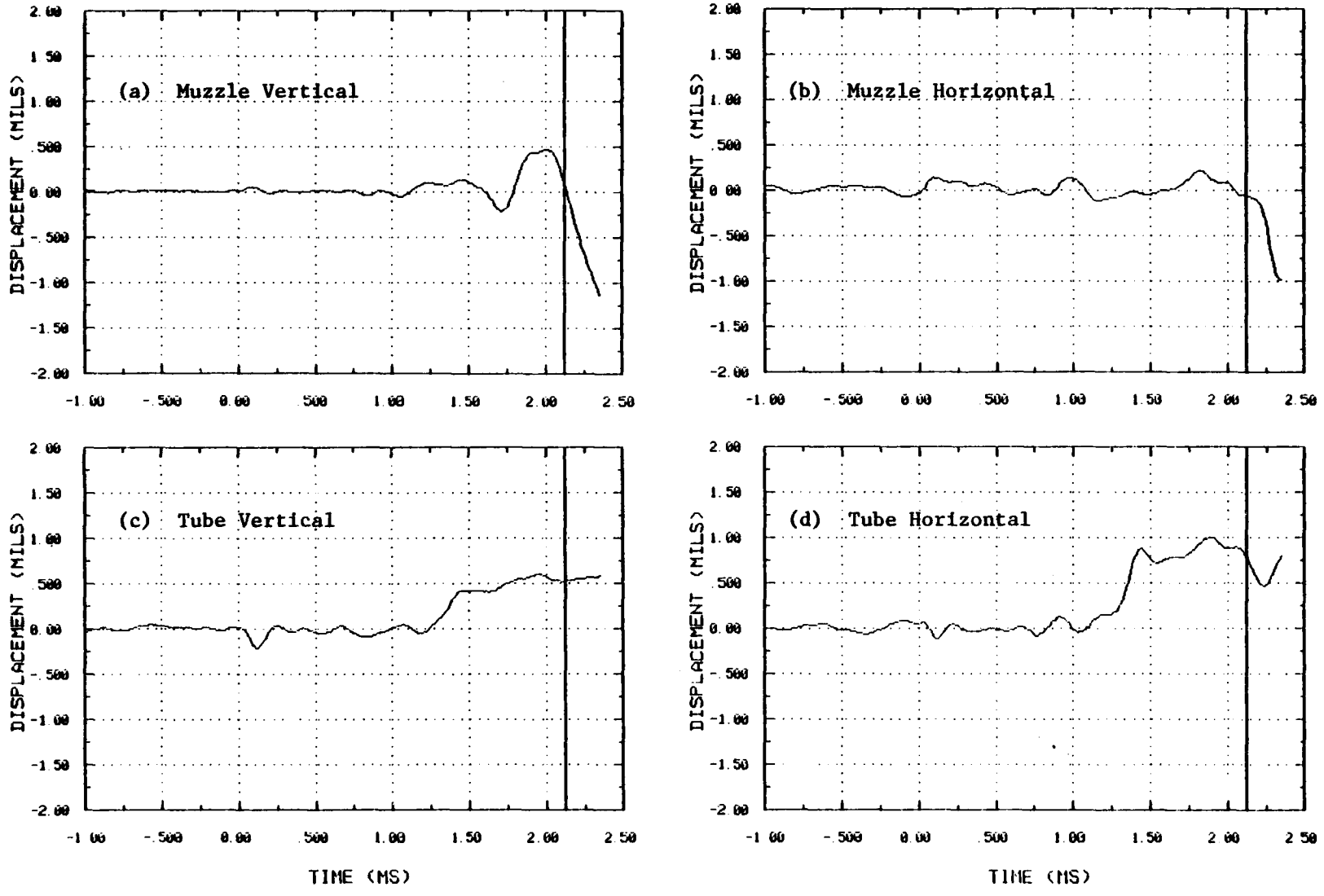

FIGURE A-12 MEASURED DISPLACEMENTS FOR TEST NO. 64 (Continued)

AD-A119 726 SOUTHWEST RESEARCH INST SAN ANTONIO TX F/G 12/1
THE INFLUENCE OF TUBE SUPPORT CONDITIONS ON MUZZLE MOTIONS.(U)
JUN 82 P A COX, J C HOKANSON DAAG29-79-C-0037

UNCLASSIFIED ARO-15722.2-EG NL

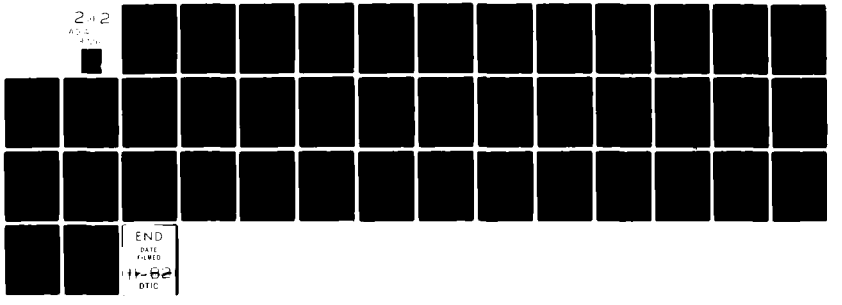

END
DATE FILMED
11-82
DTIC

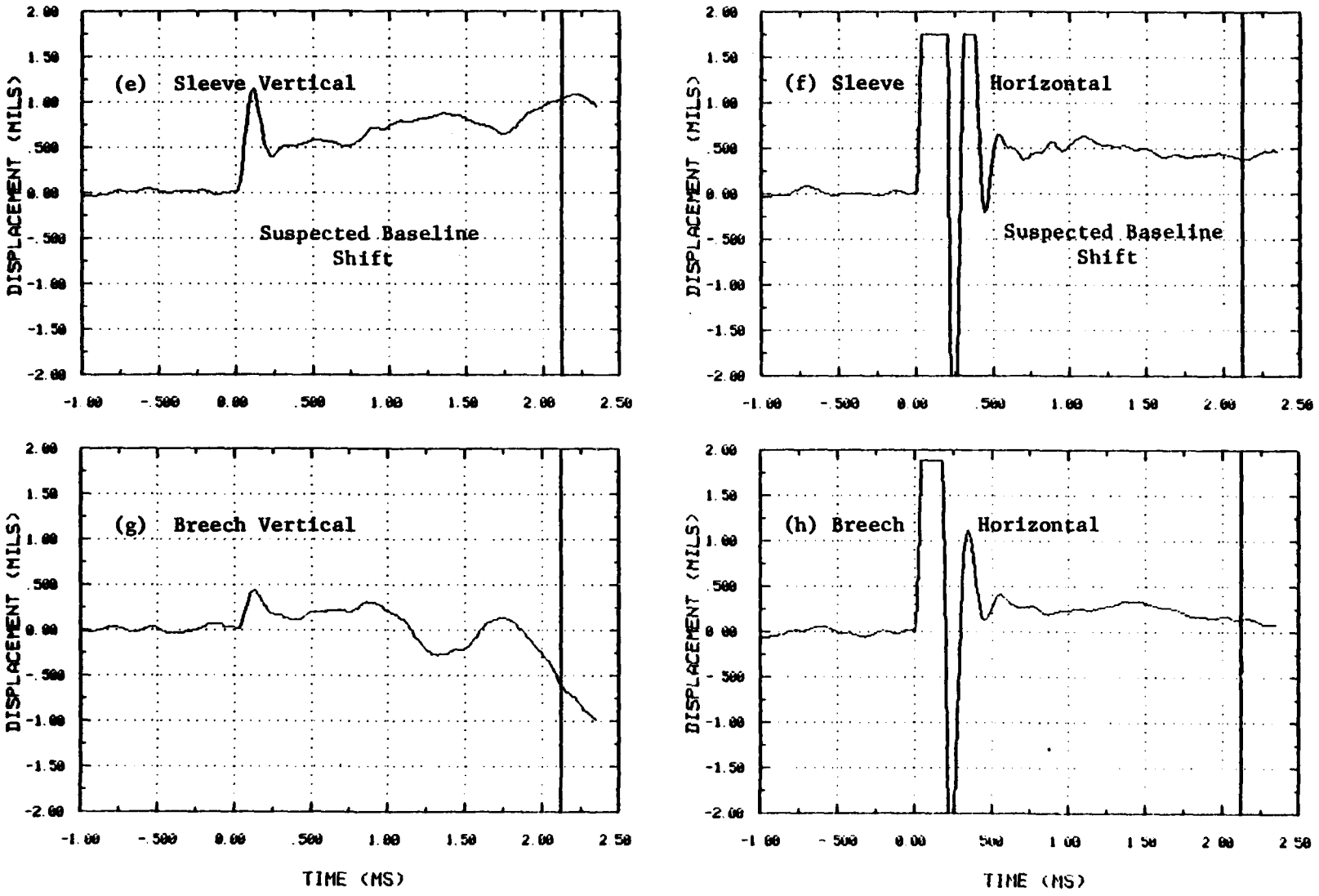

FIGURE A-12 MEASURED DISPLACEMENTS FOR TEST NO. 64 (Concluded)

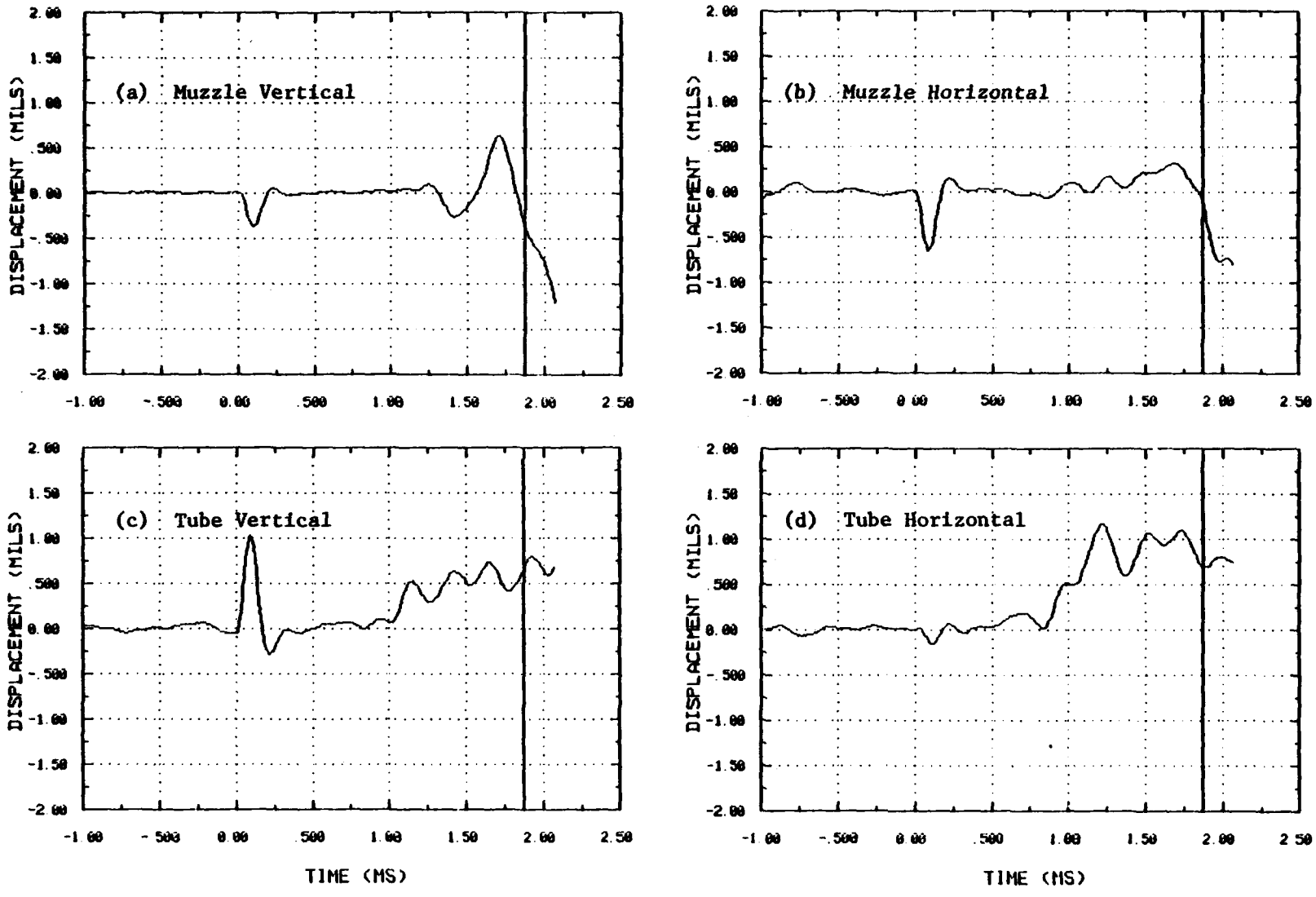

FIGURE A-13 MEASURED DISPLACEMENTS FOR TEST NO. 65 (Continued)

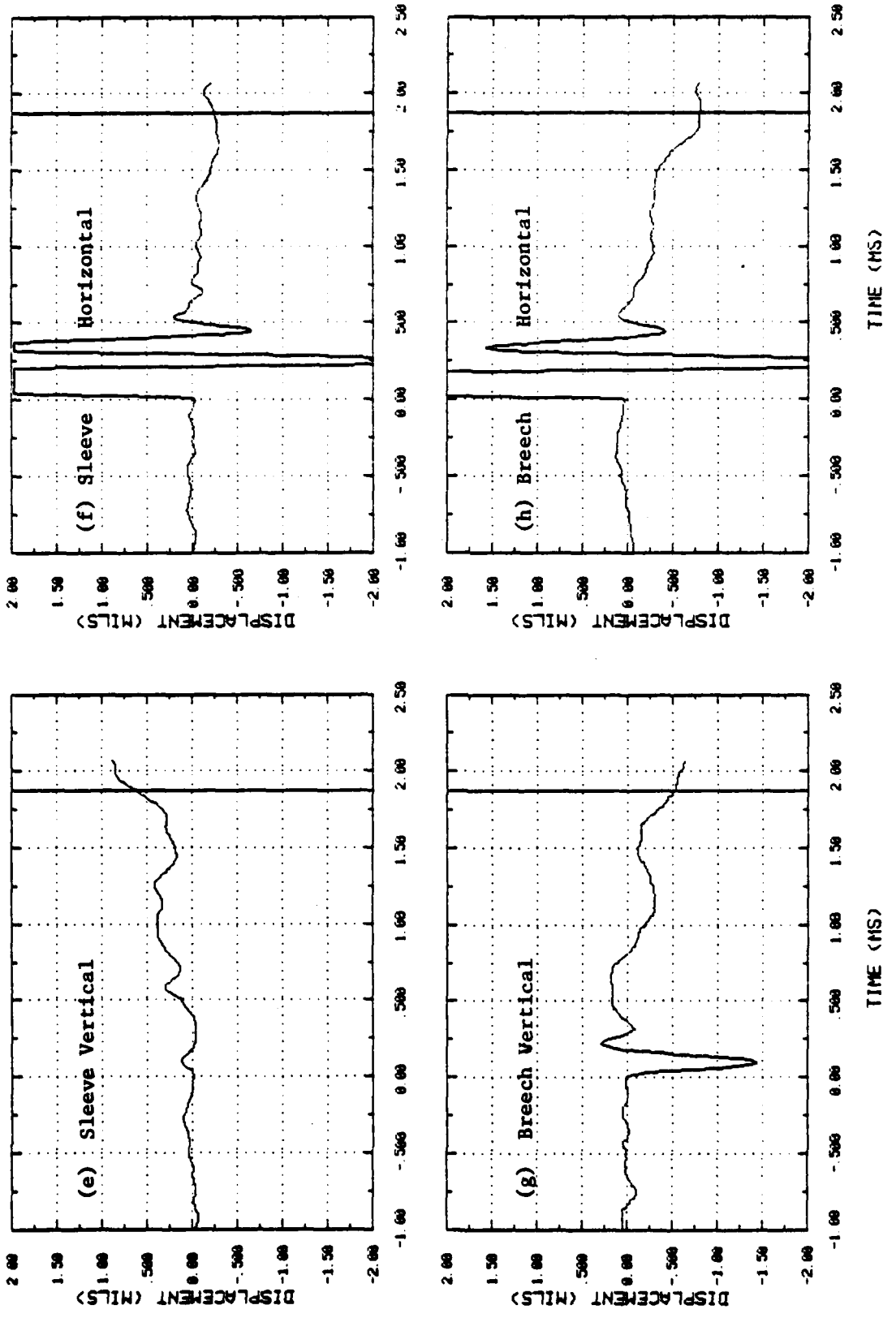

FIGURE A-13 MEASURED DISPLACEMENTS FOR TEST NO. 65 (Concluded)

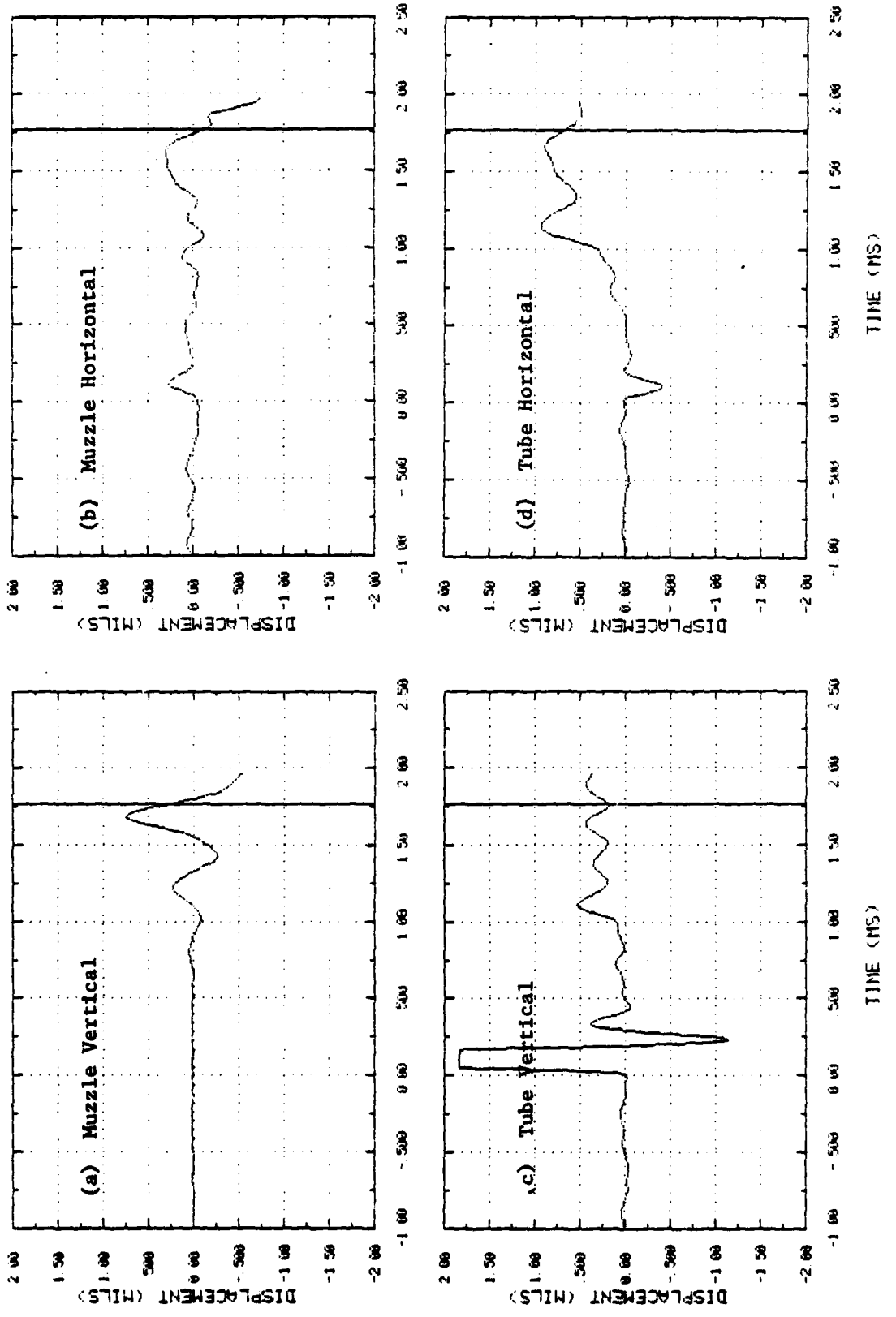

FIGURE A-14 MEASURED DISPLACEMENTS FOR TEST NO. 66 (Continued)

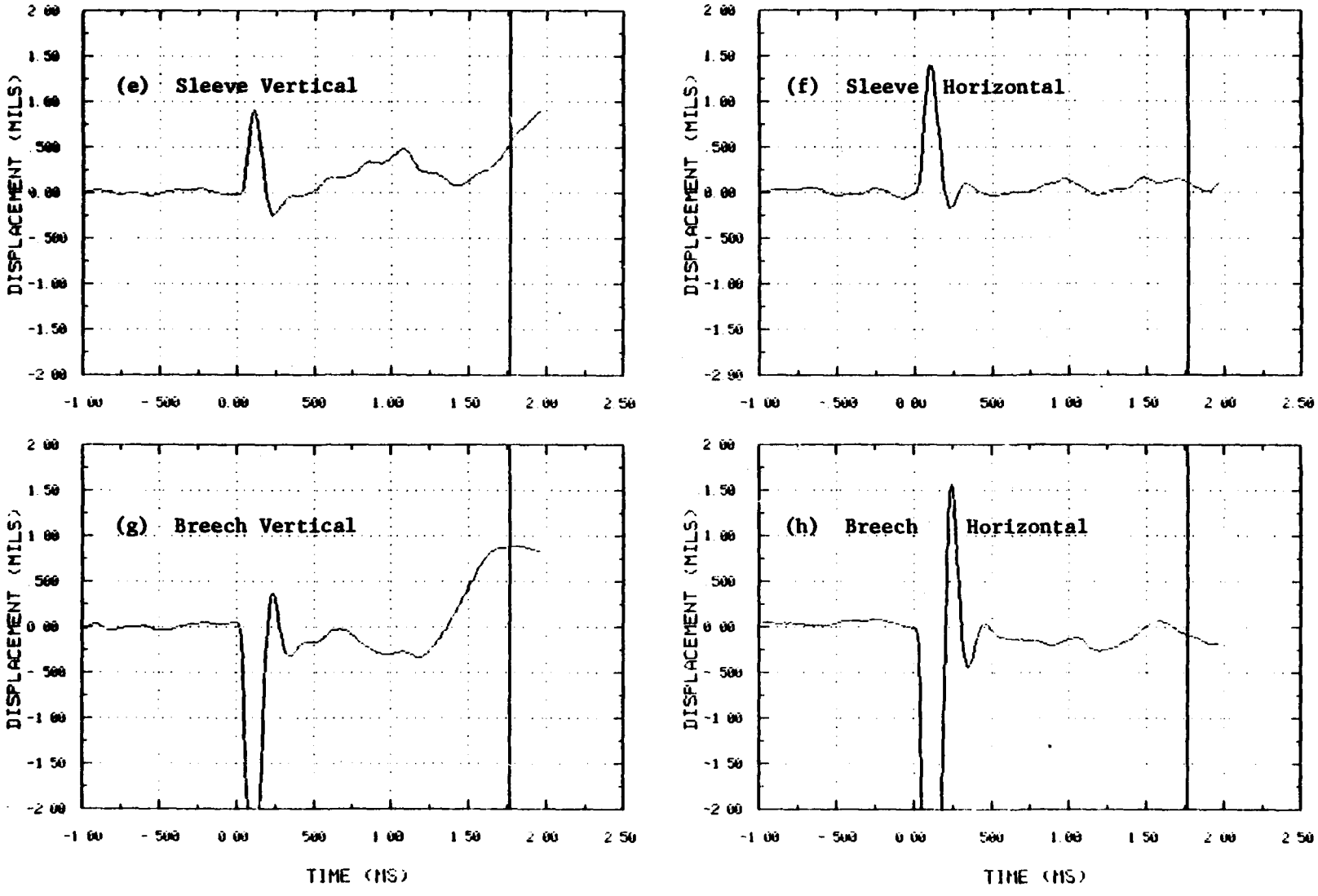

FIGURE A-14 MEASURED DISPLACEMENTS FOR TEST NO. 66 (Concluded)

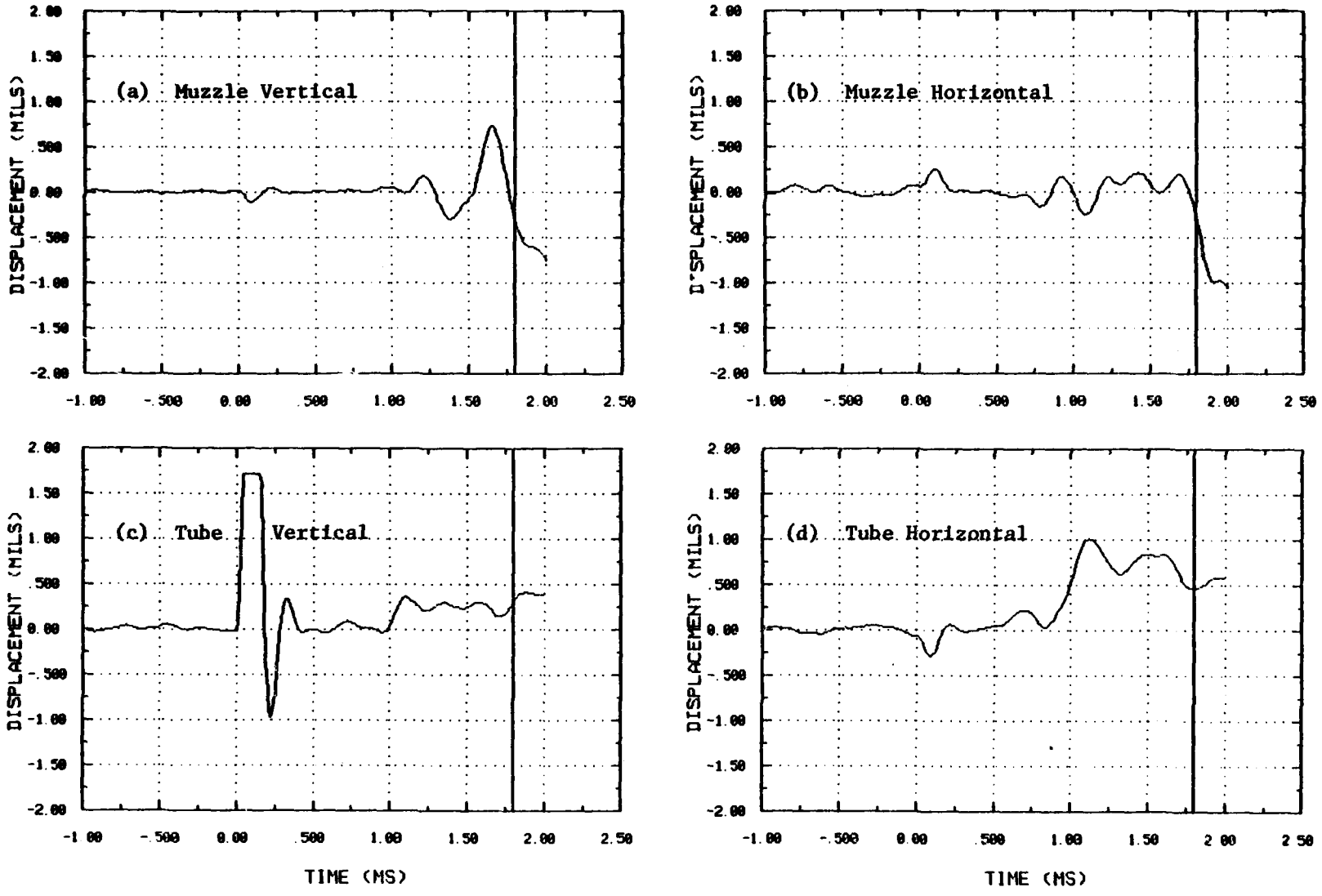

FIGURE A-15 MEASURED DISPLACEMENTS FOR TEST NO. 67 (Continued)

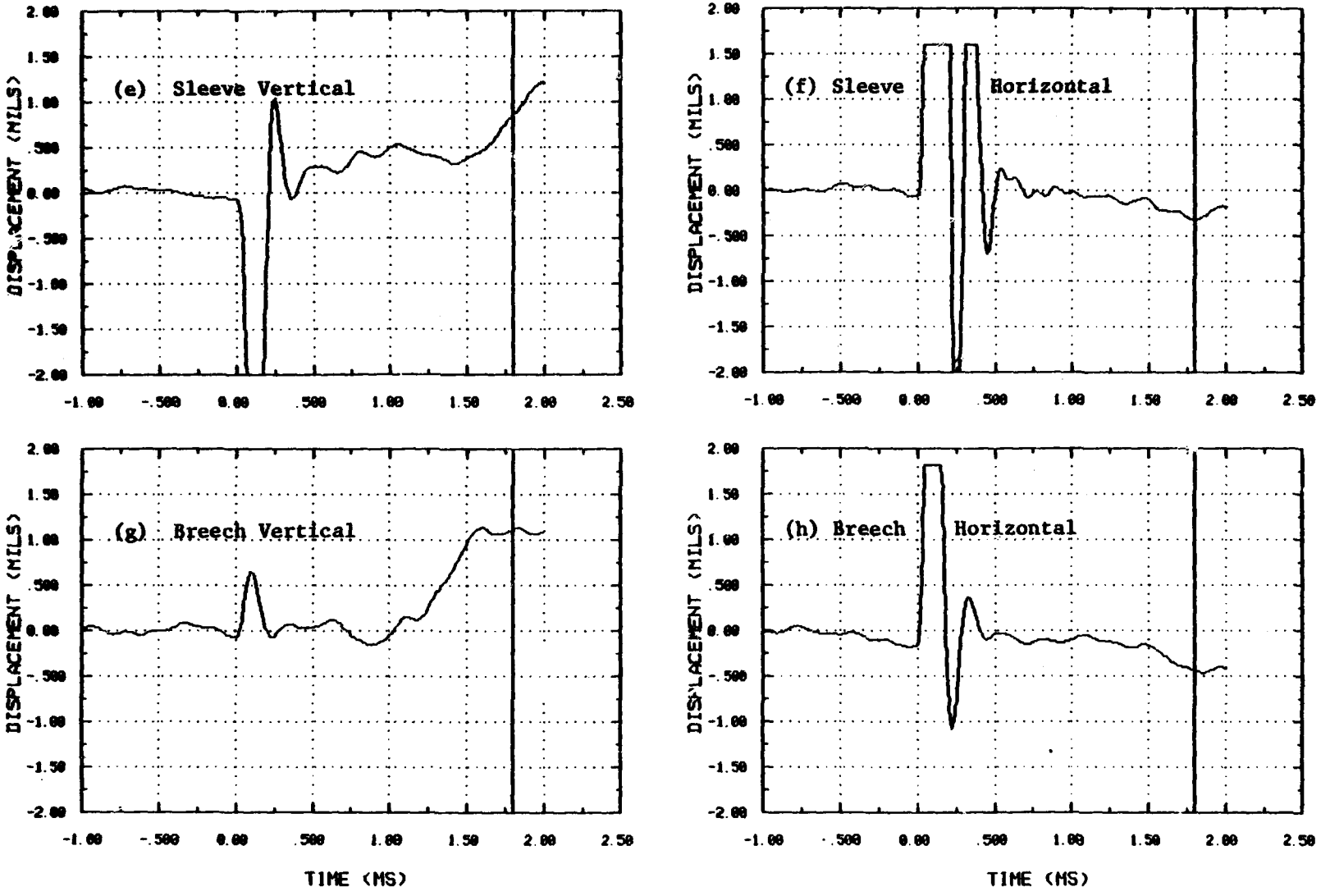

FIGURE A-15 MEASURED DISPLACEMENTS FOR TEST NO. 67 (Concluded)

APPENDIX B

GRAPHS OF CHAMBER PRESSURE
FOR TESTS

33
44
45
46
47
48
49
53
55
58
61
64
65
66
67

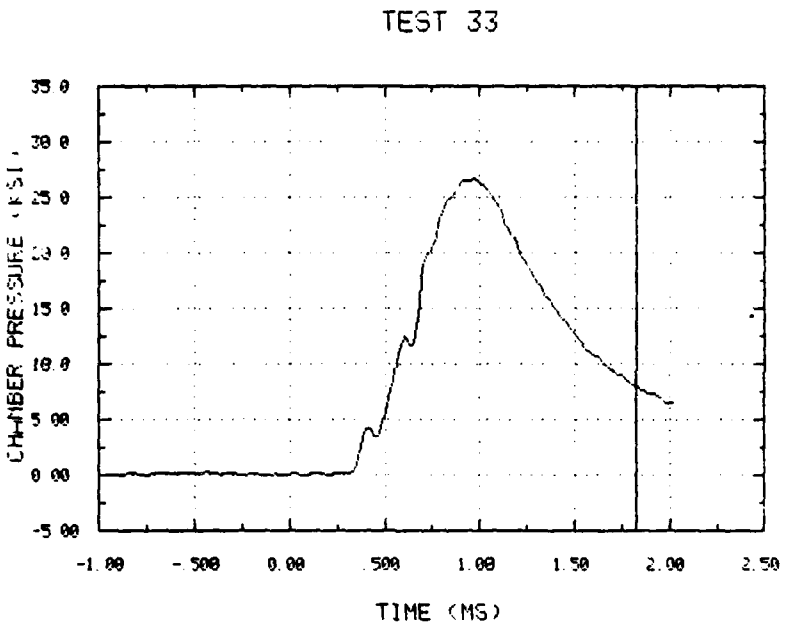

FIGURE B-1 MEASURED CHAMBER PRESSURE FOR TEST NO. 33

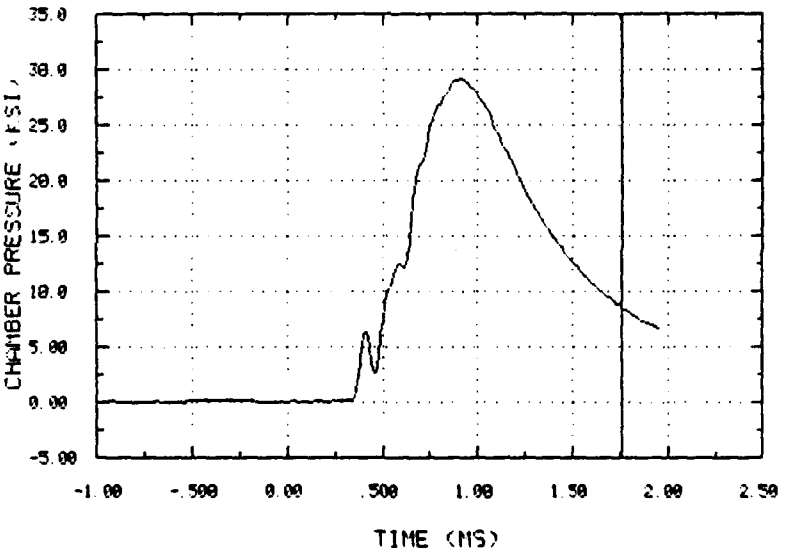

FIGURE B-2 MEASURED CHAMBER PRESSURE FOR TEST NO. 44

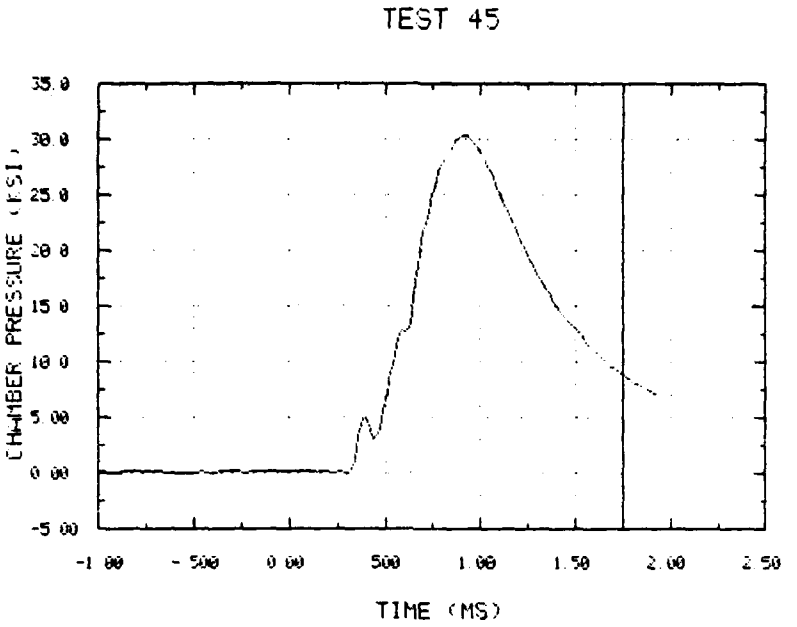

FIGURE B-3 MEASURED CHAMBER PRESSURE FOR TEST NO. 45

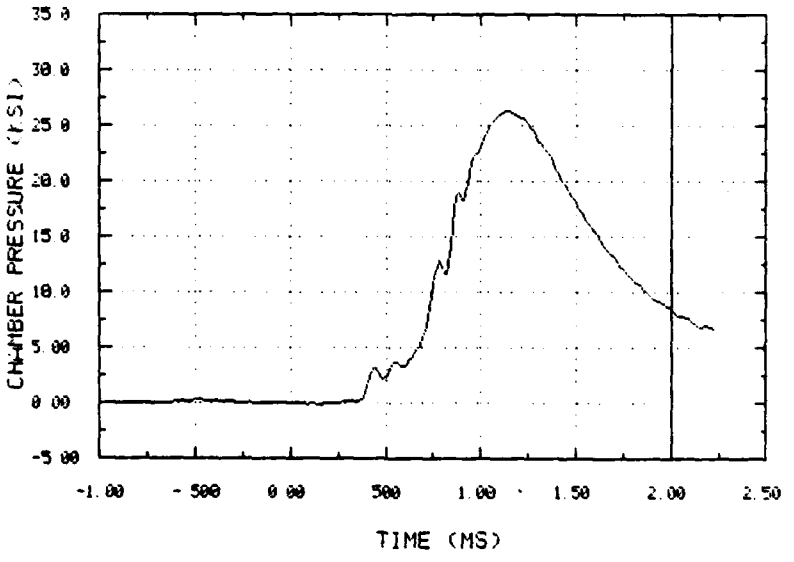

FIGURE B-4 MEASURED CHAMBER PRESSURE FOR TEST NO. 46

TEST 47

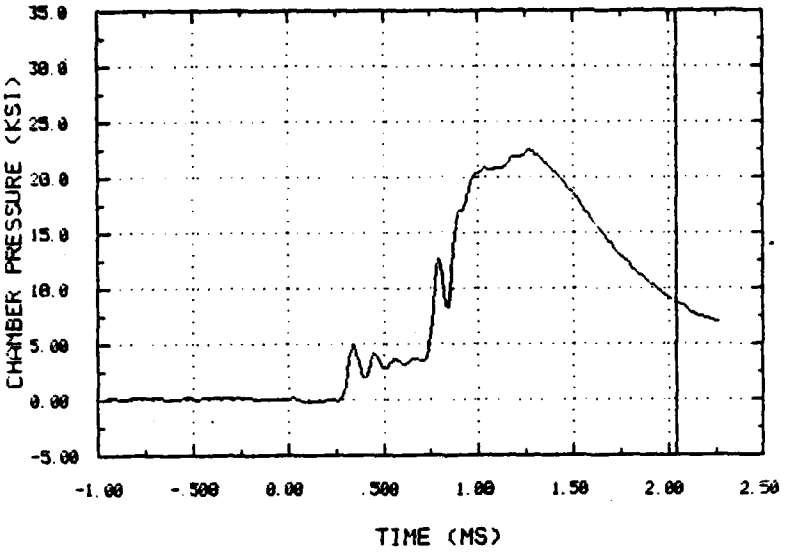

FIGURE B-5 MEASURED CHAMBER PRESSURE FOR TEST NO. 47

TEST 48

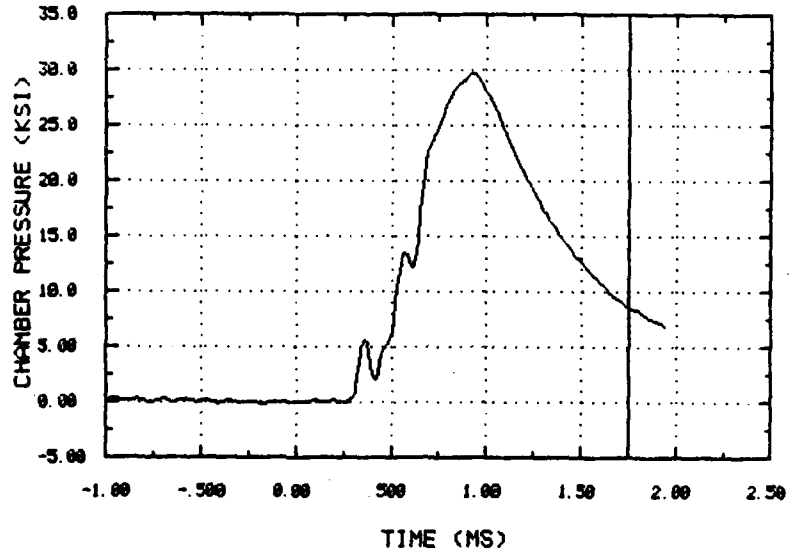

FIGURE B-6 MEASURED CHAMBER PRESSURE FOR TEST NO. 48

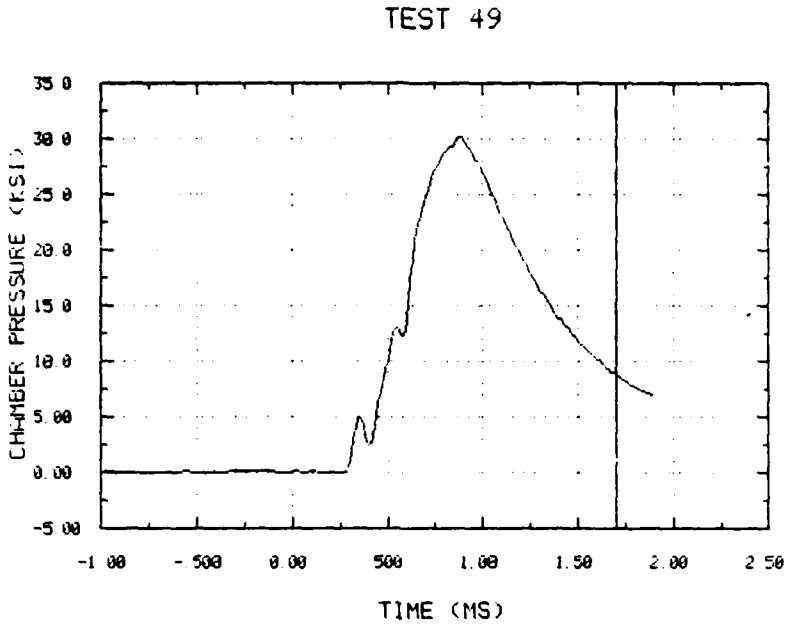

FIGURE B-7 MEASURED CHAMBER PRESSURE FOR TEST NO. 49

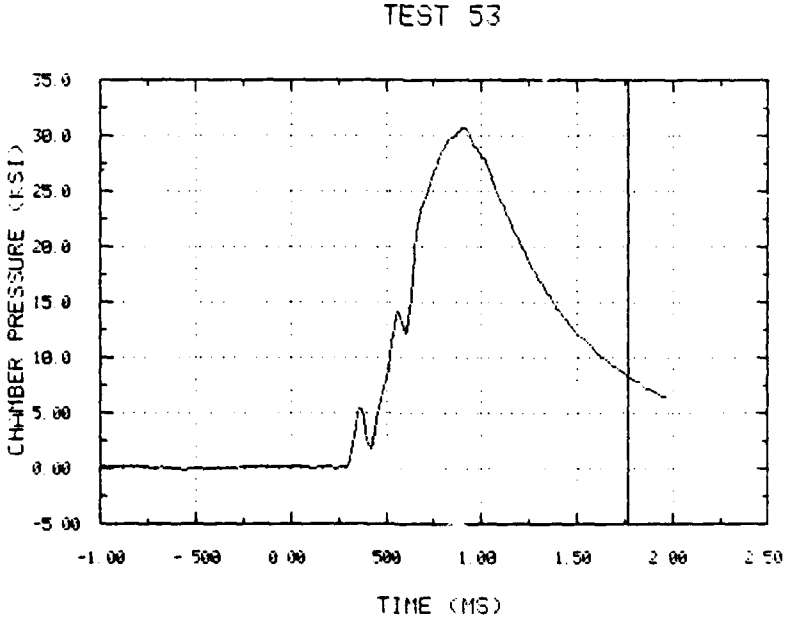

FIGURE B-8 MEASURED CHAMBER PRESSURE FOR TEST NO. 53

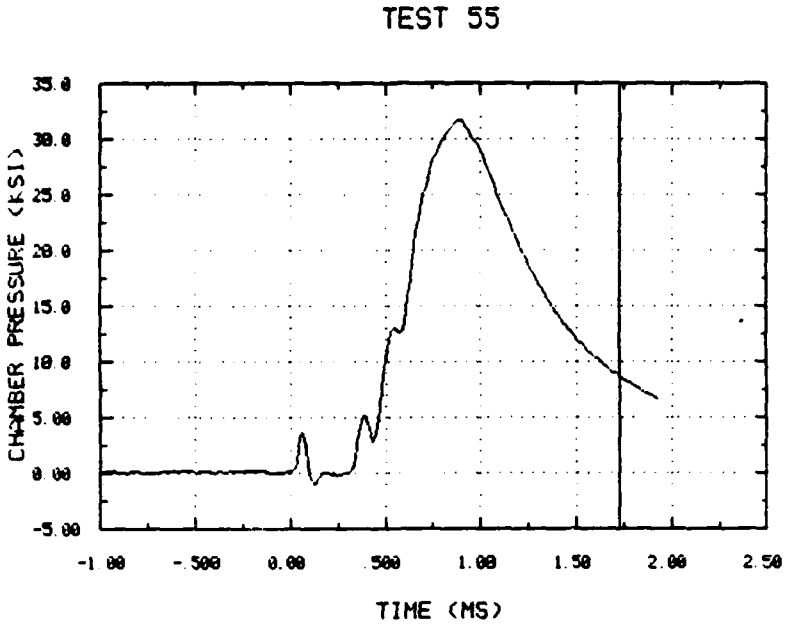

FIGURE B-9 MEASURED CHAMBER PRESSURE FOR TEST NO. 55

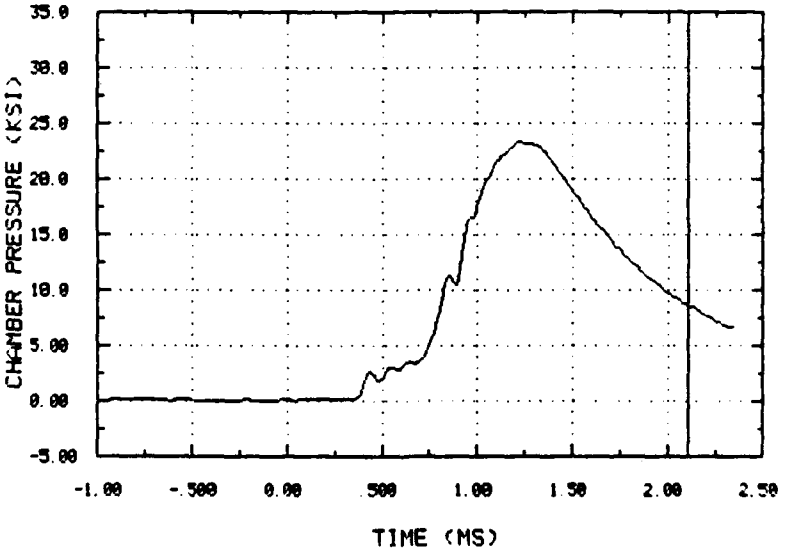

FIGURE B-10 MEASURED CHAMBER PRESSURE FOR TEST NO. 58

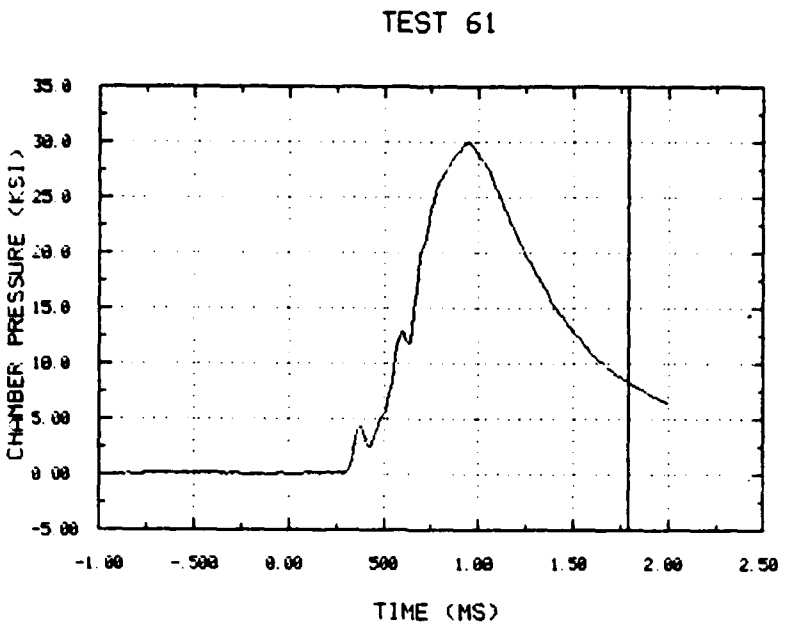

FIGURE B-11 MEASURED CHAMBER PRESSURE FOR TEST NO. 61

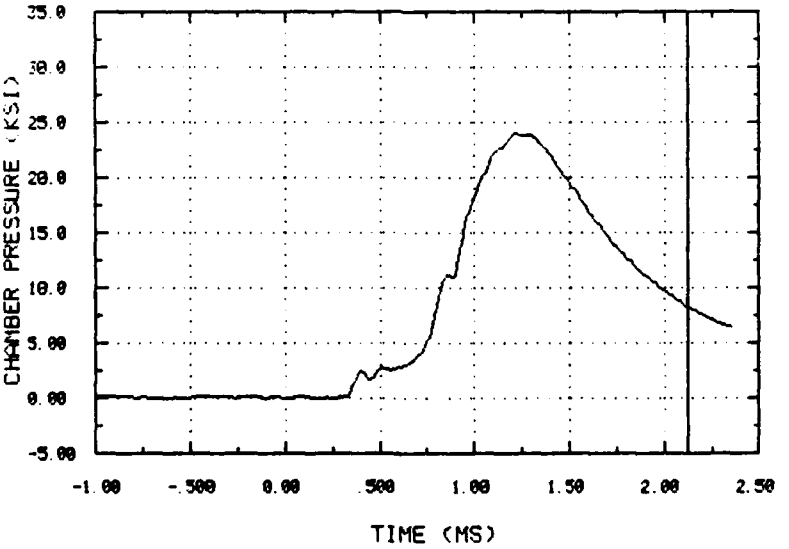

FIGURE B-12 MEASURED CHAMBER PRESSURE FOR TEST NO. 64

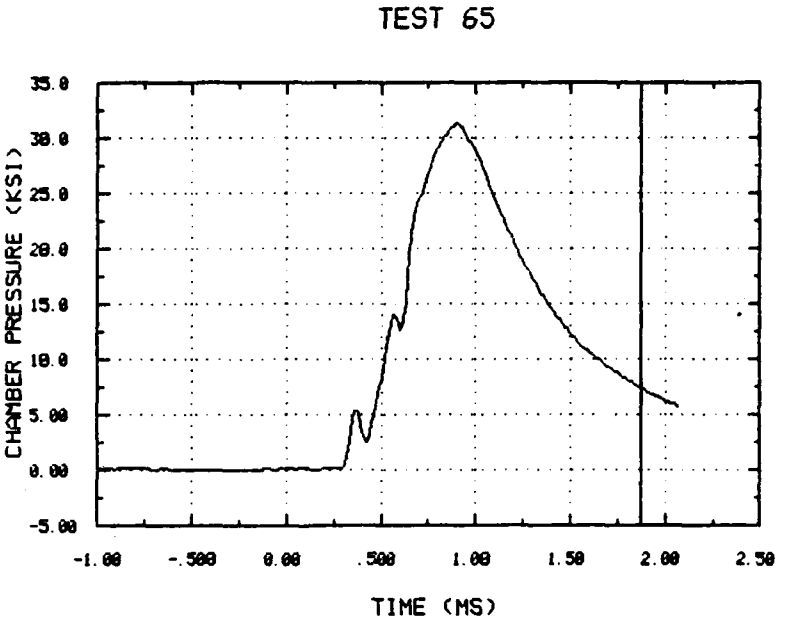

FIGURE B-13 MEASURED CHAMBER PRESSURE FOR TEST NO. 65

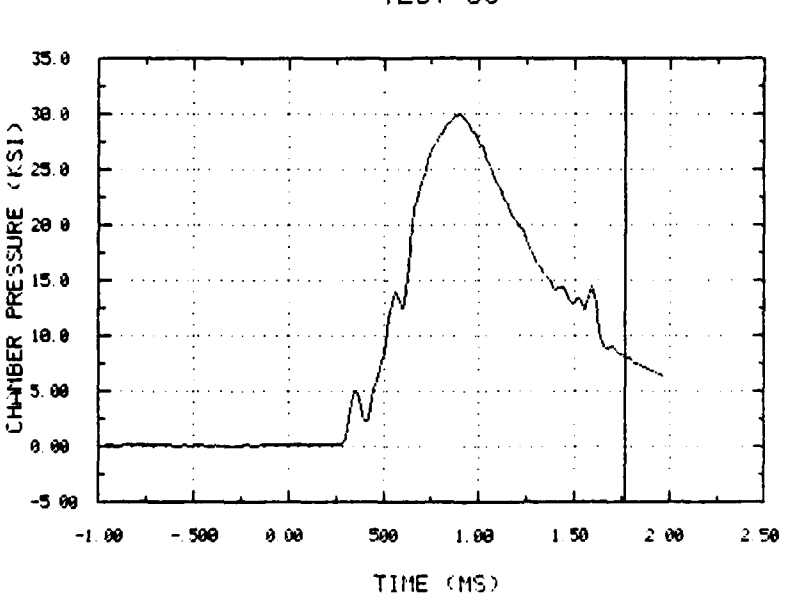

FIGURE B-14 MEASURED CHAMBER PRESSURE FOR TEST NO. 66

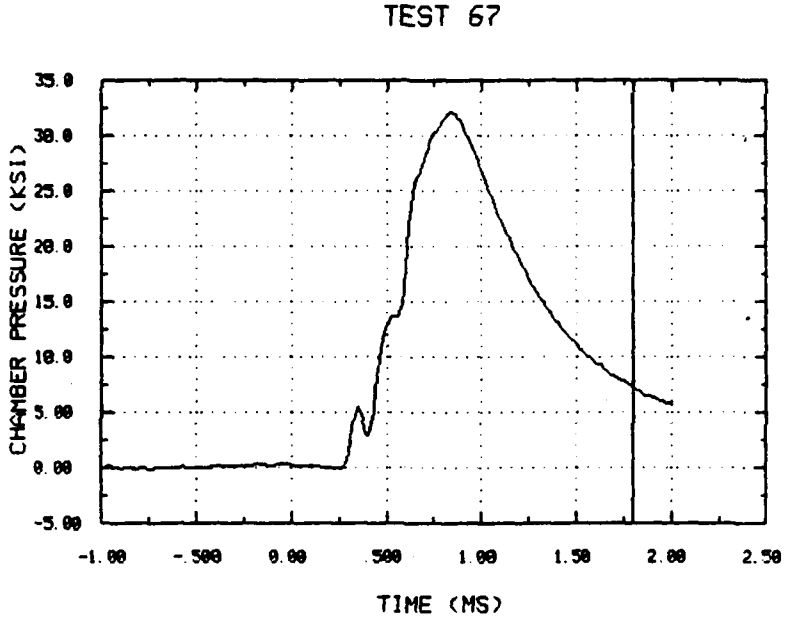

FIGURE B-15 MEASURED CHAMBER PRESSURE FOR TEST NO. 67

APPENDIX C

METHODOLOGY FOR CALCULATING PROJECTILE MOTIONS AND GRAPHS OF PROJECTILE DISPLACEMENT, VELOCITY, AND ACCELERATION FOR TESTS

33
44
45
46
53
55
58
66
67

APPENDIX C

Projectile displacement, velocity, and acceleration histories used in the muzzle motions computer program, G2DS, were calculated using the procedures described in this appendix. The chamber pressure (Appendix B) was measured in each of the experiments; however, the force driving the projectile out of the gun tube is proportional to the pressure applied to the base of the projectile, which could not be measured. A procedure was used for calculating the projectile motion, which consisted of estimating base pressures from the measured chamber pressures and integrating the resulting equations of motion. The technique used was an adaptation of the Lagrangian approximation for the projectile base pressure. This analysis assumed that the base pressure drop is inversely proportional to the momentum of the combustion products, that is:

$$\frac{P_{BASE}}{P_{CHAM}} = \frac{M_P V_P}{M_P V_P + 0.5\, A_B \rho_g x V} \qquad (C\text{-}1)$$

where M_P = projectile mass,
V_P = projectile velocity at time t,
A_B = base area of the projectile,
ρ_g = density of the reaction products at time t,
P_{BASE} = calculated base pressure at time t,
P_{CHAM} = measured chamber pressure at time t,
and x = distance traveled by the projectile up to time t.

Solving for the base pressure and simplifying the result gives:

$$P_{BASE} = \frac{P_{CHAM}}{1 + \frac{A_B \rho_g x}{2 M_P}} \qquad (C\text{-}2)$$

An empirical approach to solving Equation (2) was selected. In this case the equation can be re-written as:

$$P_{BASE} = \frac{P_{CHAM}}{1 + k x} \qquad (C\text{-}3)$$

In this equation the empirical constant k was varied in a series of calculations over a range of 0.5 to 0.75 in increments of 0.01. In any one calculation, the base pressure and projectile motions were calculated using the following equations.

$$V_F (t + dt) = V(t) + dt\, A(t) \qquad (C\text{-}4)$$

(Continued)

$$\bar{V}(t+dt) = 1 + \frac{V_F(t+dt)}{V_c} \qquad 1 + \frac{V_F(t+dt)R}{V_c}$$

$$P_{BASE}(t+dt) = P(t+dt) \quad \frac{1}{1 + kD(t)}$$

$$A(t+dt) = \frac{P_{BASE}(t+dt)\,A_B - FRICTN\,\bar{V}}{M_P} \qquad \text{(C-4)}$$

$$V(t+dt) = V(t) + \frac{[A(t+dt) + A(t)]\,dt}{2}$$

$$D(t+dt) = D(t) + \frac{[V(t+dt) + V(t)]\,dt}{2}$$

where $P(t)$ = measured chamber pressure at time t,
$P_{BASE}(t)$ = estimated base pressure at time t,
$D(t)$, $V(t)$, $A(t)$ = calculated projectile acceleration, velocity and displacement at time t,
dt = integration time step,
$VF(t)$ = initial estimate of the projectile velocity at time t,
$VC, R, FRICTN$ = empirical constants used to estimate the friction acting between the projectile and gun tube. In this effort (footnote 1):
R = 30.0
VC = $0.01 \cdot V_{ME}$ (in/s)
FRICTN = 500.0 (lb)
and V_{ME} is the measured muzzle velocity.

The initial values of the projectile acceleration, velocity, and displacement were all set to zero. The integration was carried out until the projectile displacement exceeded the available in-bore travel distance. The calculated projectile exit time and velocity were retained in each run. The empirical constant k which resulted in the best match with the measured muzzle exit time and velocity was used in the gun dynamics calculations presented in this report. The values of the empirical constant k used in these calculations are summarized in Table C-1. Plots of the calculated base pressure, projectile displacement, velocity and acceleration are given in Figure C-1 for Test 33. Chamber pressures for selected tests are given in Appendix B. Projectile motions for the other tests follow in this appendix.

(1) The form of the frictional force term was developed at the Interior Ballistics Laboratory of BRL. This form and the approximate values of the empirical constants were taken from previous work on the muzzle motions of the M68 tank gun (Reference 1).

TABLE C-1. SUMMARY OF THE CONSTANT k
USED IN THE GUN MOTION CALCULATIONS

Test No.	k	Exit Velocity (fps) Meas.	Calc.	Exit Time (ms) Meas.	Calc.
33	0.053	3380.	3377.	1.83	1.87
44	0.059	3463.	3457.	1.77	1.81
45	0.061	3502.	3497.	1.76	1.80
46	0.058	3354.	3355.	2.01	2.04
53	0.062	3499.	3494.	1.78	1.77
55	0.059	3507.	3512.	1.74	1.76
58	0.053	3253.	3253.	2.12	2.17
66	0.064	3450.	3455.	1.73	1.78
67	0.062	3535.	3533.	1.69	1.71

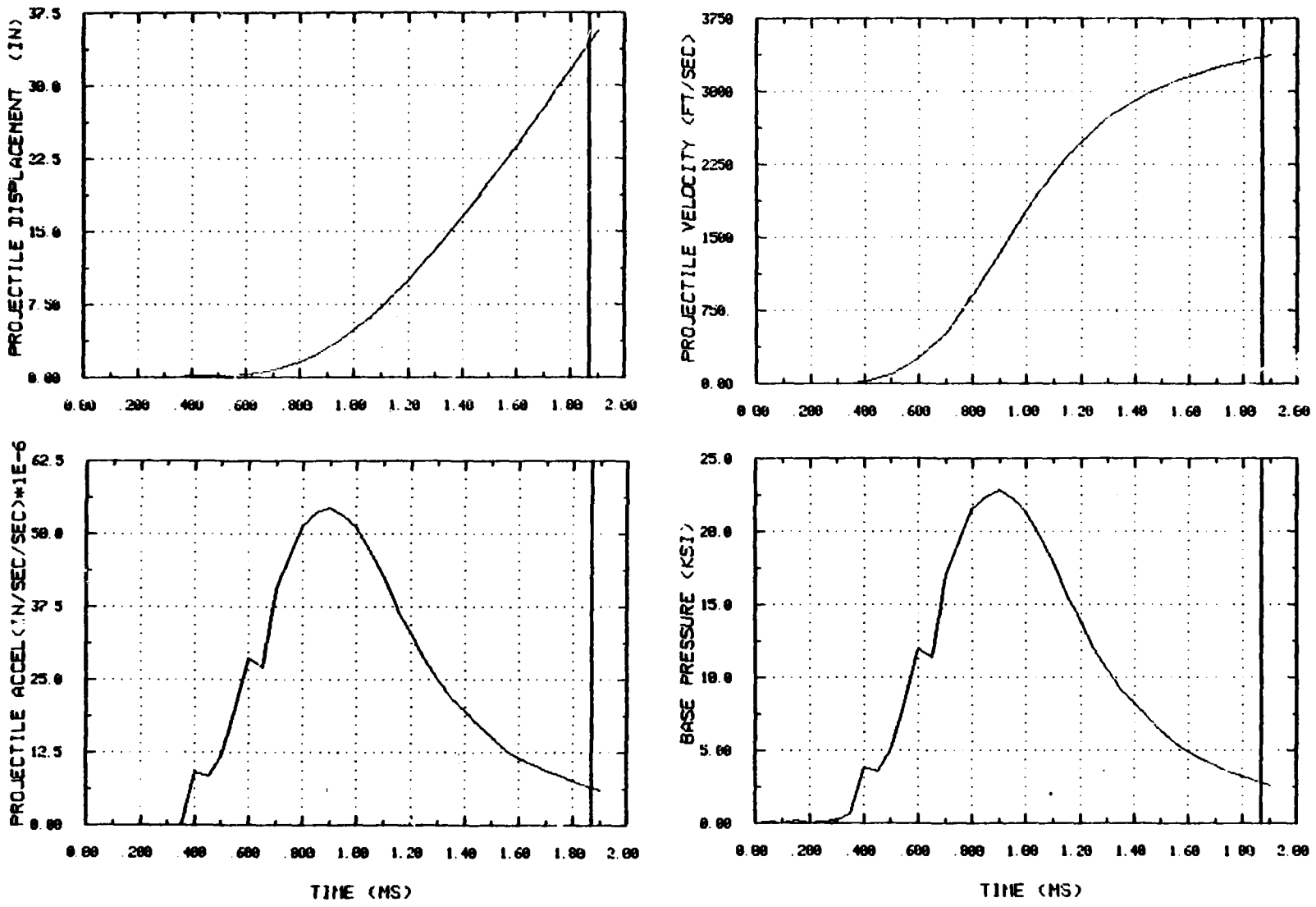

FIGURE C-1 PROJECTILE DISPLACEMENT, VELOCITY, ACCELERATION, AND CALCULATED BASE PRESSURE FOR TEST NO. 33

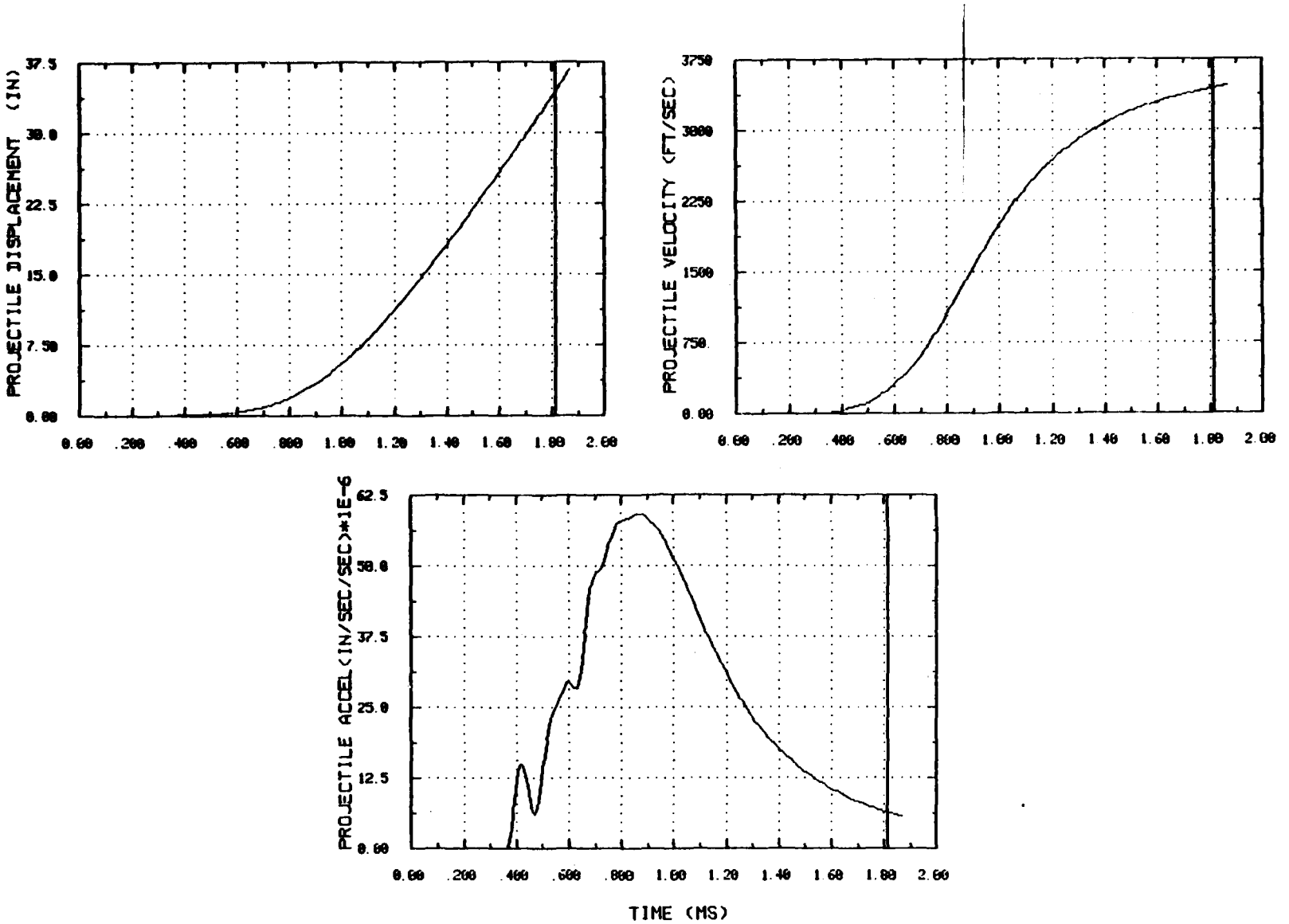

FIGURE C-2 PROJECTILE DISPLACEMENT, VELOCITY, AND ACCELERATION FOR TEST NO. 44

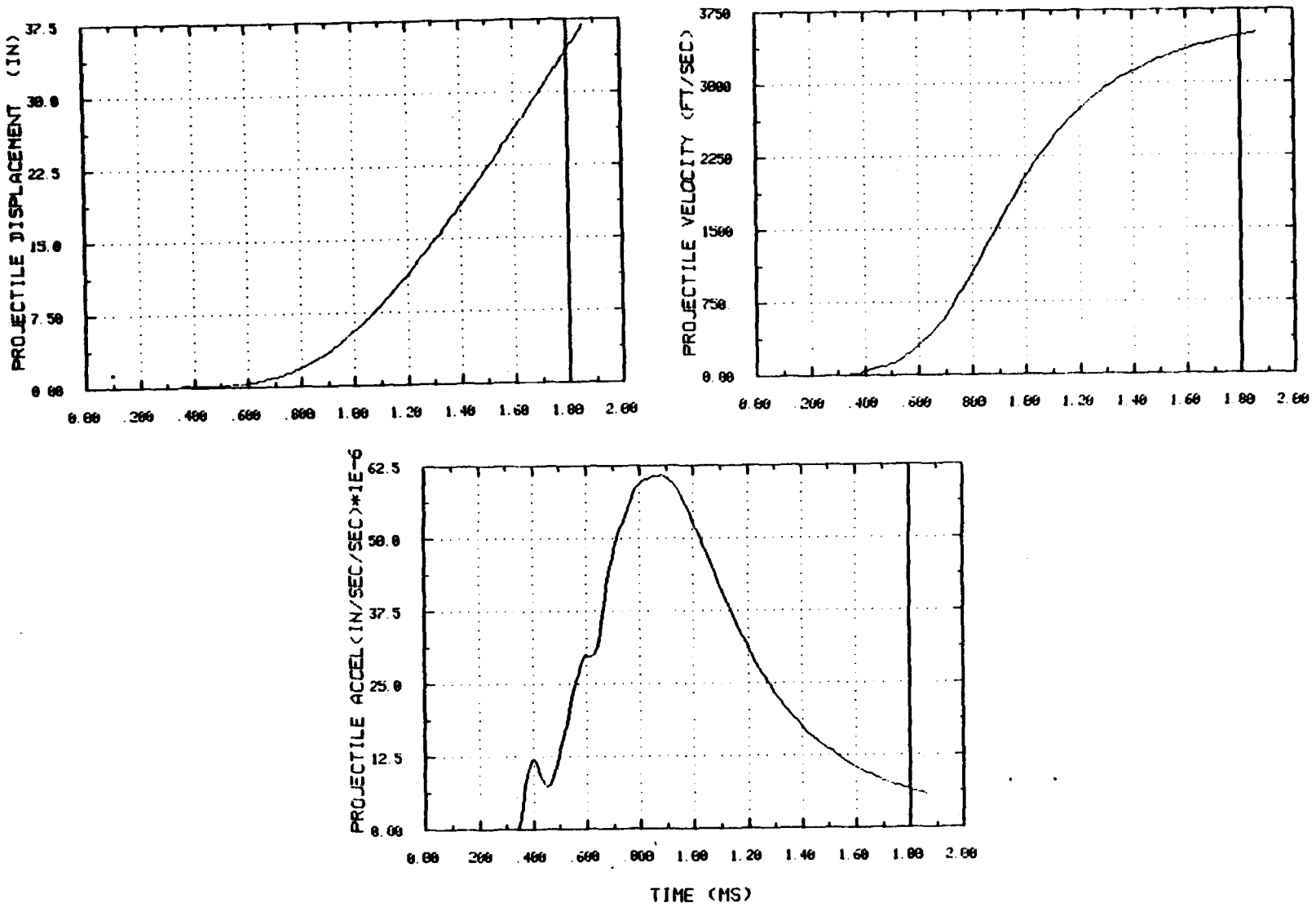

FIGURE C-3 PROJECTILE DISPLACEMENT, VELOCITY, AND ACCELERATION FOR TEST NO. 45

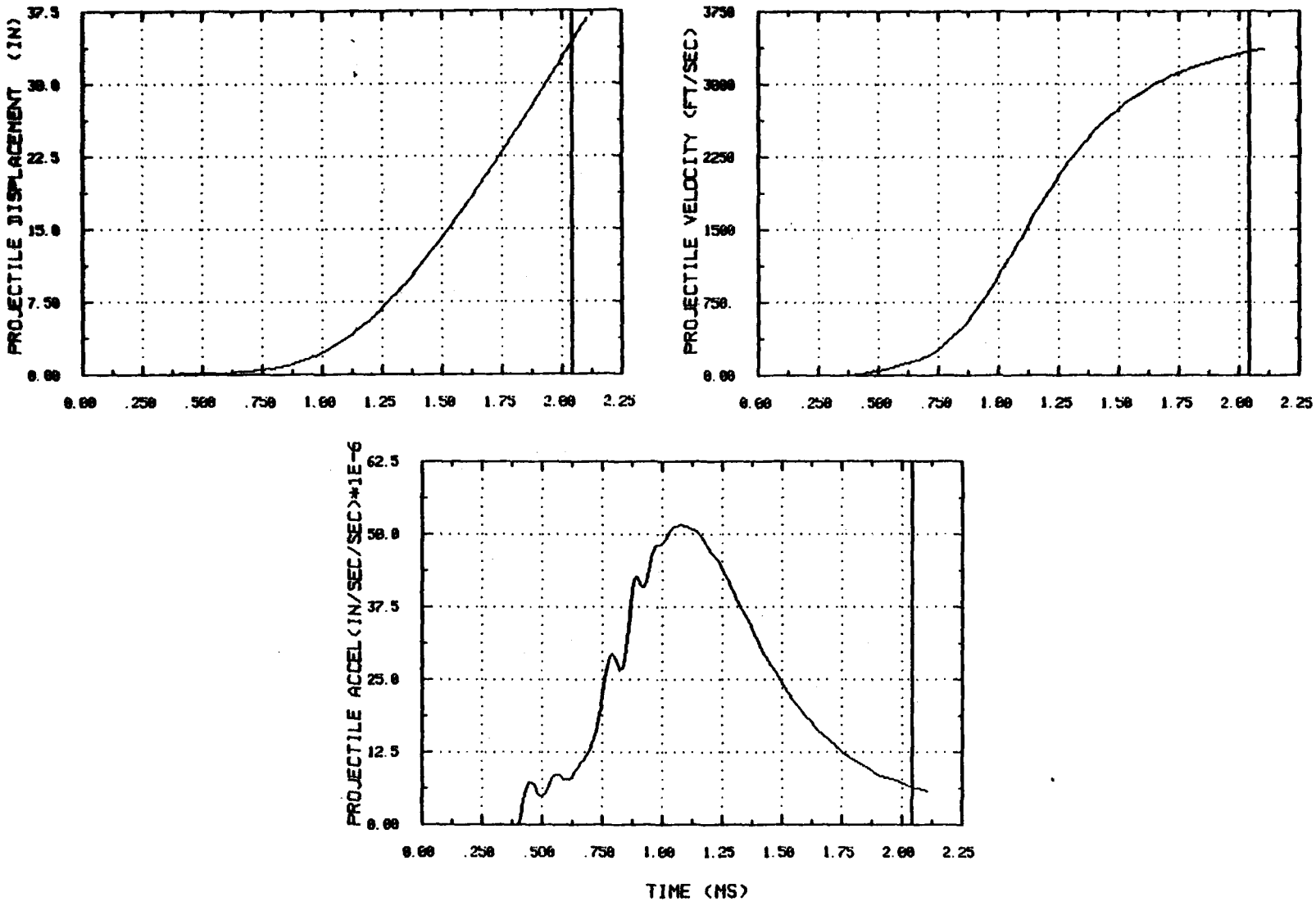

FIGURE C-4 PROJECTILE DISPLACEMENT, VELOCITY, AND ACCELERATION FOR TEST NO. 46

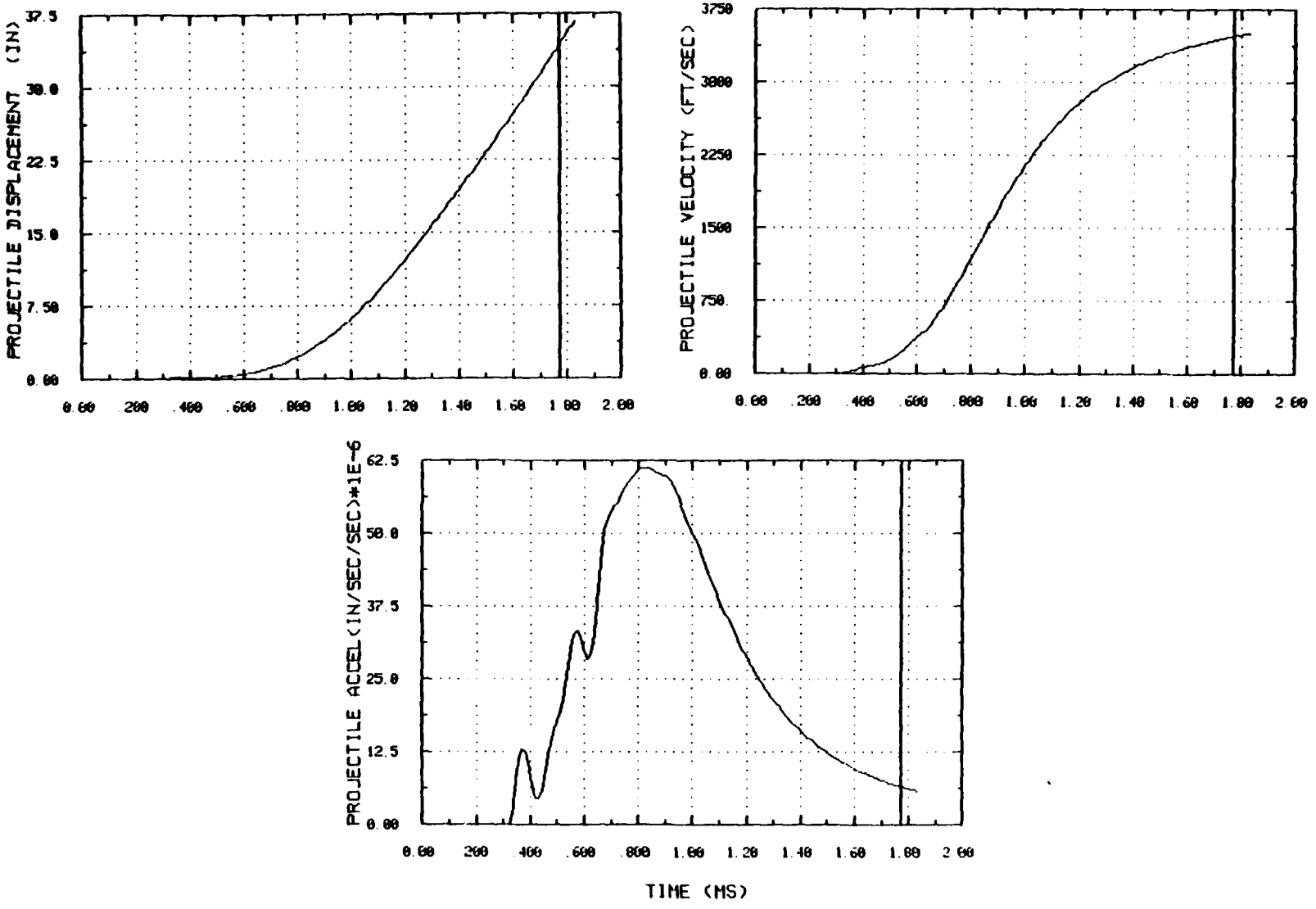

FIGURE C-5 PROJECTILE DISPLACEMENT, VELOCITY, AND ACCELERATION FOR TEST NO. 53

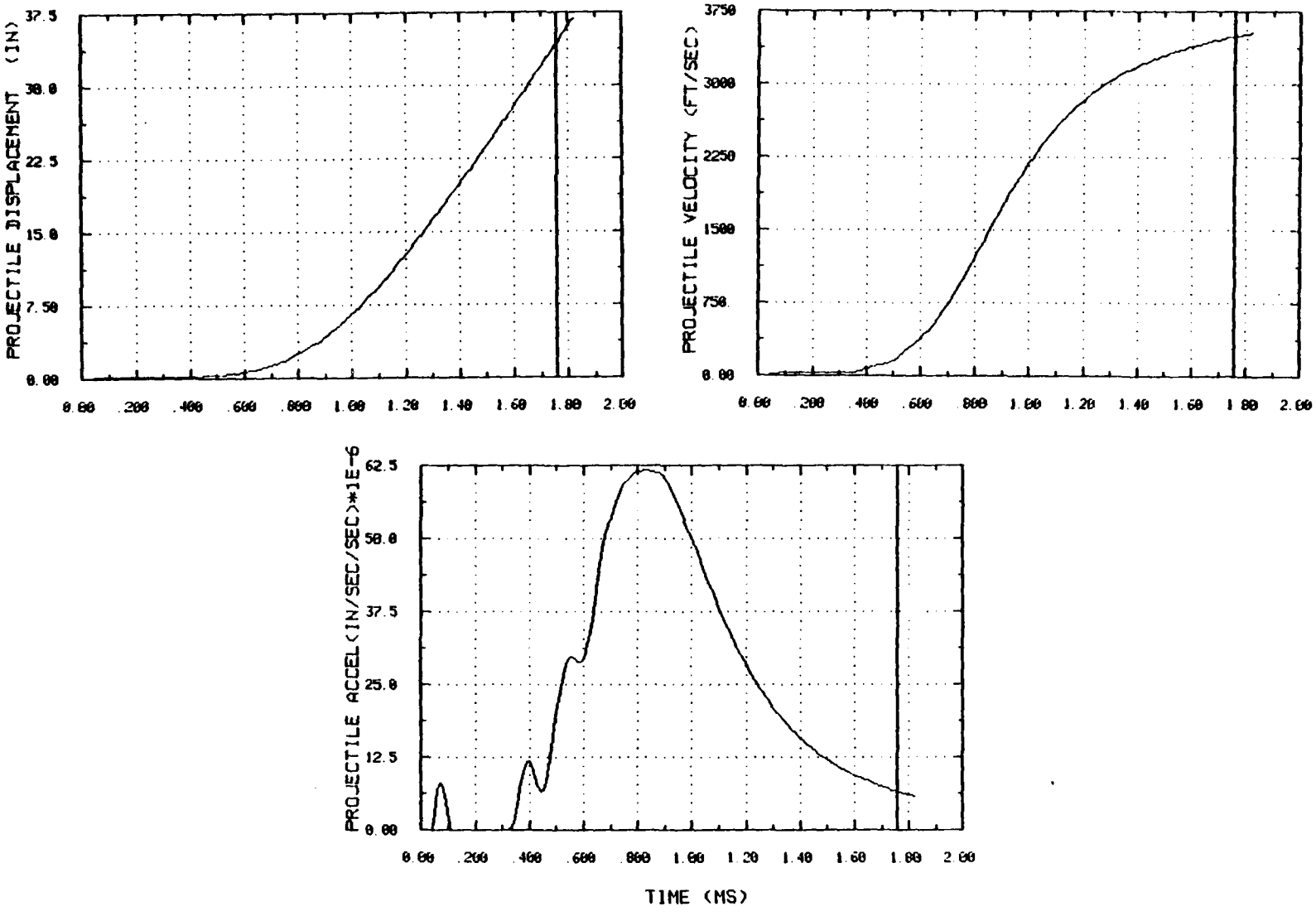

FIGURE C-6 PROJECTILE DISPLACEMENT, VELOCITY, AND ACCELERATION FOR TEST NO. 55

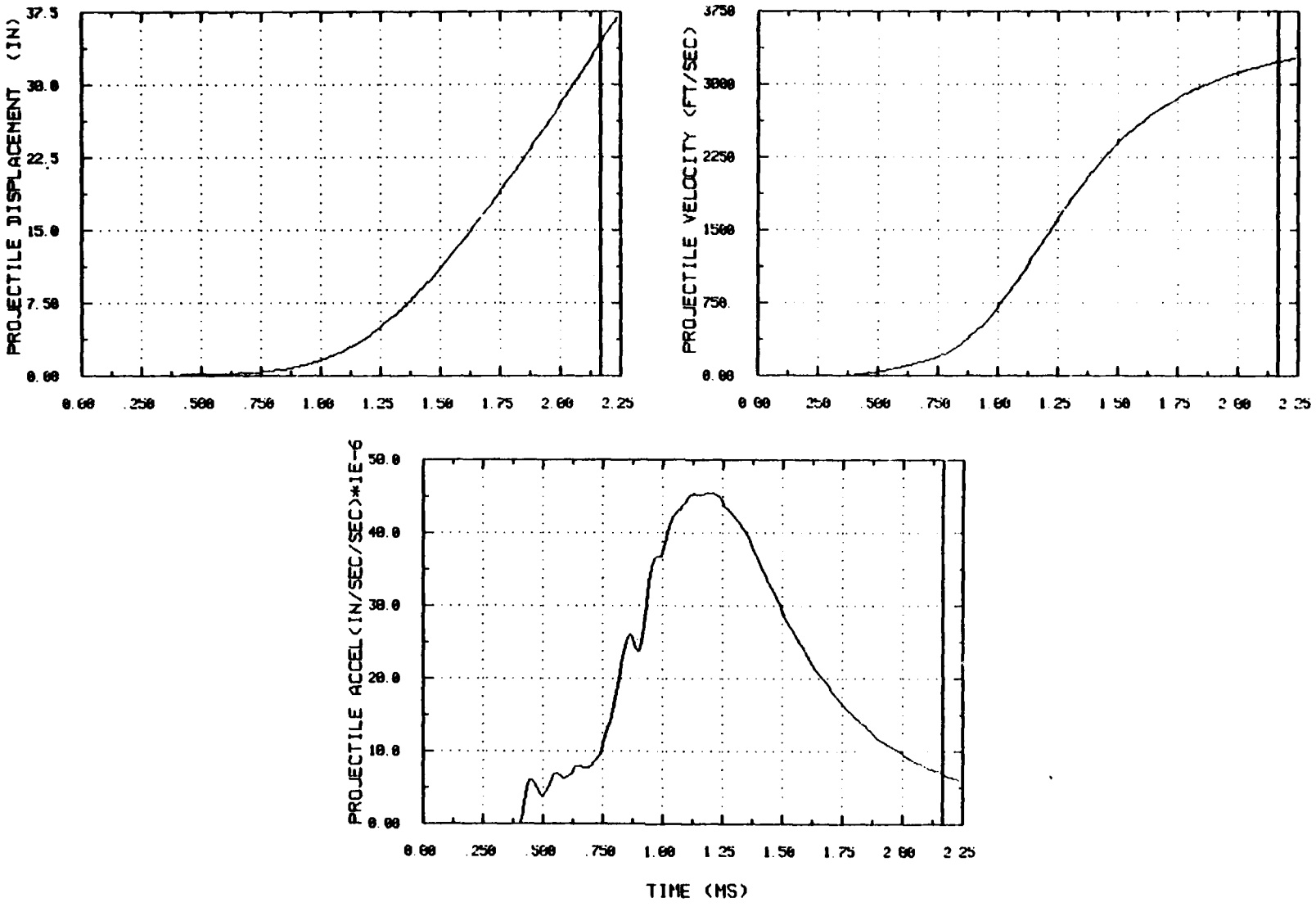

FIGURE C-7 PROJECTILE DISPLACEMENT, VELOCITY, AND ACCELERATION FOR TEST NO. 58

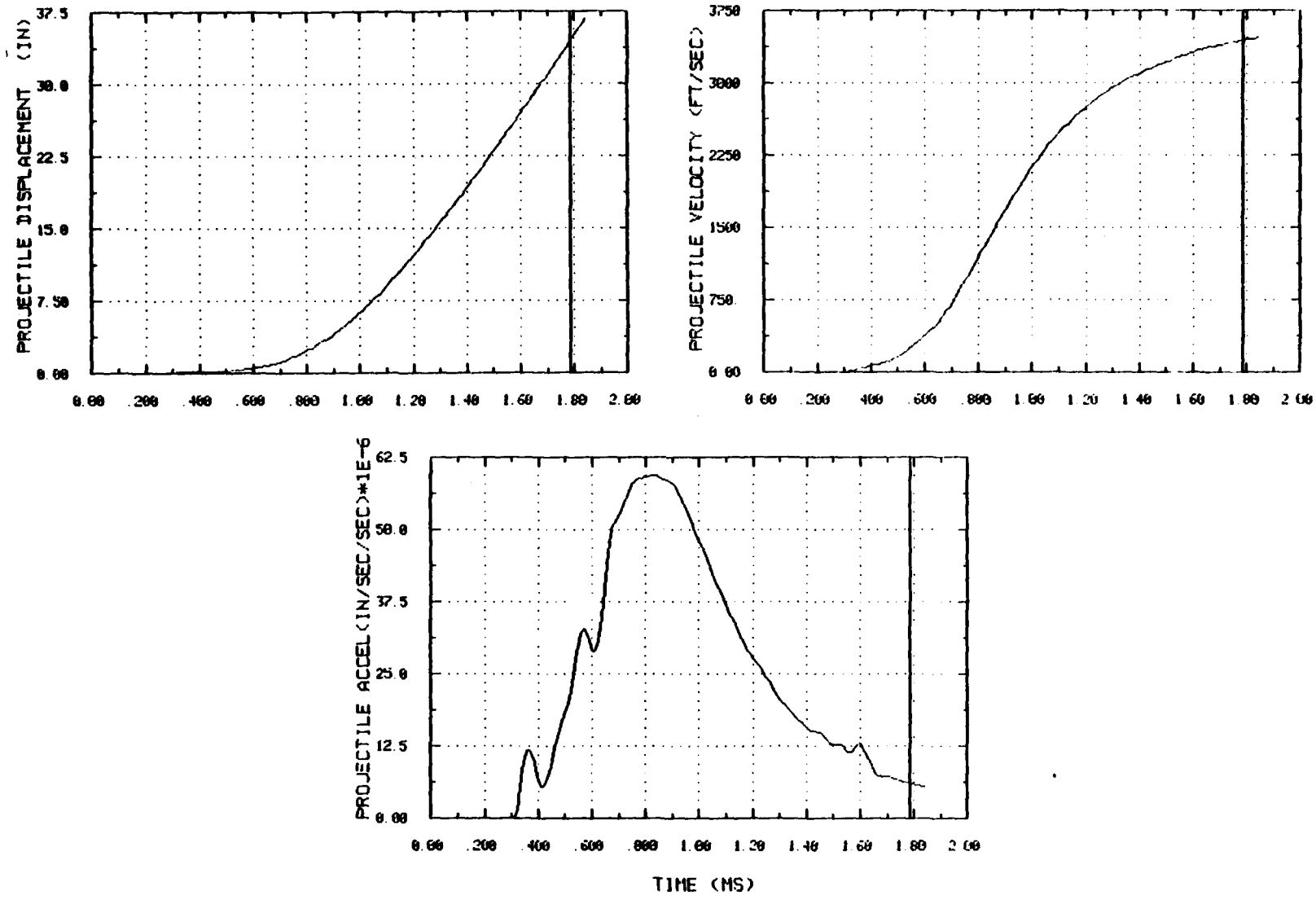

FIGURE C-8 PROJECTILE DISPLACEMENT, VELOCITY, AND ACCELERATION FOR TEST NO. 66

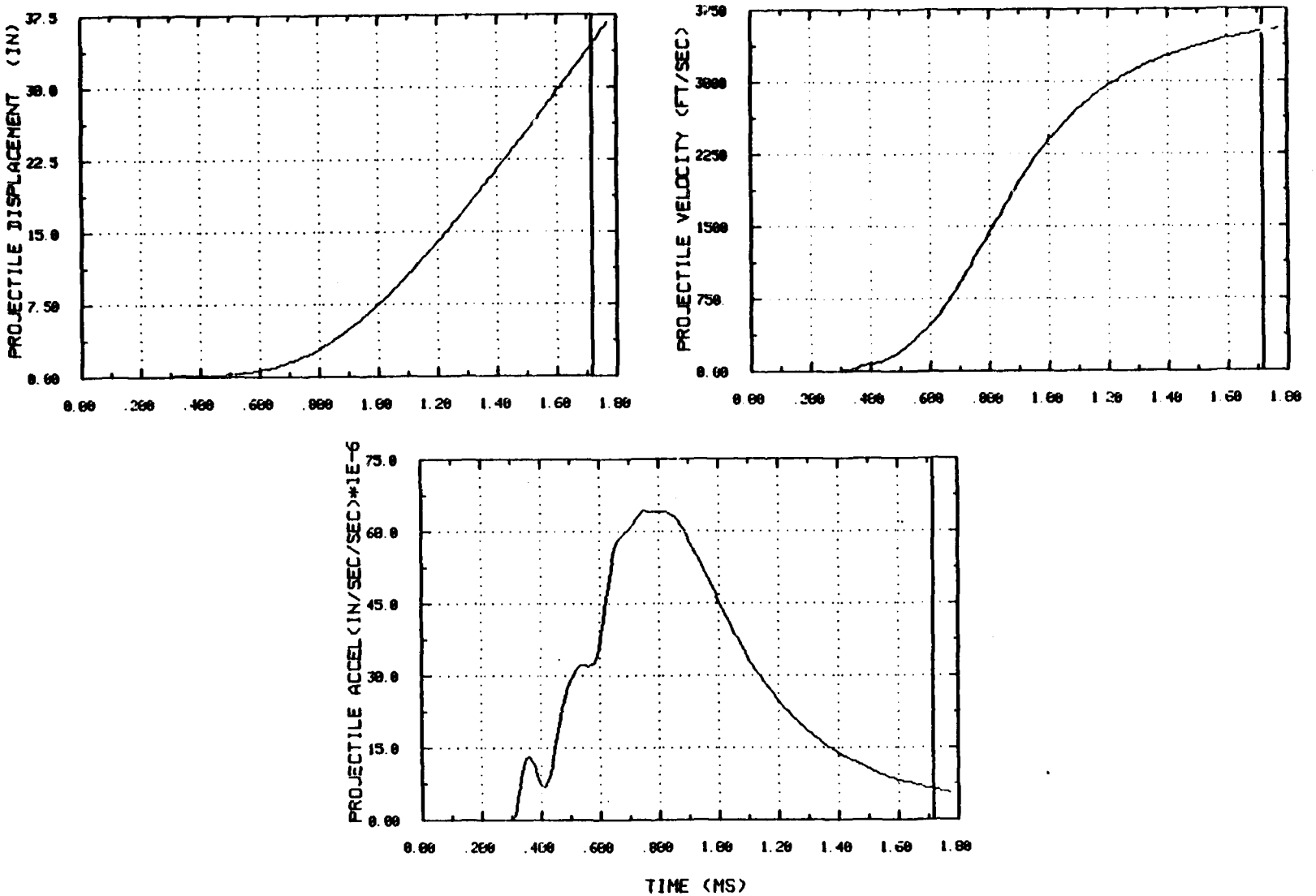

FIGURE C-9 PROJECTILE DISPLACEMENT, VELOCITY, AND ACCELERATION FOR TEST NO. 67

APPENDIX D

CALCULATED DISPLACEMENTS OF THE MODEL TEST WEAPON FOR TESTS

33
44
45
46
53
66

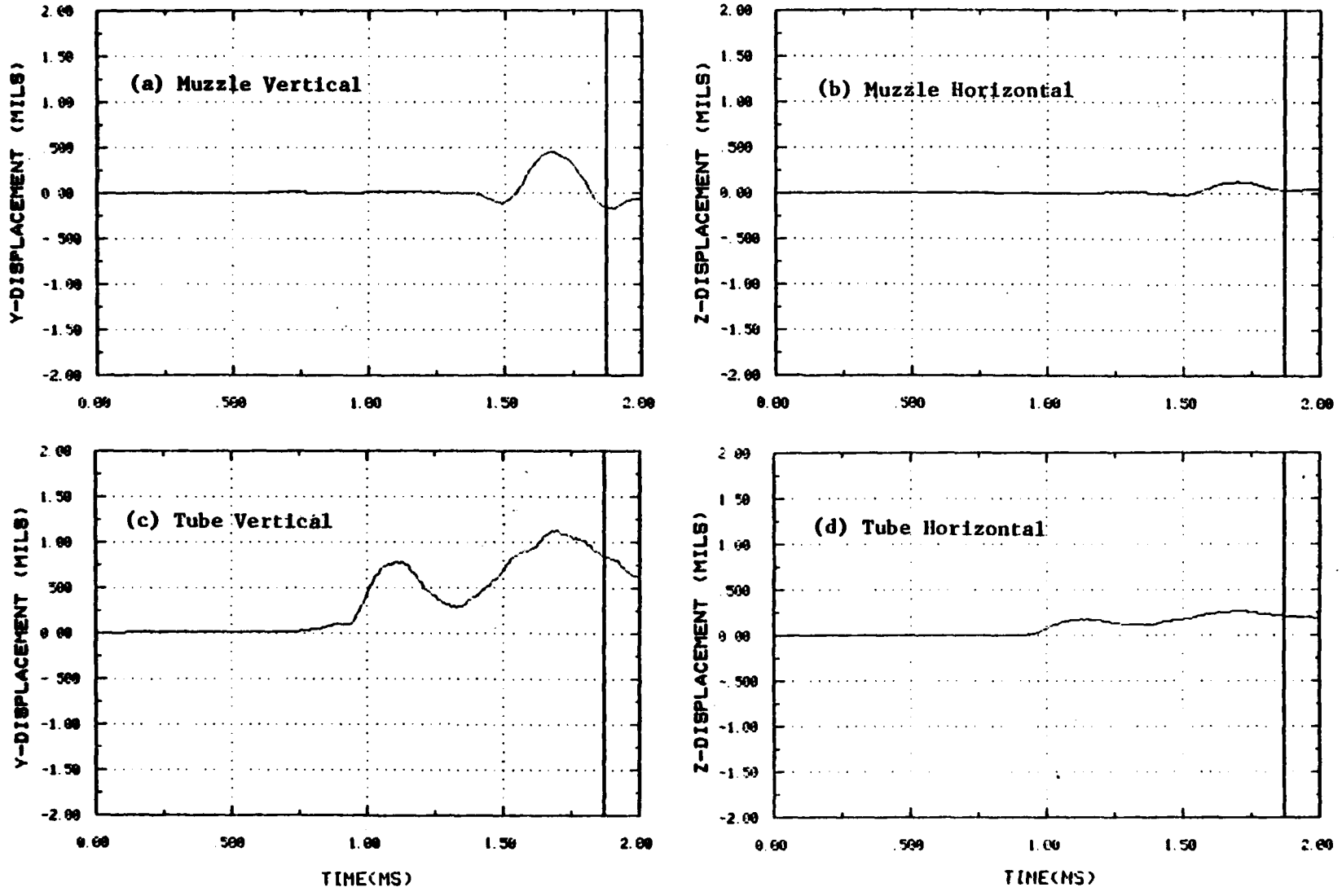

FIGURE D-1 CALCULATED DISPLACEMENTS FOR TEST NO. 33 (Cont'd)

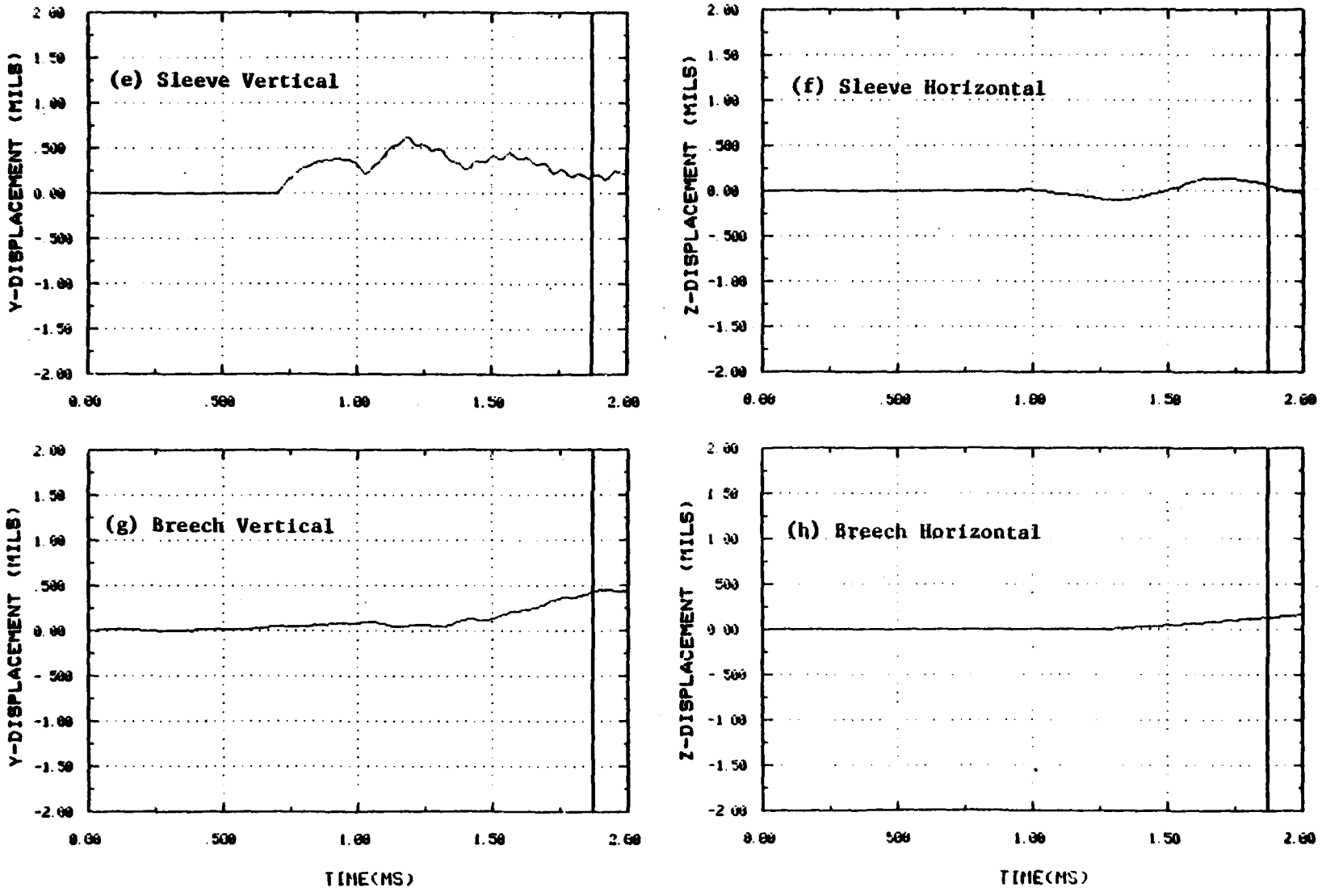

FIGURE D-1 CALCULATED DISPLACEMENTS FOR TEST NO. 33 (Concl'd)

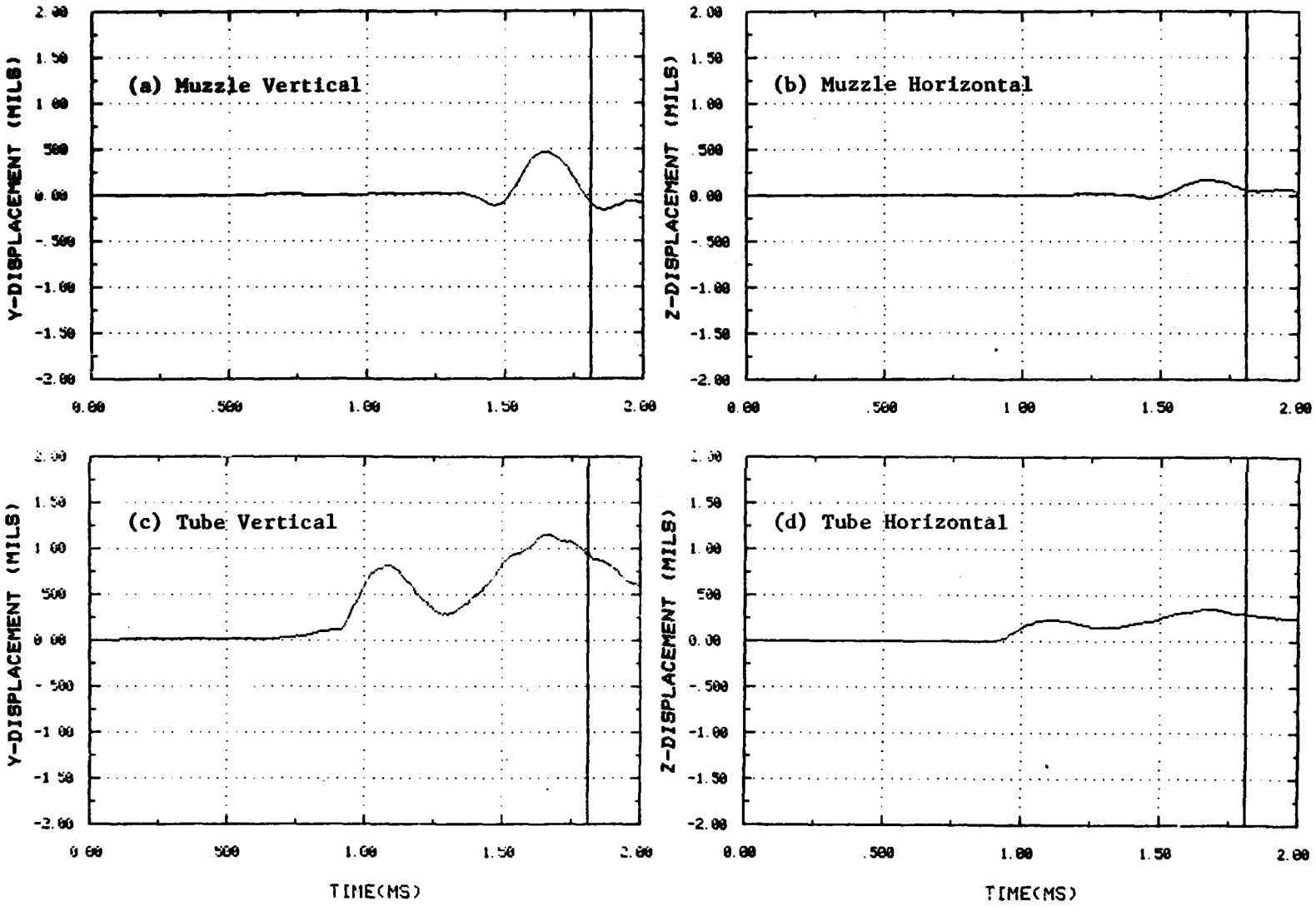

FIGURE D-2 CALCULATED DISPLACEMENTS FOR TEST NO. 44 (Cont'd)

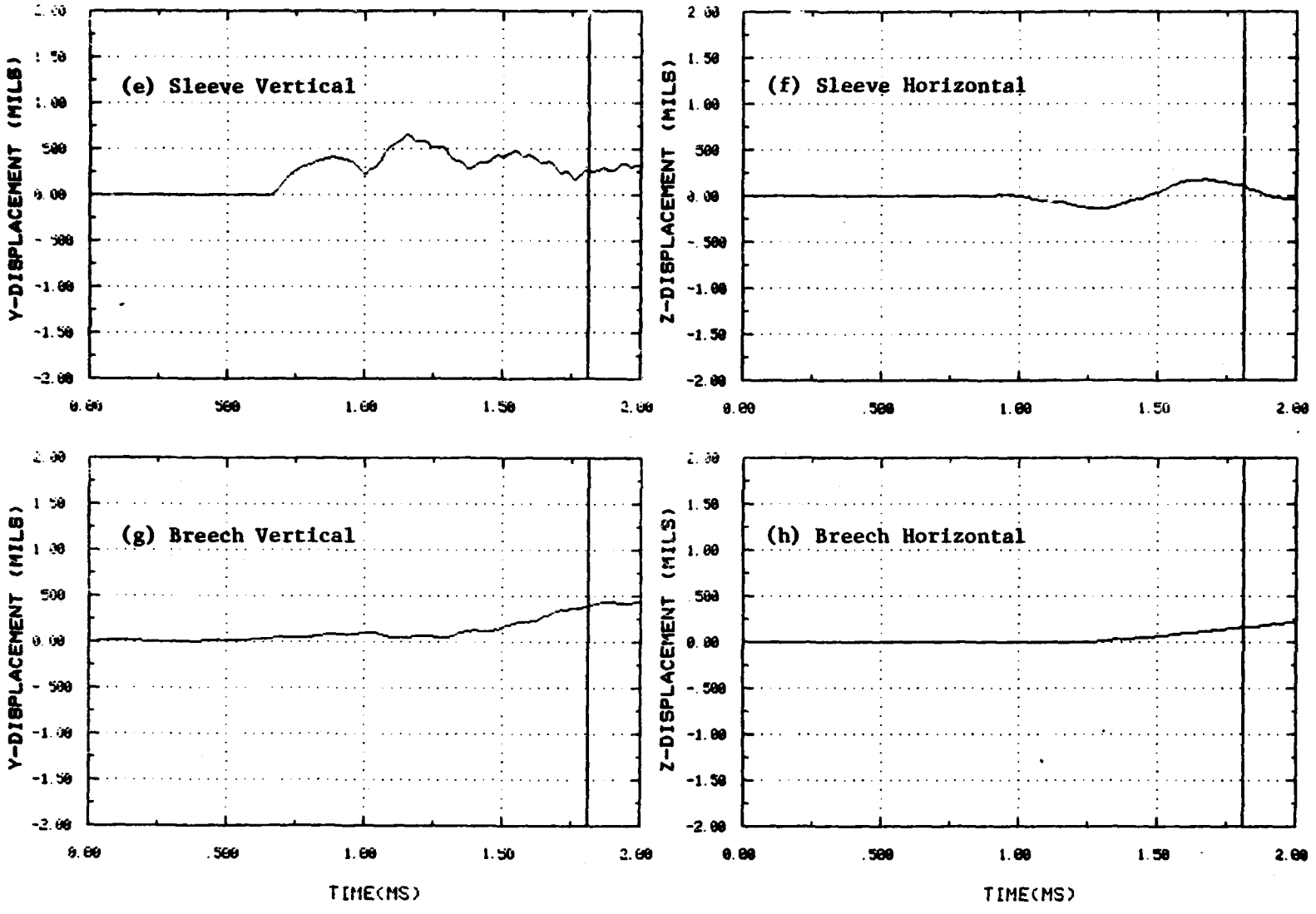

FIGURE D-2 CALCULATED DISPLACEMENTS FOR TFST NO. 44 (Concl'd)

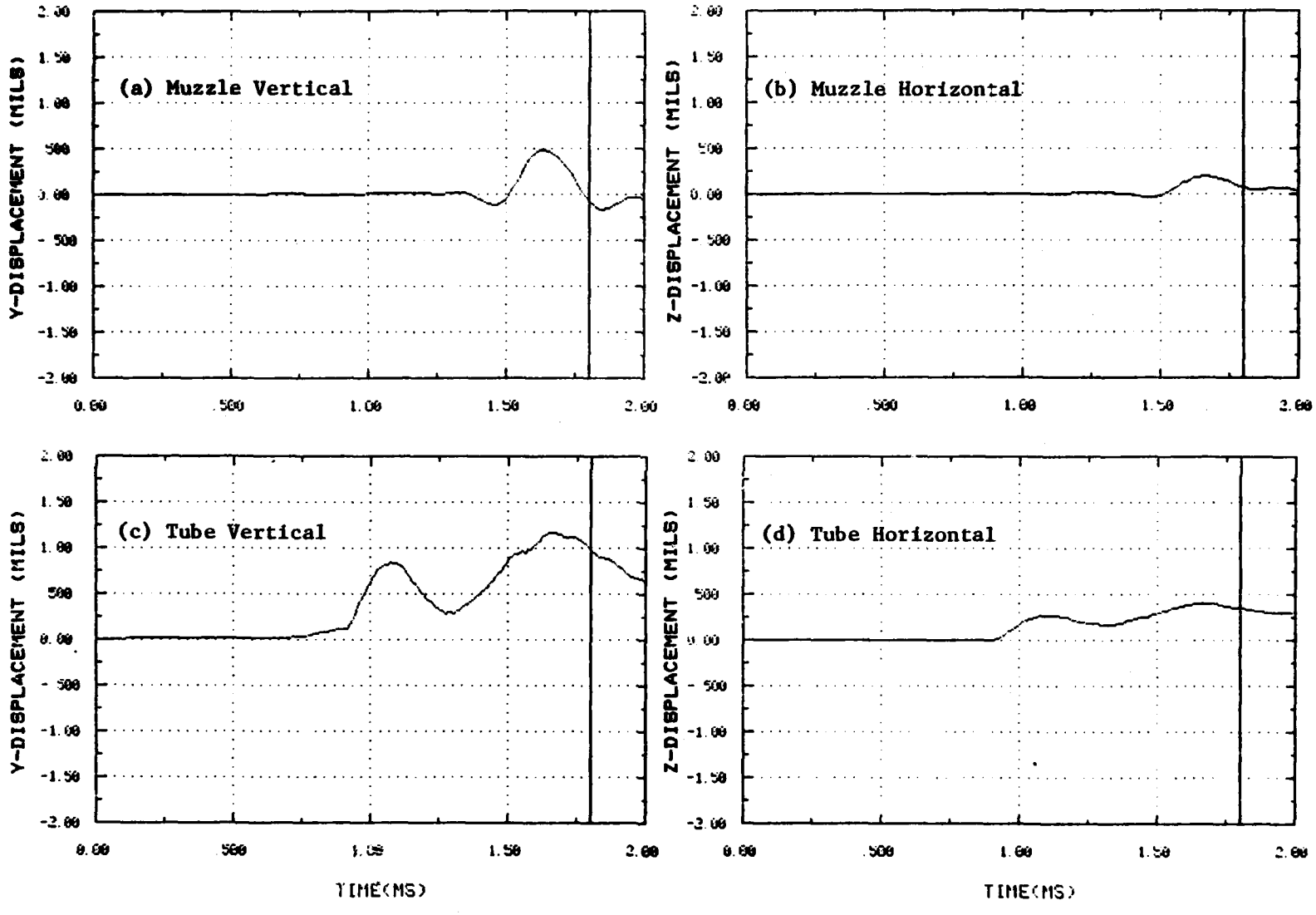

FIGURE D-3 CALCULATED DISPLACEMENTS FOR TEST NO. 45 (Cont'd)

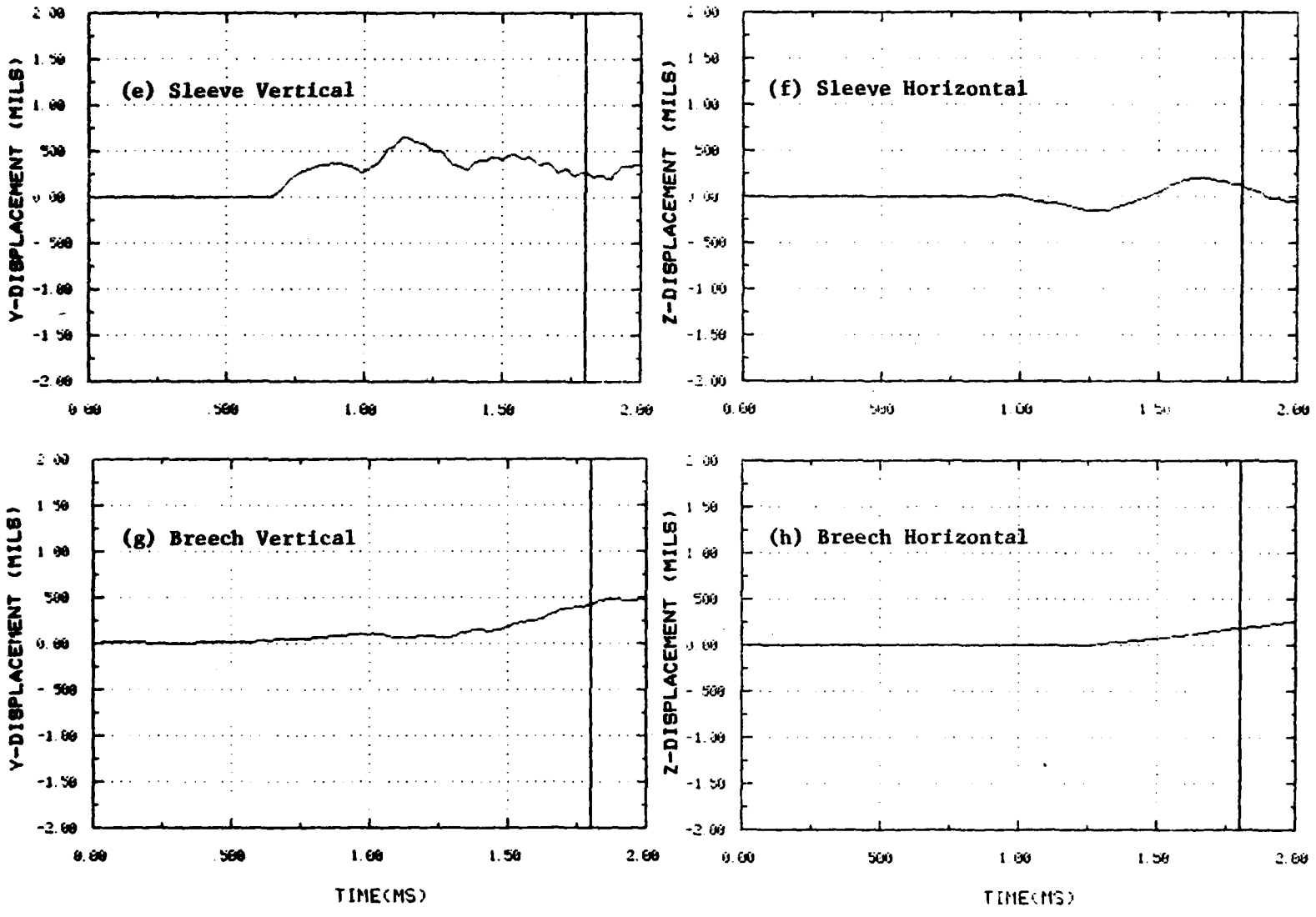

FIGURE D-3 CALCULATED DISPLACEMENTS FOR TEST NO. 45 (Concl'd)

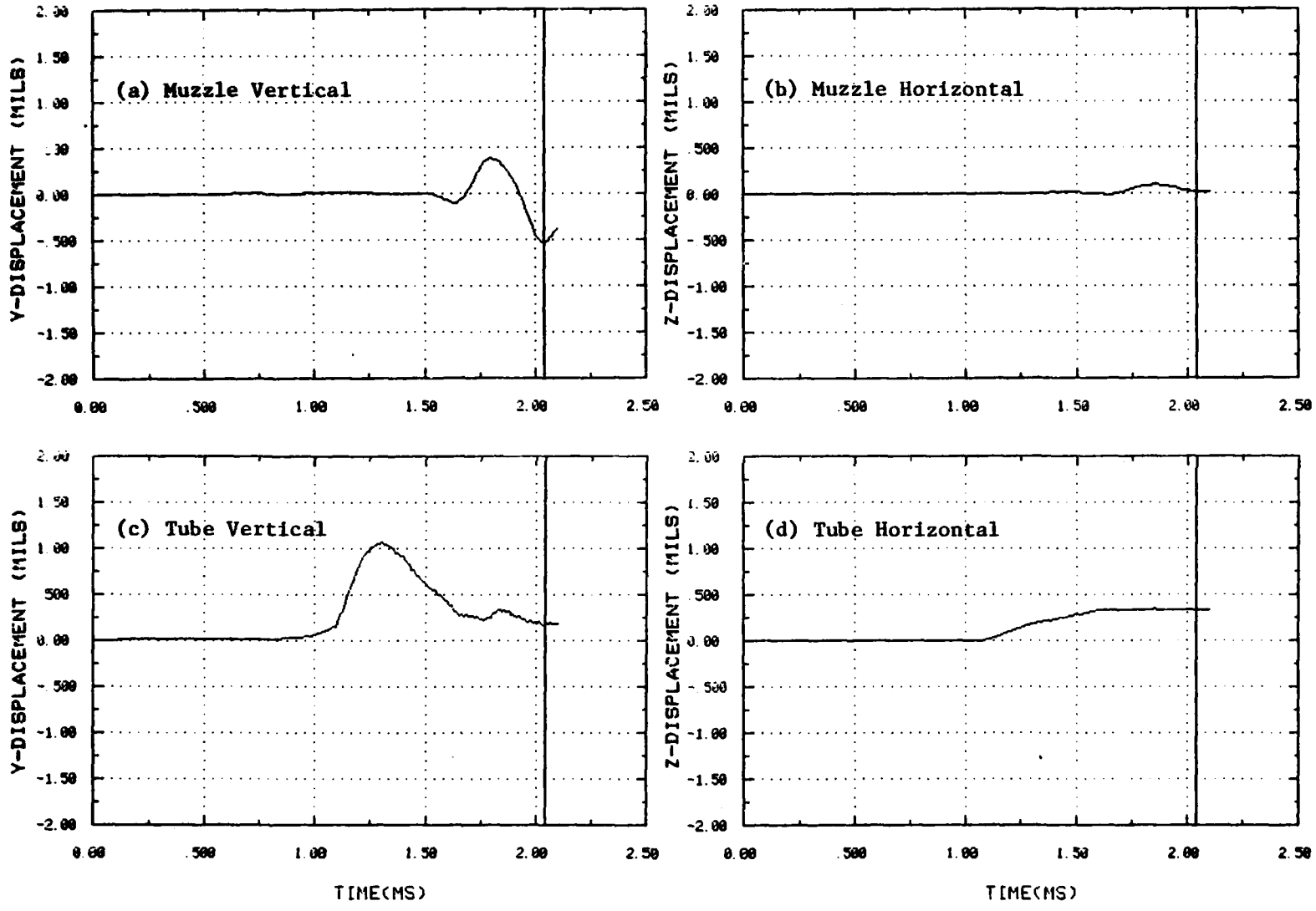

FIGURE D-4 CALCULATED DISPLACEMENTS FOR TEST NO. 46 (Cont'd)

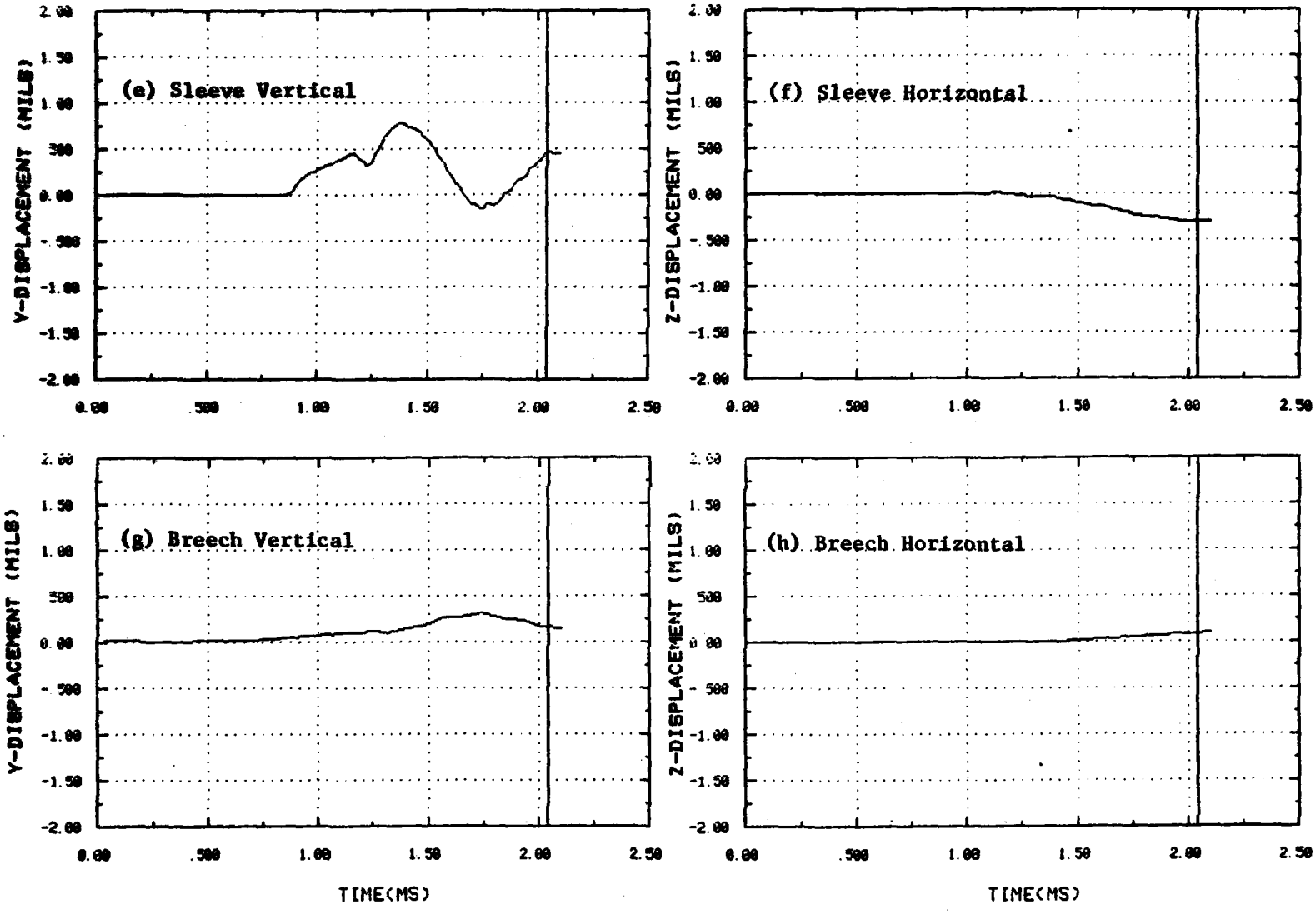

FIGURE D-4 CALCULATED DISPLACEMENTS FOR TEST NO. 46 (Concl'd)

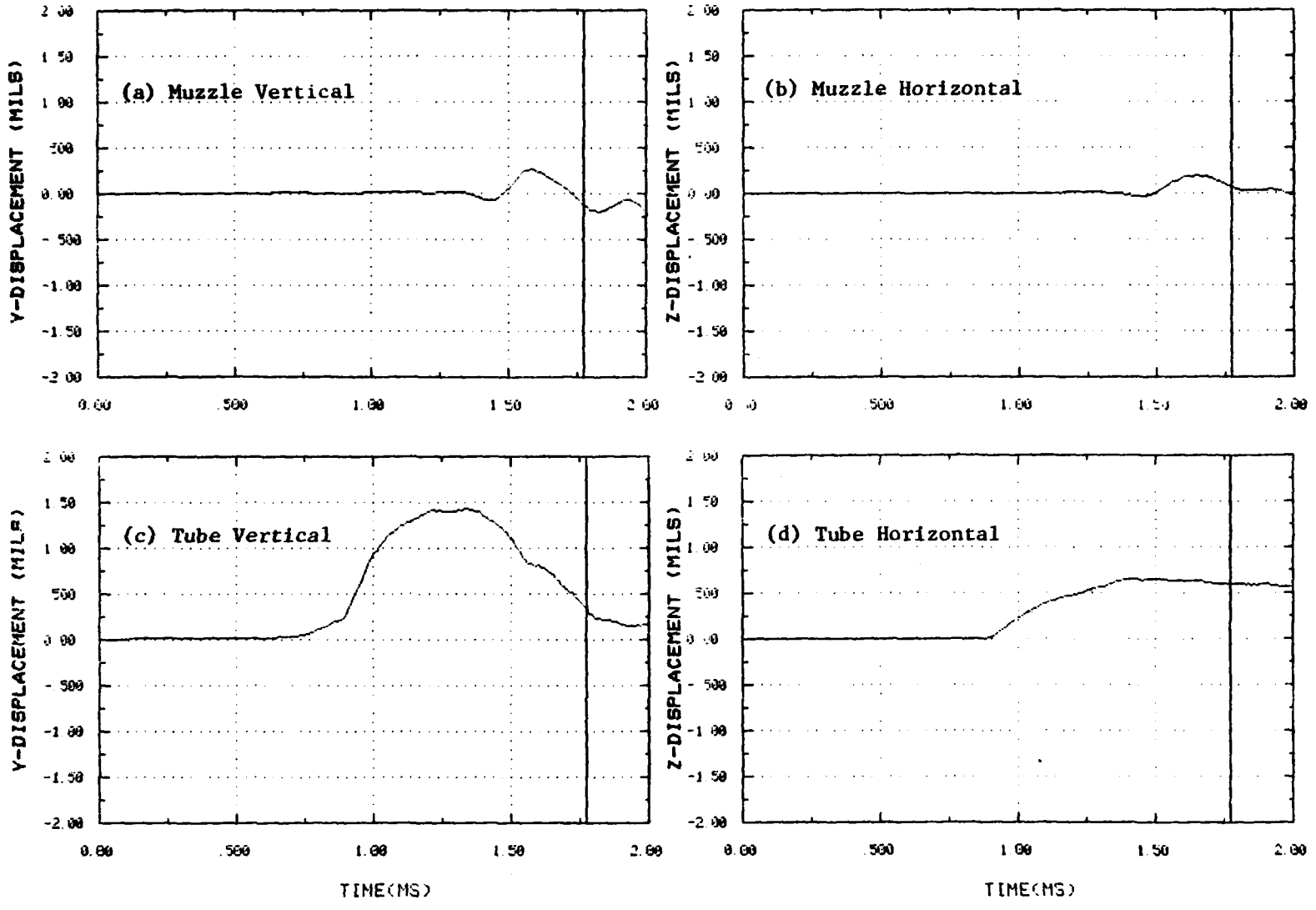

FIGURE D-5 CALCULATED DISPLACEMENTS FOR TEST NO. 53 (Cont'd)

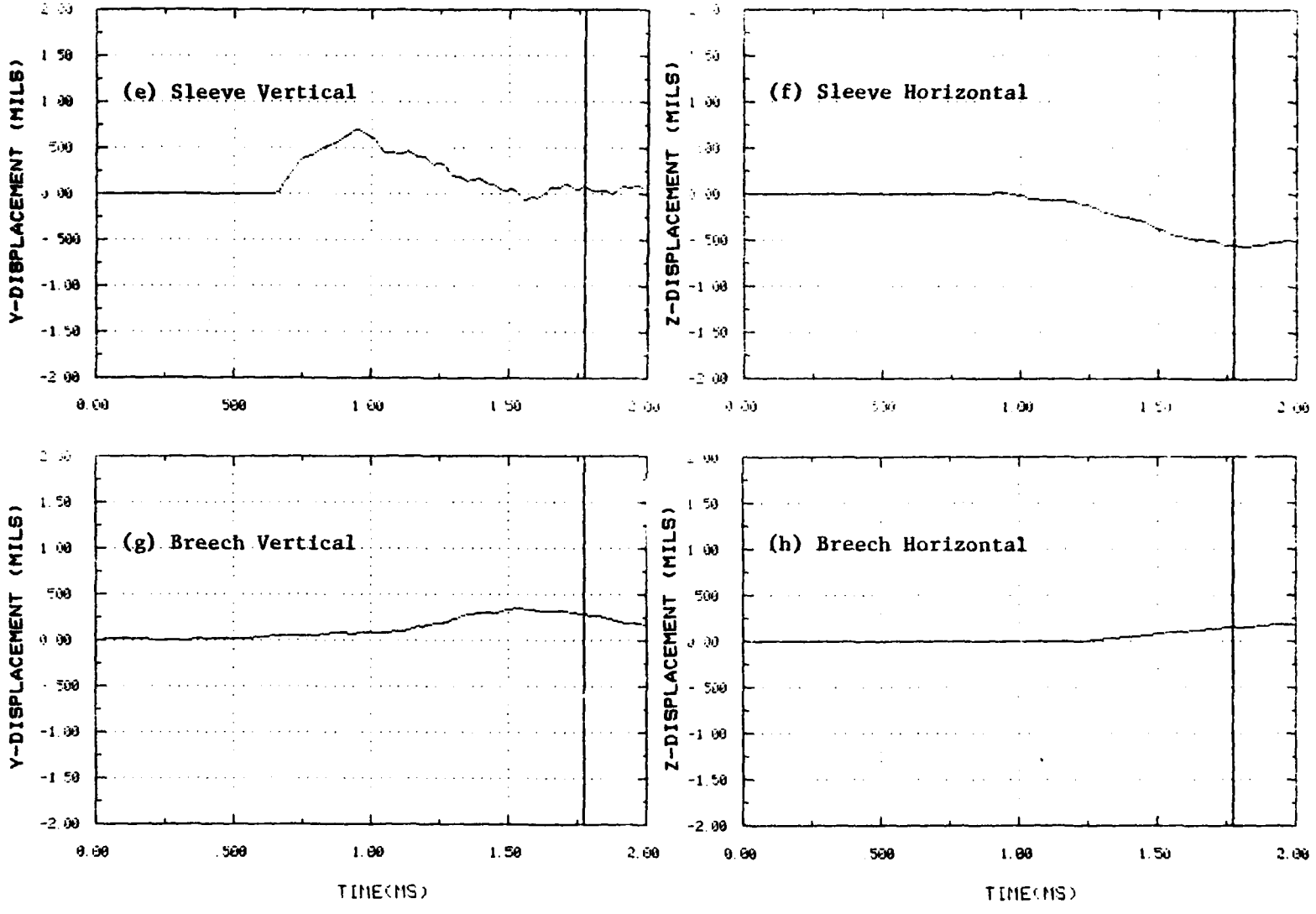

FIGURE D-5 CALCULATED DISPLACEMENTS FOR TEST NO. 53 (Concl'd)

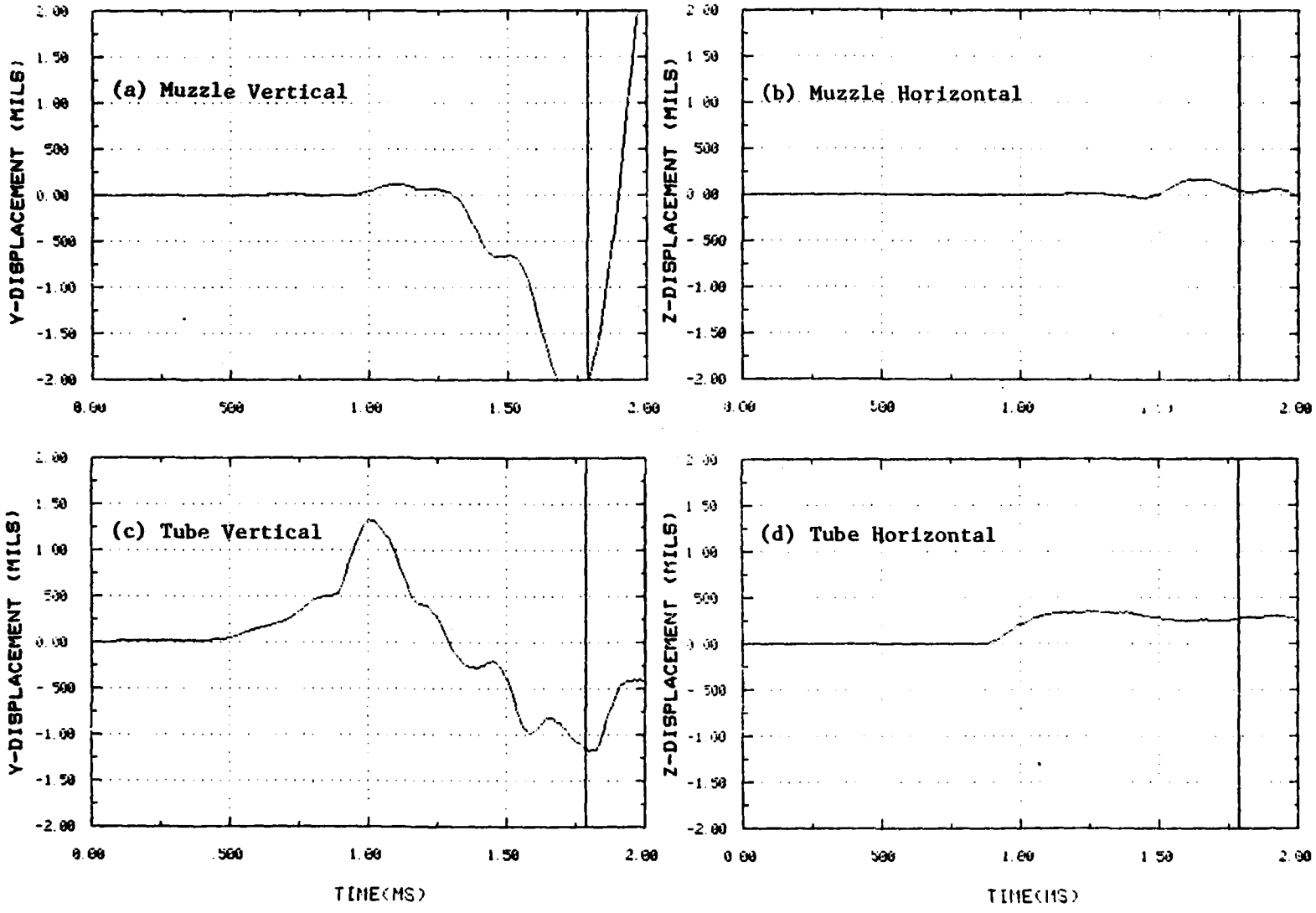

FIGURE D-6 CALCULATED DISPLACEMENTS FOR TEST NO. 66 (Cont'd)

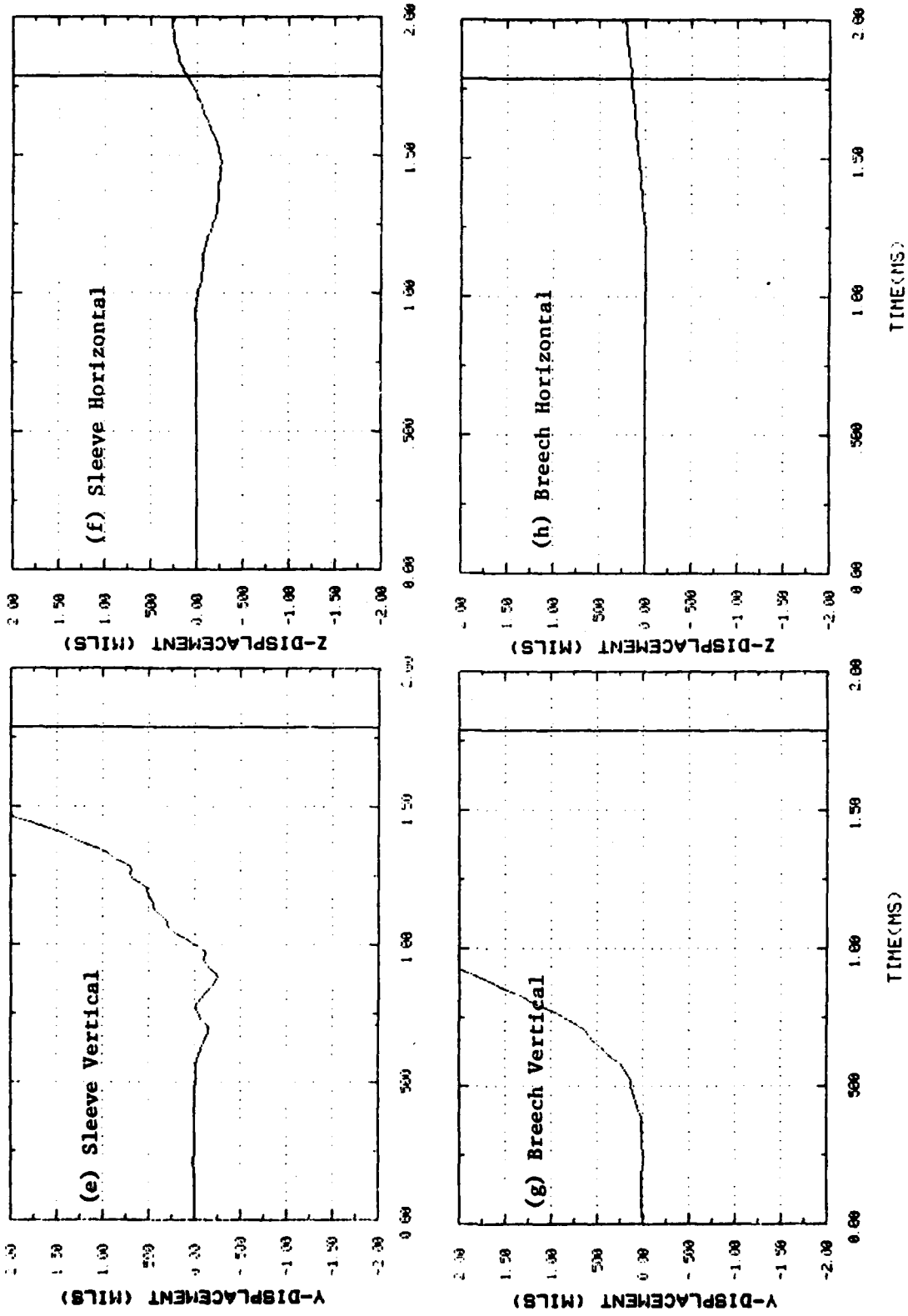

FIGURE D-6 CALCULATED DISPLACEMENTS FOR TEST NO. 66 (Concl'd)